EXPERIMENTAL AND SIMULATIVE STUDY OF CHARACTERISTICS OF "SITE ERROR" INHERENT TO MAGNETIC DIRECTION-FINDER (DF) LIGHTNING LOCATING TECHNIQUE

LU TAO

Ph.D

The Hong Kong Polytechnic University

2014

The Hong Kong Polytechnic University

Department of Building Services Engineering

Experimental and Simulative Study of Characteristics of "Site Error" Inherent to Magnetic Direction-Finder (DF) Lightning Locating Technique

LU TAO

A thesis submitted in partial fulfillment of the requirements

for the Degree of Doctor of Philosophy

July 2013

Certificate of Originality

I hereby declare that this thesis is my own work and that, to the best of my knowledge and belief, it reproduces no material previously published or written, nor material that has been accepted for the award of any other degree or diploma, except where due acknowledgment has been made in the text.

LU TAO

Department of Building Services Engineering

The Hong Kong Polytechnic University

Hong Kong SAR, China

July, 2013

Abstract

For lightning research and other applications, such as forest-fire detection, management of electric power lines and airplane protection etc, lightning locating systems have been developed. To locate a lightning striking position, time-of-arrival (TOA) and gated wideband magnetic direction-finding (DF) technologies are mostly utilized. One of the major factors of DF performance is its “site error”.

Firstly, the properties of the “site error” as a function of the source azimuth have been examined. It is found that for a given DF, its “site error” as a function of source azimuth appears as a complicated waveform with a dominant sinusoidal cycle of either 360° or 180°. A different DF has a different “site error” pattern but this pattern is timely invariant unless the DF's site environment is changed.

Secondly, with the magnetic field waveforms recorded by the two crossed magnetic loops of a broadband direction finder (DF), characteristics of “site error” in determination of lightning stroke direction have been investigated in frequency domain in bands of 100 Hz to 600 kHz. For a given lightning stroke, it is found that the source directions determined by ratios of signals from the two crossed magnetic loops vary at different frequencies. The variation of the source directions versus frequencies for a stroke usually shows a fluctuation with some sharp mono-polar and

bi-polar pulses superposed on a relative flat line. Such a fluctuation in the source directions determined is usually attributed to the “site error” in literature.

Thirdly, theoretical interpretation and modeling of such characteristics of the “site error” have been attempted based on an electromagnetic dipole model. It shows that the mono-polar shape fluctuations of “site error” in frequency domain are due to re-excitation of lightning signal by ‘electric-dipole-wise' objects near the DF, while the bipolar ones are due to re-excitation by ’magnetic-dipole-wise' objects near the DF. The proposed model can also interpret well the azimuthal properties of the ‘site error’ reported in literature. Furthermore, possible approaches for making “site error” correction have been discussed.

Fourthly, although lightning location network (LLN) has been widely used all over the world, its performance is still constrained by the “site error” as long as the direction-finder technique is deployed. Based on lightning data from a regional LLN consisted of 25 DF/TOA combined sensors, a method for “site error” estimation and correction has been proposed and practiced. By comparing the lightning locations reported by at least 4 sensors between DF and TOA techniques, the spatial and seasonal signatures of “site error” for individual sensors are found and discussed. The signatures found are well consistent with those in literature. The “site error” obtained are then used to correct and improve the accuracy of lightning locations reported by only 2 sensors. Results show that the proposed “site error” correction method could

significantly improve the location accuracy of the LLN.

Finally, an improved approach for locating close lightning strokes based on single station with broadband DF technique has been proposed and practiced. In the approach, a lightning stroke is modeled with an electrical dipole carrying current components in very low frequency and low frequency (VLF/LF) bands, as wavelengths in these frequency bands are much longer than the effective length of the channel of a lightning stroke. For a close lightning stroke, the ratio of the spectra of the vertical electrical field and horizontal magnetic field at ground is theoretically a function of the frequency and the distance to the stroke. The distance of the stroke can then be obtained by fitting the theoretical function with the observed data. The approach was examined by applying it to broadband VLF/LF electrical and magnetic field waveforms observed simultaneously at one station for several strokes in a range of about 10 to 50 km. Furthermore, a prototypal single-station lightning location system (S-LLS), which can be analogized to a modified VLF/LF broadband DF programmed with our proposed lightning stroke distance determining approach, has been built up and tested. Comparisons of individual stroke locations with the local LLN show that the S-LLS has a good location accuracy of about 0.1 – 4 km for close lightning strokes in ranges of 15 to 60 km, but has a poor location accuracy of about 12.4 – 26 km for distant lightning strokes in ranges of 80 to 130 km.

Publications Arising from the Thesis

Journal Paper

1. Mingli Chen, Tao Lu, Ya-ping Du: Properties of "Site Error" of Lightning Direction-Finder (DF) and Its Modeling, *Atmospheric Research,* Vol. 129–130, pp.97–109, 2013.
2. Mingli Chen, Tao Lu, Ya-ping Du: An Improved Technique for Locating Close Lightning Stroke from Single Station Observation and Its validation with Experiment, *IET Generation, Transmission & Distribution* (submitted), 2013.

Conference Paper

1. Tao Lu, Mingli Chen: Characteristic of "Site Errors" and Its Interpretation for a Broadband DF by Frequency Domain Analysis, *XIV International Conference on Atmospheric Electricity*, August 08-12, 2011, Rio de Janeiro, Brazil.
2. Mingli Chen, Huaibin Wang, Tao Lu: Experimental Study of Locating Close Lightning Strokes based on Single-Station Observations, *XIV International Conference on Atmospheric Electricity*, August 08-12, 2011, Rio de Janeiro, Brazil.
3. Mingli Chen, Tao Lu, Ya-ping Du: Performance of TOA/DF Lightning Location Network in China – Site errors and Detection Efficiency, *7th Asia-Pacific International Conference on Lightning,* November 1-4, 2011, Chengdu, China.
4. Tao Lu, Mingli Chen, Ya-ping Du: Site Errors Estimation and Correction for MDF/TOA Combined Lightning Location Network, *31st International Conference on Lightning Protection (ICLP)*, September 2-7, 2012, Vienna, Austria.

Acknowledgments

I must express my sincere gratitude to my Chief Supervisor, Dr. Chen Mingli, my Co-Supervisor, Prof. Deng Shiming, and Prof. Du Ya-ping, of Department of Building Services Engineering (BSE), The Hong Kong Polytechnic University, for their effective supervisions, valuable suggestions and encouragements throughout the course of the work. They have serious research attitude and become role models to fellow.

Thanks to The Hong Kong Polytechnic University and Hong Kong Government. I have satisfactory access to books, Journals and equipments. My special thanks go to Dr. Gou Xueqiang from the College of Physics and Electronic Engineering, Northwest Normal University, China, for his assistance in my data processing and literature review. I would like to also thank Mr. Xu Yazhong, Miss Shen Yanchi and Miss Ding Xunyun for their assistance in all aspects of my study and live. Furthermore, I am grateful to Prof. Zhang Yijun, Prof. Dong Wansheng, Dr. Zheng Dong, Dr. Zhang Yang, Dr. Lu Weitao, Dr. Chen Shaodong, Dr. Liu Hengyi, Dr. Wang Fei, Mr Zhu Biao, Mr Yan Biwu, Mr Shi Yuheng, Mr Gao Hong, and Mr Zhou Enwei for their helps on my field experiments. Thanks to Mr. Wang Huaibin for his technical supports during my experimental works.

Thanks to my roommates, Guo Daoqin, Peng Jinqng, Chen Xi, and Zhang Liang.

They make my life full of variety.

Finally, I would like to express my appreciation to my mother and father. They lead a simply life and always encourage me to work hard although I am far away from them. I wish them good health and happy.

Table of Contents

Page

List of Figures

List of Tables

Chapter 1

Introduction

1.1 Lightning phenomenon

Lightning is a kind of strong discharge phenomenon happens in atmosphere with large-current in nature. It is usually accompanied by a strong convective weather. In general, there are two forms of lightning flashes: cloud discharge and cloud-to-ground lightning. More than a half of all lightning flashes are cloud discharges which mainly occur between the positive and negative electric charge zones within a thunder cloud. Those rare inter-cloud discharges and cloud-air discharges are also called cloud discharges [Wang et al., 2000]. Cloud discharge is especially dangerous to aero and space vehicles although it does little harm to human and animals on ground [Rakov and Uman, 2003]. Cloud-to-ground lightning discharge (CG) occurs between cloud and ground surface. Its duration ranges from tens of milliseconds to 1 second. A typical CG may contain several electric discharge pulses which is called “return stroke”. The time interval between two continuous return strokes is about tens of milliseconds [Uman, 1987]. The return stroke is the most severe event during a lightning flash. The magnitude of return stroke peak current is about a few tens or hundreds kA. However, the return stroke also exposes the position of the lightning flash due to its strong electromagnetic signals. After a preliminary breakdown, the stepped leader is formed. When the stepped leader connects the cloud and ground with its conducting channel, a return stroke happens. The return stroke emits light,

sound and electromagnetic signals. Light and sound also give the clue of its position. However they can just be a reference since they have a limited propagation distance. People also are seeking the speed of return stroke. They used optical equipment such as Boys camera and photomultipliers to record the light information of lightning [Jordan and Uman, 1983]. The speed of return stroke derived by the light signal is about one third of the speed of light. People have already known some features of the lightning return strokes, but there are still some features that could not be detected at present.

Hypothesis is the guidance of scientists. They know something, then make a hypothesis and do some experiments to exam and refine the hypothesis. In order to disclose the characteristics of return stroke, pioneers also made some hypotheses and models to represent the return stroke channel. These engineering and physical return stroke models got improved with the pass of time and the development of technique. Here are some typical return stroke models.

In an engineering model, the cloud and ground are usually viewed as two planes of a huge capacity. When a lightning flash is generated, there will be a transmission line that connects these two planes. Then the ground impedance and cloud impedance can be taken into account. The cloud, ground, and the conducting channel left by the stepped leader or dart leader form a (Inductance-Capacitance-Resistance) LCR circuit. People can solve this circuit by either theoretic or numerical calculation. LCR circuit and some experimental data help people to get the return stroke current waveform. Fig. 1.1 is a typical current waveform shape used by most of current propagation models. The current waveform has a form of double exponential function which is consistent

with the solution of LCR circuit.

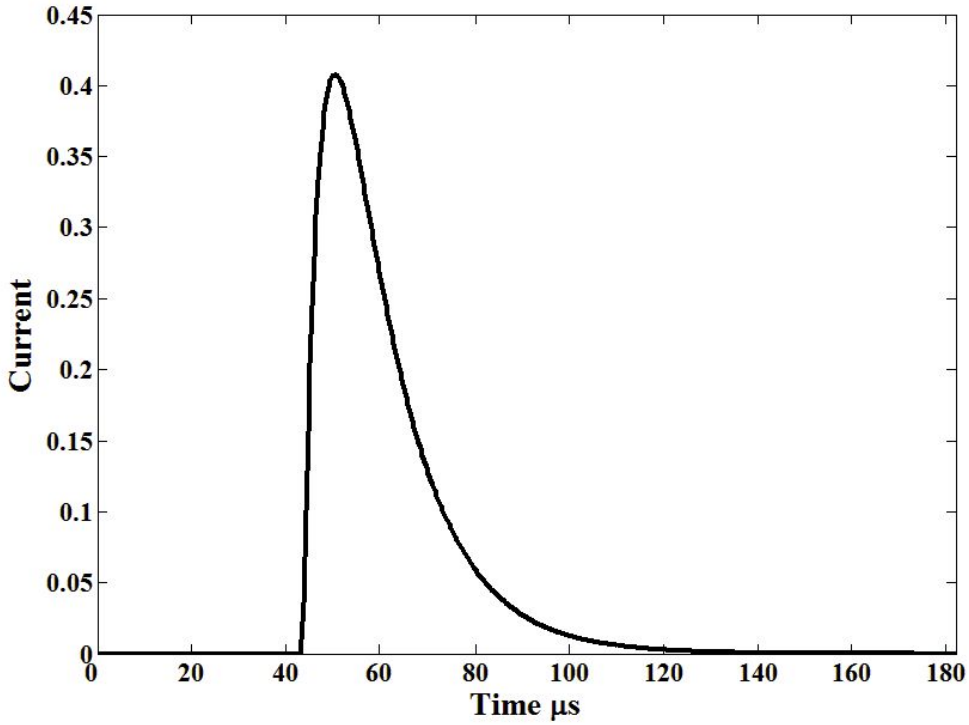

Fig. 1.1 Typical 8/20 μs lightning current waveform. Its front time is 8 μs and time to half value is 20 μs

Nucci et al. gave a modified transmission line model (MTL) which can be on behalf of current propagation model [Nucci et al., 1988]. Suppose the current of Fig. 1.1 is $I_b(t)$, then the current at a given height z in Nucci's model can be expressed as $I(z,t) = \exp(-\frac{z}{\lambda_c}) I_b(t-\frac{z}{v})$, when $t > \frac{z}{v}$, and $I(z,t) = 0$ when $t < \frac{z}{v}$, here v is the speed of return stroke front and the current pulse has the same speed with the return stroke front. Term $\exp(-\frac{z}{\lambda_c})$ is account for the neutralization action in the return stroke front and λ_c equals 2000 m.

The current generation models are concerned with the mechanism how current was generated and the current was not just simply pumped into the channel base as the current propagation model.

Lin et al. gave a model which is the combine of current propagation and current generation model [Lin et al., 1980]. He decomposed the return stroke current into three parts: i) A uniform, low frequency current, which is assumed to be left by the stepped leader or dart leader. It decreases with height in the form of $\exp(-\gamma z)$; ii) An upward propagating current pulse, which can be treated in the form of Nucci's in above; iii) Corona current, which comes from the neutralization action and propagates alone the channel.

Owing to its large current, high power, intensive electromagnetic radiation and uncertainty, lightning especially CG has high potential to cause damage to human life and property. In 2004, 617 people died in lightning-related natural disaster in the mainland of China and the number is keeping growing year by year [Mei et al., 2007]. Besides the direct damage, electromagnetic radiation would cause indirect harm. Electric and electronic devices have been widely used since 1980s. People are getting more and more relied on electric and electronic equipment with the progress of information technology. Computers and other related semiconductor devices are playing important roles in politics, economy, and military. All these electronic devices are vulnerable to electromagnetic interference of lightning flashes. According to a classified statistic of lightning strike accidents, 63 percent of accidents were associated with electric and electronic equipment damage [Mei et al., 2007].

Lightning is also the major cause of fires in forest. From 1990 to 2006, 591 forest fires events occurred in Daxing'an Ling mountain area in China and 60.7 percent of them were ignited by lightning strike [Tian et al., 2009]. So with the development of economy and society, problems brought by lightning have arisen. Lightning research becomes an important means of protecting country and people's life and possessions.

1.2 Lightning locating network

Knowing the location of a lightning discharge provides people with time to protect themselves and devices. The lightning location information also gives convenience to the maintenance of electric-power line, forest-fire detection and airplane protection etc. In addition, lightning location information is very important for lightning research, such as the research of flash densities and spatial characteristics of lightning activity versus terrain [Chen et al., 2010].

Transient lightning discharge emits out a broadband electromagnetic impulse ranging from VLF to UHF [Shen et al., 2003] and its spectral distribution is illustrated in Fig. 1.2. Lightning signal especially those return strokes' emission around VLF and LF is relatively strong and its power spectrum gets peak at about 10 kHz. Based on the sound, light, and electromagnetic signal emitted by a lightning source, people are able to tell the spatial location of lightning, its magnitude and polarity.

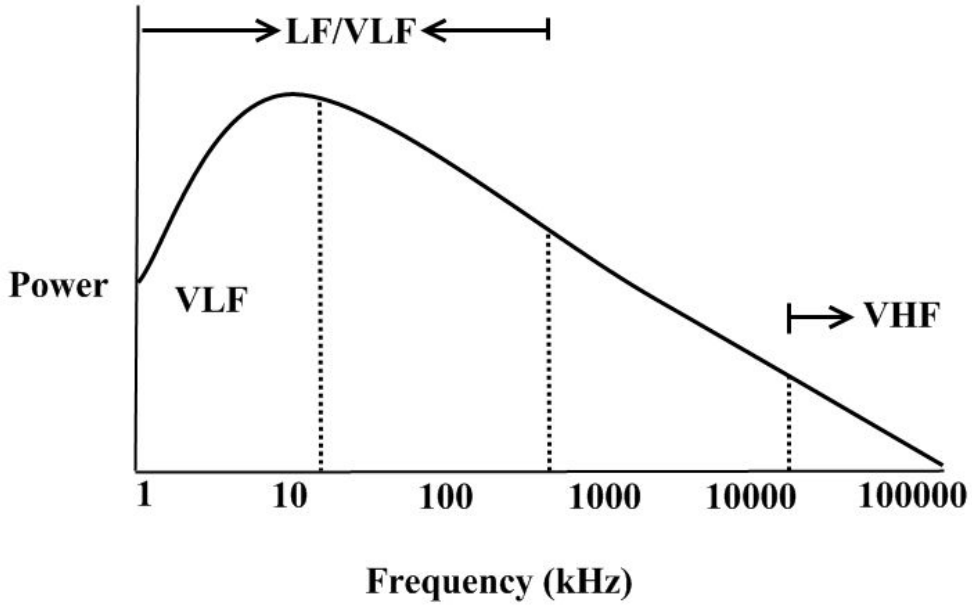

Fig. 1.2 Lightning power distribution diagram

Most of lightning location techniques have a form of multiple stations. As mentioned in [Chen, 2009], four kinds of multi-station techniques have been used in practice. They are magnetic direction finder (DF), time-of-arrival (TOA), interferometric and TOA/DF combined techniques.

A typical DF is composed of two orthogonal magnetic loop antennae and one flat plate electric antenna. Vertical and orthogonal magnetic field loops are used to obtain lightning source direction, as the ratio of the signals in the two detectors is proportional to the tangent of the angle to the source [Uman, 1987]. The polarity of a lightning flash and its strength are determined from the electric signal. In addition, with built-in criteria, DF technique can also distinguish the CC and CG flashes

[Krider et al., 1976]. A DF network requires at least two stations and the intersecting point of two directions from the two DFs gives the source location. Higher accuracy can be achieved if more than two DFs are arranged.

The TOA technique is based on the fact that a lightning signal arrives at two different stations at different times [Casper and Bent, 1992]. A time difference, which means a certain distance difference from the two fix stations to the lightning source, forms a hyperbola. And the intersecting point of 2 hyperbolas from three stations reveals the position of the lightning source. Either the electric or the magnetic signal can be adopted in TOA system. The antenna of TOA system is less complicated than that of DF. The TOA's performance is dependent on the accuracy of time synchronization. Up to date, the pure TOA system working at high frequency has achieved accuracy as high as tens of meters such as the LMA (Lightning Mapping Array) system in New Mexico [Thomas et al., 2004]. It is a set of three dimensions lightning source locating system operating at 60~66 MHz. Each sensor has synchronized with a GPS clock. Its locating results' time resolution is 100 microseconds. Locating error especially the source height information would increase with the distance between source and sensor. In addition, as shown in Fig. 1.3, two hyperbolas may have two points of intersection when the lightning source is far from the envelope of TOA stations. Therefore a TOA network needs at least 4 stations to make sure that the position of source is unique.

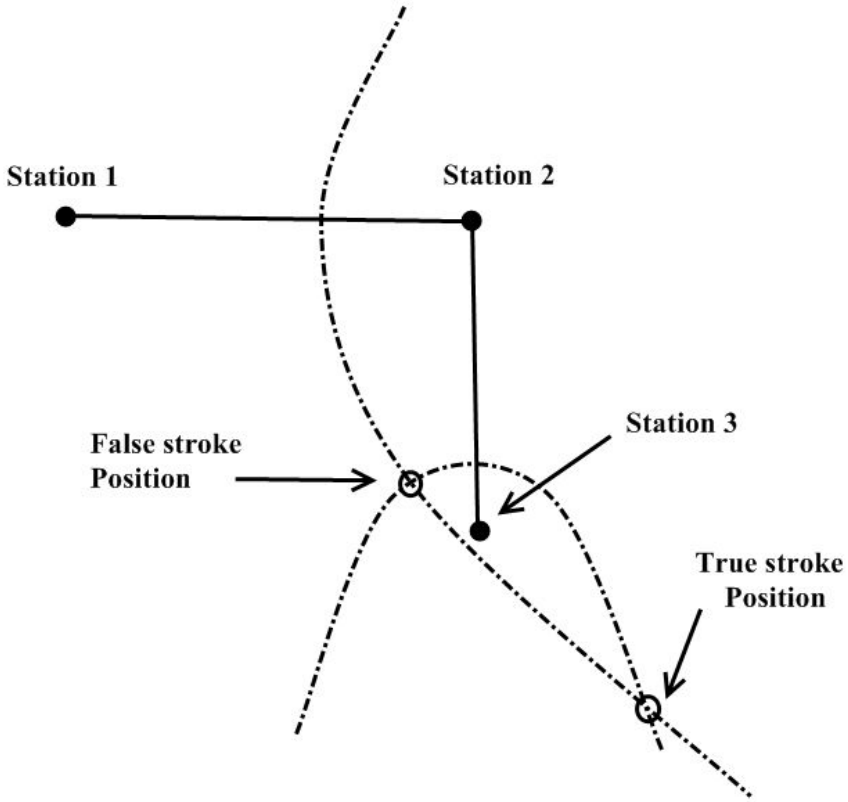

Fig. 1.3 Circumstance of ambiguous stroke positions when the lightning source is far from the envelope of TOA stations. Dotted lines represent hyperbolas determined by time differences

The detection efficiency (DE) of pure TOA systems is unsatisfactory. Another typical TOA lightning locating network is WWLLN (World Wide Lightning Location Network). It was sponsored by University of Washington then normally operating till today through extensive and international cooperation. This system is working at VLF (3-30 kHz) and lightning source position was given by time of group arrival algorithm based on at least five WWLLN sensors synchronized with GPS clock. Its location accuracy is about 10 km. This network's DE for strokes whose peak current is about 30 kA is 30% through world wide. At present this system has 40 sensors spread all over the earth surface and the number is still keeping growing [Website_1, 2013].

In order to gain higher location accuracy and have discrimination between CC and CG, IMPACT (Improved Accuracy Using Combined Technology) system has been developed, where the DF and TOA techniques were combined together [Cummins et al., 1998]. Each detection station in this system records not only lightning source's direction but also its arrival time. Both of the two methods mentioned above contribute to the final results. The National Lightning Detection Network (NLDN) is a typical IMPACT system. From 1989 to 2005, it experienced 9 times upgrade. In this progress, NLDN evolved from pure DF arrays to IMPACT and had national reach [Biagi et al., 2007]. Another merit of the IMPACT is that it has higher DE than that of a pure TOA system since it can detect a lightning signal by as few as two sensors. The DE of the NLDN for a flash has reached 90-95% and stroke DE has reached 60-80% after its 2002-2003 upgrade [Cummins and Murphy, 2009]. Nowadays, the most of LLNs are based on DF/TOA combined technique.

The interferometric technique is based on the fact that phase differences of lightning signal at an antenna array contain the information of the source position, which usually operates at VHF bands between tens and hundreds MHz. In article [Richard and Auffray, 1985] interferometric technique was introduced. Antennae of interferometer system just separated at several meters, so the electromagnetic signal can be viewed as parallel radiation. For a certain frequency, which mainly between tens and hundreds of MHz, the azimuth of source has fixed relevancy with phase differences of those antennae. One set of interferometer gives the azimuth and elevation of the source since the elevation is also a dimension of angle. Two sets of interferometers are able to add on the distance information. Shao has built a set of

narrowband interferometer whose center frequency was 274 MHz and its bandwidth was 6 MHz. It is able to observe cloud to ground lightning in two dimensions with a time resolution of 1 microsecond [Shao et al., 1995].

1.3 Research objective and thesis outline

Lightning's danger and mystery have drawn much attention. People made research on lightning from different spatial scales. Lightning channel's detailed structure can be visualized by detecting its very high frequency radiation. Even when lightning source is 1000 km far away, its very low frequency signal is able to reach the sensor and expose its position. Lightning detection within several hundred kilometers in low frequency range is close to common population and has been studied extensively.

Nowadays the lightning location network (LLN) system in determining the position of lightning source within wide area has already achieved an accuracy of several hundreds of meters, such as the Hong Kong Observatory [Website_2, 2013] and NLDN. However, it still left some spaces to get improved. High accuracy of LLN owes to its TOA portion. The DF portion still has appreciable errors. As long as the DF technique is involved, it is always suffering from the problem of "site error", which leads the detected source azimuth deviating from the true source direction by tens of degrees [Mach et al., 1986].

To contribute to "site error" correction issue, this work mainly aims at following aspects:

1) The properties of “site error” as a function of either the source azimuth or the receiver frequency band are to be investigated and affirmed based on experiments.

- *The results on this aspect are summarized in Chapter 2 and Chapter 3.*

2) A physical or semi-physical model is to be built for theoretical interpretation of the properties of “site error” observed. The model should contain the major factors which caused the site error to a DF. It should be able to explain the experiment phenomenon in both the azimuth and frequency domains.

- *The results on this aspect are summarized in Chapter 4.*

3) Adequate algorithms that can be incorporated into a DF system to identify and correct the “site error” both in post-analysis or real-time for individual lightning strokes are to be explored and verified with experimental data.

- *The results on this aspect are summarized in Chapter 5.*

4) Comparing to a multiple-station LLN, a single station lightning location system is easy to install, does not need precise time synchronization and lower maintenance costs. Therefore, the last objective of this work is to seek a reliable algorithm to derive source-observer distance based on a single-station observation of a lightning stroke in close distance, say within 100 km or some things like that, since this distance range is enough to provide early warning of the hazards for people. The existing DF technique allows recording the electric and magnetic signal of a lightning stroke in broadband simultaneously. Based on electromagnetic wave transmission theories, the source-observer distance may be obtained by a combined analysis between the broadband electric and magnetic fields. A prototypal single-station

lightning location system is to be built based on the proposed algorithm and comparison of individual stroke location with local lightning locating network is made to validate the single-station technique.

- *The results on this aspect are summarized in Chapter 6.*

Chapter 2

“Site error” and its properties in azimuth domain

2.1 Background on “site error” issue

The DF technology uses a pair of vertical and orthogonal magnetic field loops to obtain lightning direction. It includes narrowband DFs and gated wideband DFs. Narrowband DFs have been used to detect distant lightning since 1920s [Horner, 1954]. The narrowband DF generally operates in a narrow frequency band centered at a frequency in the range of 5 to 10 kHz, where the lightning signal is relatively strong [Horner, 1957]. The major disadvantage of narrowband DFs is that they have inherent azimuthal errors of order 10 degree when lightning is relatively close to the DFs [Krider, 1973]. Non-vertical channel sections and "site error" which would be discussed later contribute to the azimuthal errors.

Gated wideband DFs were developed by Krider et al. to overcome the disadvantage mentioned above. One of the major advantages of gated wideband DFs compared to narrowband ones is that they are able to avoid non-vertical channel sections' influence by means of displaying only the initial ground wave portion of the VLF signals. In addition, the gated wideband systems are relatively insensitive to intra-cloud

discharges due to a proper choice of trigger level and sample gate width [Krider et al., 1976]. The gated wideband DF was originally designed to detect only negative ground flashed, and in the late 1980s, this kind of system was modified to accept both negative and positive ground flashes by sensing the polarity of charge lowered by a ground flash.

However, both the narrowband and wideband DFs have the problem of “site error”. The “site error” refers to the azimuthal error caused by unwanted magnetic field components due to effects such as non-horizontal topography near the DF and re-radiation by nearby conducting structures. The “site error” was reported to be as large as 30° for narrowband DF [Horner, 1957], and 10° for wideband one [Mach et al., 1986]. It is believed that the “site error” was caused by DFs' nearby structures, such as buildings, power lines and cables, and by variations in the surrounding terrain. In contrary, the total random error arisen from non-vertical channels, noises of background and DF electronics is usually 1–2° only [Krider et al., 1980].

As mentioned in chapter 1, As long as the DF technique is involved in a LLN, it always suffers from the problem of “site error”. For instance, in a TOA/DF network, lightning strokes detected by 4 or more sensors are usually located by the TOA technique, while those detected by less than 4 sensors are located by DF/TOA mixed approach. Therefore, “site error” corrections are still essential for the use of lightning data of a TOA/DF type LLN.

2.2 Existing methodologies for “site error” corrections

“Site error” is a kind of system error. It is a sum of rotation error during installation and the error cause by surrounding structures. The rotation error is a constant and azimuthal properties of the “site error” are found when people do the “site error” correction. There are two basic approaches for the estimation and correction of the “site error” “nonparametric method” and “parametric method”.

Nonparametric method is subdivided into two categories. One is statistical analysis and calculation and the second is using different instruments such as video camera or radar to correct the “site error” of a DF.

Mach et al. first developed a statistical method by using redundant DF data as reference. If a lightning signal has been detected by at least three DFs, the difference between first DF’s azimuth and the other two DFs’ combined results was recorded. The deviation was viewed as an initial “site error” of the DF at that azimuth. This procedure would be done at other azimuths for this DF. All initial “site errors” at all azimuths of the DF were kept in storage. “Site error” table of second DF was obtained by the same algorithm but the data of first DF had been corrected using its initial “site error” information. When it comes to the third DF, it is able to using other two DFs’ corrected data. This operation was repeated again and again until all the “site error”

versus azimuth curves of three DFs become stable [Mach et al., 1986].

Mach also made comparison between all-azimuth TV results and DF azimuths. “Site error” was plotted in Fig. 2.1 as a function of DF azimuths. It has an odd-cycle variation [Mach et al., 1986].

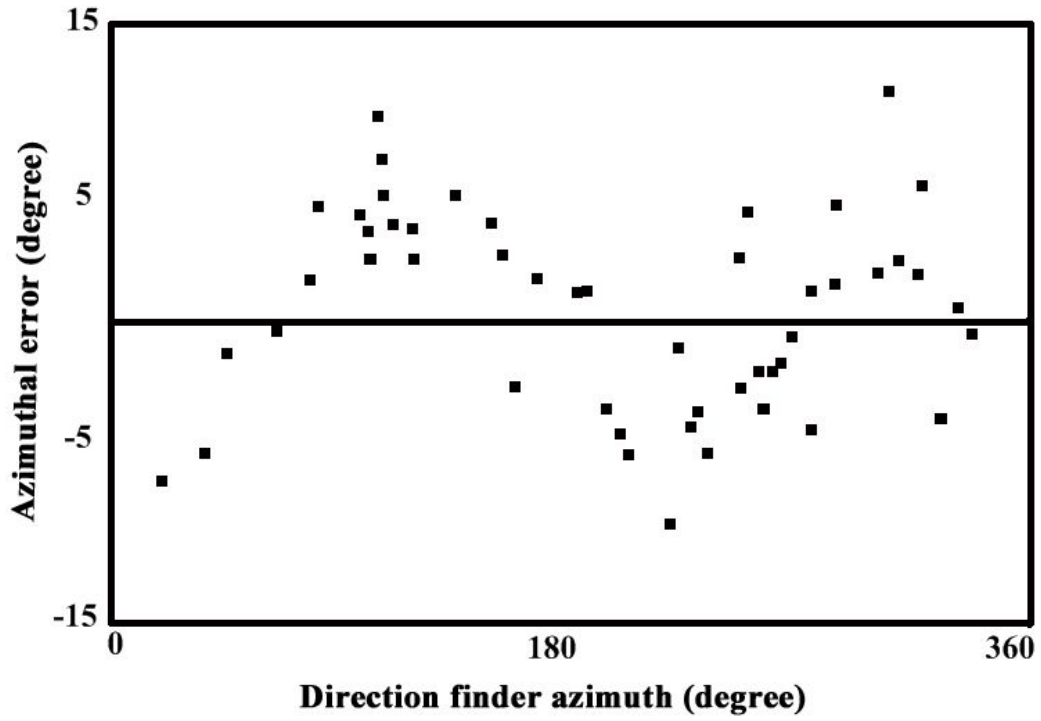

Fig. 2.1 Azimuthal error versus azimuth from DF (re-plotted from Mach et al., 1986). The error is the difference between the all-azimuth TV and his DF azimuth, negative value means anticlockwise displacement of the TV (source direction) to the DF azimuth

Hiscox first tried a parametric method [Hiscox et al., 1984]. “Site error” was

expressed by him in a form of two-cycle sinusoidal function. A weighted sum of square of the difference between optimized lightning azimuth and each DF's detected azimuth was calculated. Then this sum of square or so called variance was processed by a nonlinear least square method so as to find the amplitude and phase of that sinusoidal function. However, those optimized lightning azimuth were determined when the "site error" still existed. So the sin function was not exact "site error" curve.

An improved parametric method depends on an optimization approach using lightning locations detected by at least three DFs in a network. An essential assumption of this method is that "site error" has a form of limited order trigonometric series. It has been changed to a non-linear unconstrained optimization problem with the help of Orville's eigen technique [Orville, 1987]. "Site error" curve was obtained by minimizing the objective function. Parametric method focused on the calculation of parameter and did not need to determine each lightning source's optimal position by iterative optimization solution. So the major advantage of the method is that it is suitable for processing huge amounts of data.

Here are some results presented by Chen in early 1990s in Figs. 2.2, 2.3 and 2.4 using the method mentioned above for a 3-DF network in Beijing area. Each of them represents "site error" versus azimuth pattern of a DF [Chen et al., 1991]. In the same paper, lightning stroke positions were plotted on a figure to make some comparison with radar echoes. Before correction, lightning source position could be far away from

radar echoes as large as tens of kilometers. After correction, all lightning position were covered by radar echoes or got really close to them. So the consistency between The LLN and radar echoes was improved.

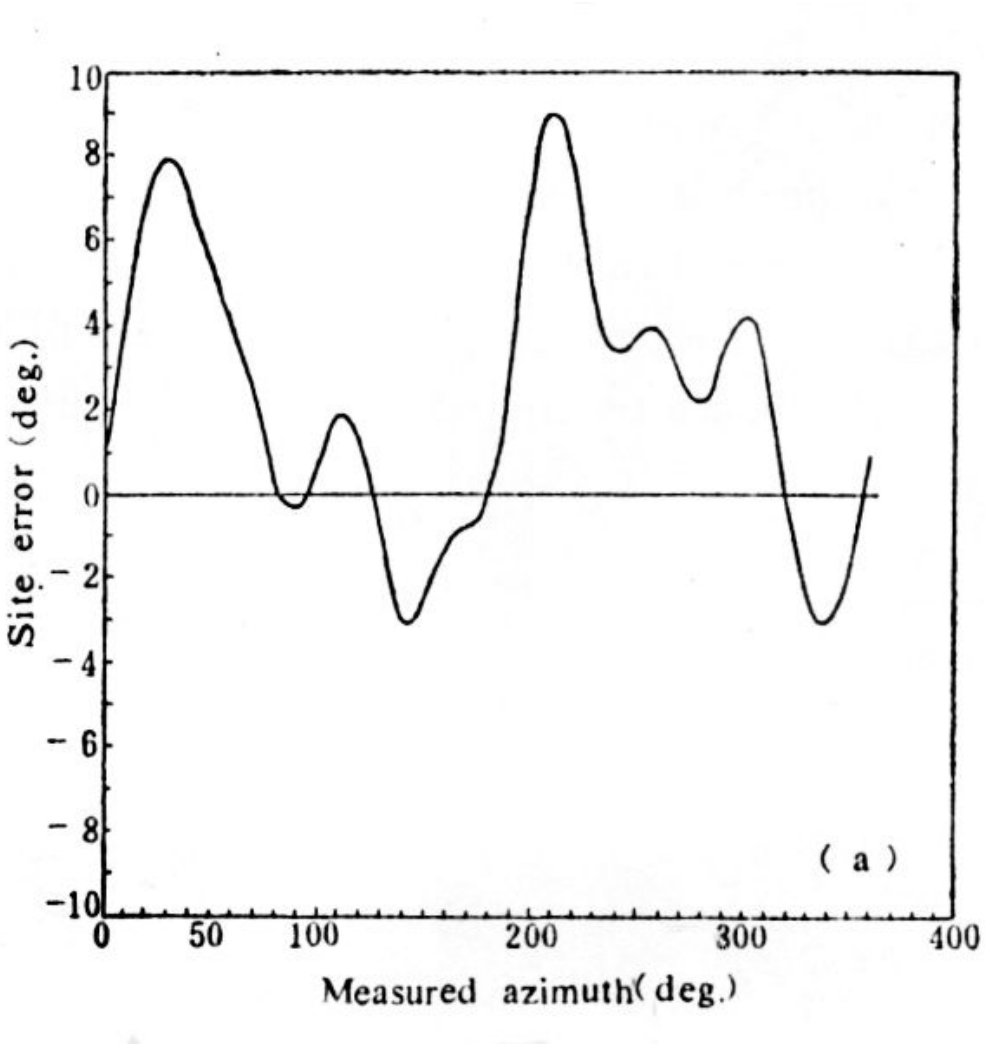

Fig. 2.2 “Site error” of DF1 in a 3-DF network in Beijing (Chen et al., 1991)

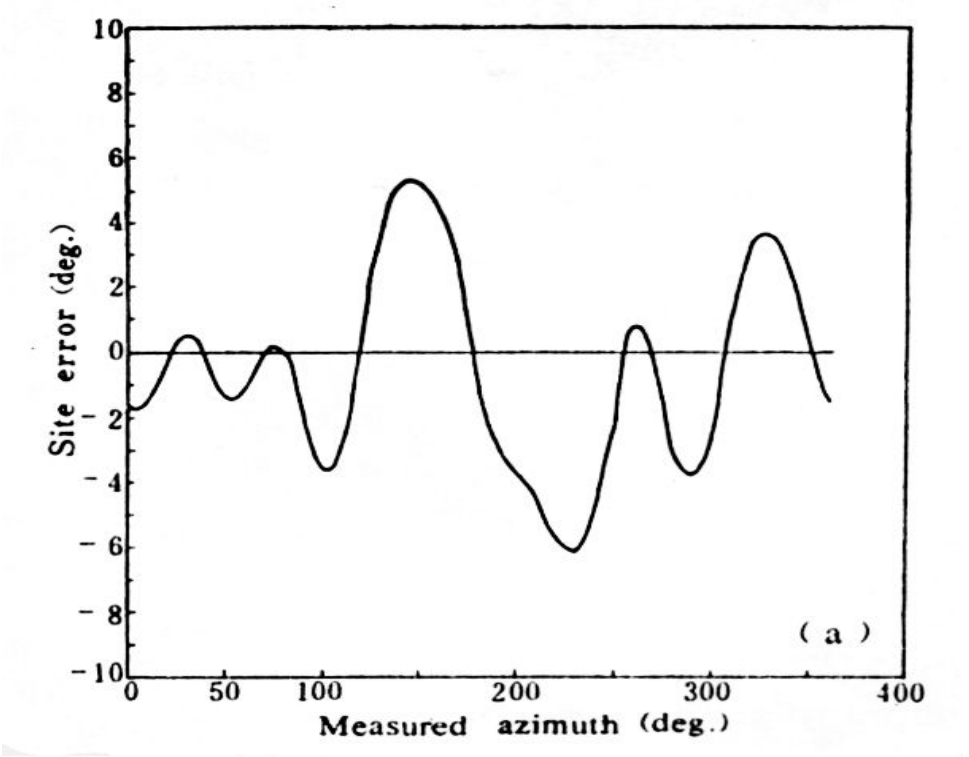

Fig. 2.3 “Site error” of DF2 in a 3-DF network in Beijing (Chen et al., 1991)

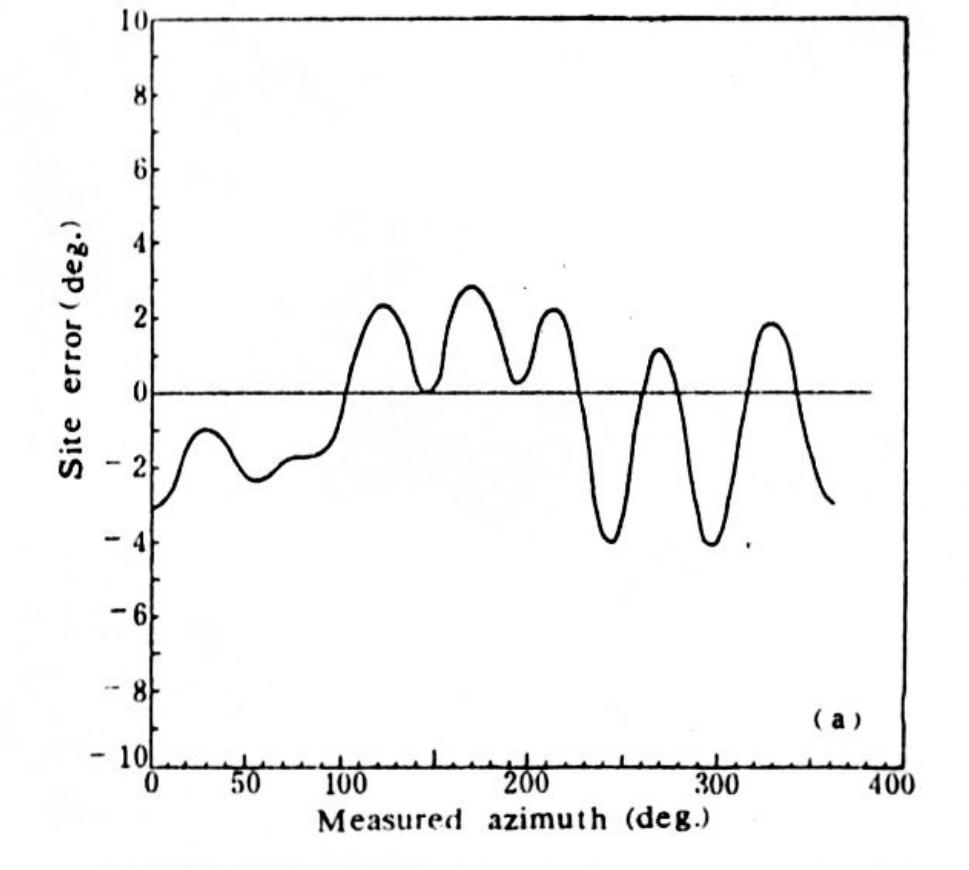

Fig. 2.4 “Site error” of DF3 in a 3-DF network in Beijing (Chen et al., 1991)

2.3 Properties of "site error" versus azimuth

Passi and Lopez represented "site error" in forms of sum of several two-cycle sinusoidal functions [Passi and Lopez, 1989]. This expression was then employed to recovery artificially simulated "site error" from pure direction finder network [Lopez and Passi, 1991]. In their simulation, two-cycle sinusoidal "site error" and random error were coupled into different DFs. "Site error" correction works well when a network has four or more DFs. As shown in Fig. 2.5, DFs in elaborate alignment also does good to "site error" recovery because most location problems occurred close to the cross point of two closest DFs [Stansfield, 1947].

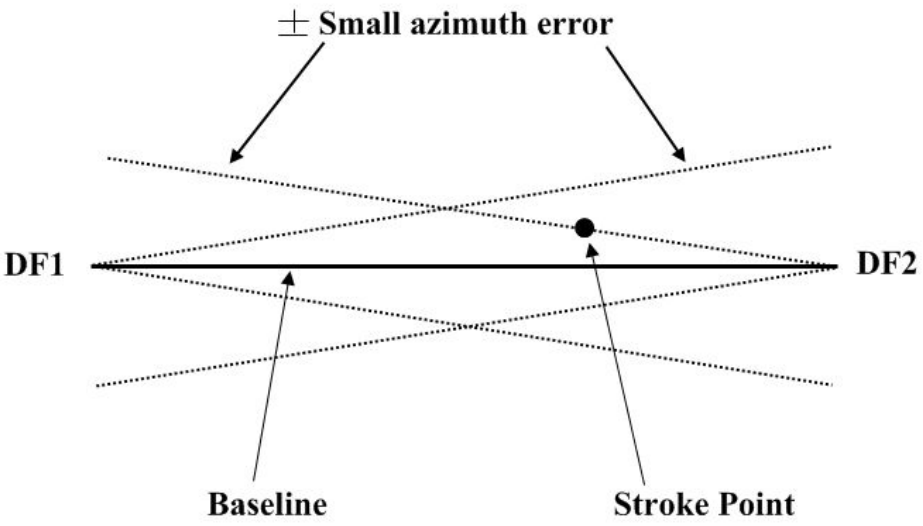

Fig. 2.5 Lightning stroke point near baseline of two sensors has large location error even for small azimuth error

Based on the parametric method, Chen et al. studied the azimuthal characteristic of the “site error” of a wideband 3-DF LLN in China [Chen et al., 1991; Chen et al., 1993]. Figs. 2.6 and 2.7 show the “site error” versus source azimuths for two DFs in the 3-DF LLN, marked as “CPM” and “NMB” respectively. The “CPM” represents the DF sensor at Chang Ping Meteorology station in suburban area of Beijing, where there were relatively less artificial structures nearby the sensor. The “NMB” refers to the DF at National Meteorology Bureau in urban area of Beijing, where there were relatively more artificial structures nearby the sensor. Beside those dual cycles as presented by Lopez [Lopez and Passi, 1991], it was found that the “site error” curves shaped either odd cycles or dual cycles with respect to the source azimuth. A different DF had a different “site error” curve due to a different surrounding environment. However, the “site error” curves for the same DF in two continuous years were very similar, indicating that the “site error” was a constant during a certain time period. It is this property that makes the corrections of the “site error” in real-time feasible and practical.

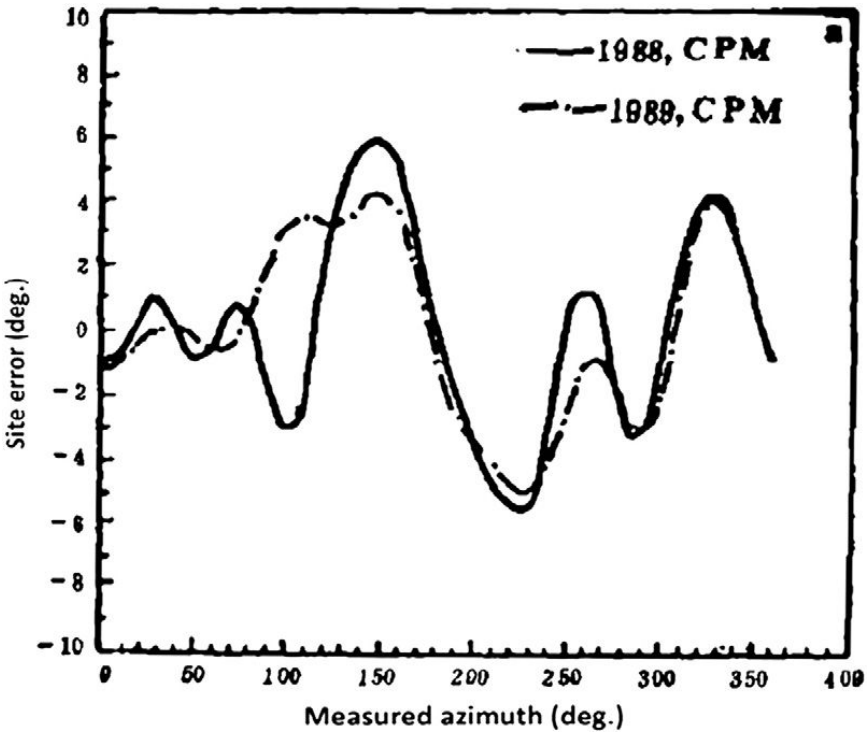

Fig. 2.6 “Site error” versus source azimuth for the “CPM” DF in a 3-DF network for the year 1988 (solid line) and 1989 (dash line)

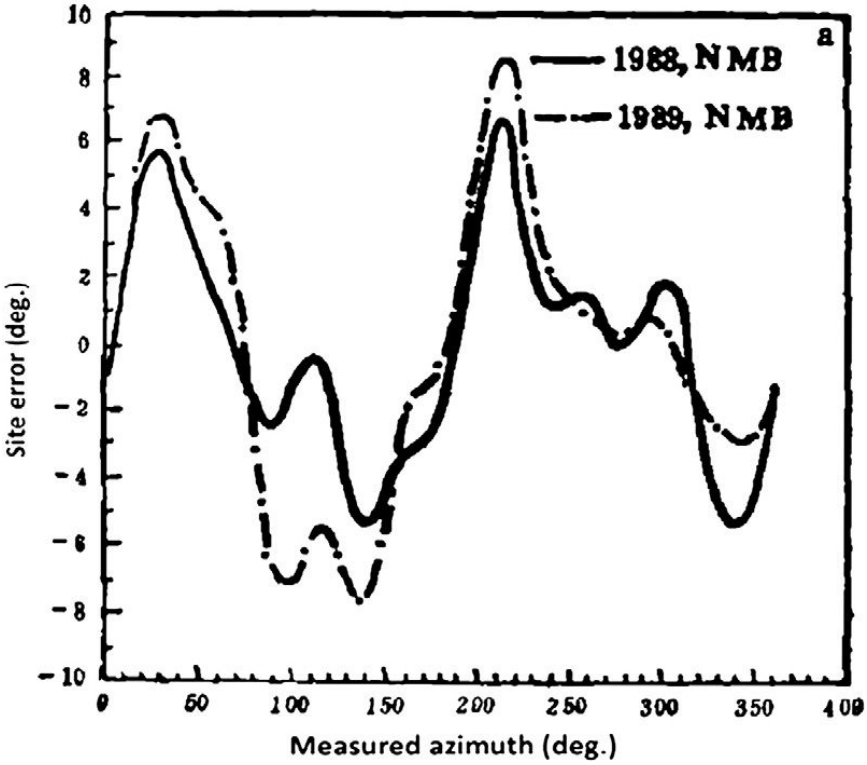

Fig. 2.7 Similar to Fig. 2.6 but for the “NMB” DF in the same network

2.4 Conclusion

In this chapter, the “site error”’ properties in azimuth domain have been reviewed. The “site error” of a DF is inevitable but it fellows certain rules.

“Site error” versus azimuth curve is not just a sum of two-cycle sinusoid function; it also contains odd-cycle trigonometric function components. Two-cycle variation of “site error” is due to magnetic dipole radiation and odd-cycle variation is due to electric dipole radiation. It is noted that those curves characterized by large “site error” contained relatively large amount of two-cycle components.

“Site error” is caused by the conducting structures in the vicinity of a DF which may reflect or scatter incoming electromagnetic field signal such as buildings, power lines, under ground metallic conduit mountain and so on. Noticeable large conducting objects should be avoided when install a DF. In addition, all DFs should be distributed as homogeneous as possible.

Different DFs has different “site error” versus azimuth curves since they are not in a same installation environment. However, one DF’s “site error” variation law has time stability which becomes the basis of “site error” correction. Lightning source locating result would become more close to its actual position after “site error” correction.

Chapter 3

Properties of “site error” in frequency domain

A lightning stroke channel can be viewed as an electric dipole antenna that carries currents with different frequencies, mainly in VLF/LF frequency bands. This simplified model has been used to evaluate the distance of lightning since 1990s [Korol and Nickolaenko, 1993].

When it comes to properties of “site error” in frequency domain, DFs were developed from narrowband to wideband [Krider, 1980]. The shapes and polarities of the lightning-produced electric and magnetic field waveforms are well-preserved due to the wideband of the DFs system, which can then be used for analysis of “site error” in frequency domain.

3.1 Experiments and data

The data used in this study was obtained by using an integrated lightning detector (ILD), which can be used as a broadband DF [Chen et al., 2007]. The ILD included a flat-plate electric field antenna with a bandwidth of 100 Hz to 3.5 MHz and three identical orthogonal magnetic field loops (two in vertical and one in horizontal) with a

bandwidth of 100 Hz to 600 kHz. It also included four light detectors oriented to north, south, east and west respectively for optical direction finding. All the outputs were digitized and recorded on a multiple-channel recorder (8 channels) at a sampling rate of 10 MHz with a recording time up 1 second per channel per event. Data were reprocessed by picking out 8192 data points around the peak value in an interval of every 20 samples. They have covered a time range of 16 ms.

The electric field antenna has a double flat-plate structure with an area of 0.07 square meters. Its working principle has been described by [Krider et al., 1977]. A simplified circuit and antenna to measure electric field of lightning is shown in Fig. 3.1. When plate antenna exposed to the outside electric field E, relevance between the change of electric field E and electric charge Q on antenna can be expressed as:

$$\Delta Q = A_{eff}\varepsilon_0 \Delta E \quad .$$

Where, A_{eff} is the effective area of plate antenna and the permittivity ε_0 is equal to 8.854×10^{-12} F/m.

Output voltage variation and external environment electric field's change have following relations:

$$\Delta V = \frac{\Delta Q}{C} = \frac{A_{eff}\varepsilon_0}{C}\Delta E \quad .$$

Where, C is a total feedback capacitor of the whole circuit.

Sensitivity of the measuring system is influenced by the area of antenna and the value

of capacitor. The integrator decay constant (=RC) can be changed by selecting an appropriate feedback resistor R. The electric field antenna system used in ILD has a RC time of 2 milliseconds and a gain of 91 dB. It was designed to reflect a fast change of the lightning-produced electric field.

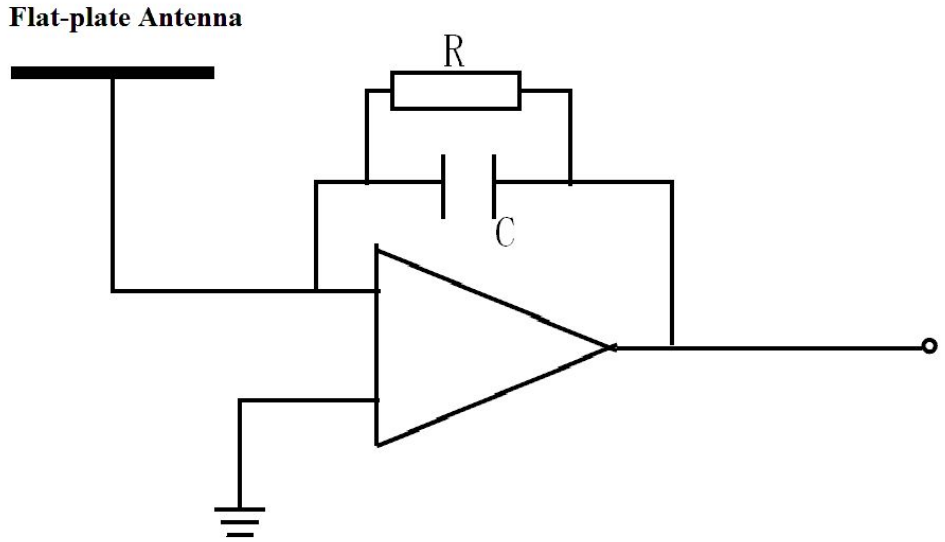

Fig. 3.1 Schematic diagram of the electric field antenna system used in ILD

The loop antenna for lightning-produced magnetic field detection has been firstly introduced by [Krider and Noggle, 1975]. It is mainly consisted of a loop antenna and an integral circuit. Fig 3.2 is a pattern of the loop antenna and its equivalent circuit. According to Faraday's law of electromagnetic induction, when the magnetic flux Φ through the loop varies, induced electromotive force *U(t)* is expressed in the formula below:

$$U(t) = -\frac{d\phi}{dt} = -\frac{dB}{dt} \bullet S ,$$

where, *B* is magnetic field density and *S* is the effective area of the loop antenna.

Since U is equal to the change rate of B, the magnetic field density should be the integral of U. This procedure is realized by an integral circuit. When integrator decay constant (RC) is much larger than U's change cycle, the output voltage U_0 would be proportional to the integral of $U(t)$, i.e. the magnetic field density B.

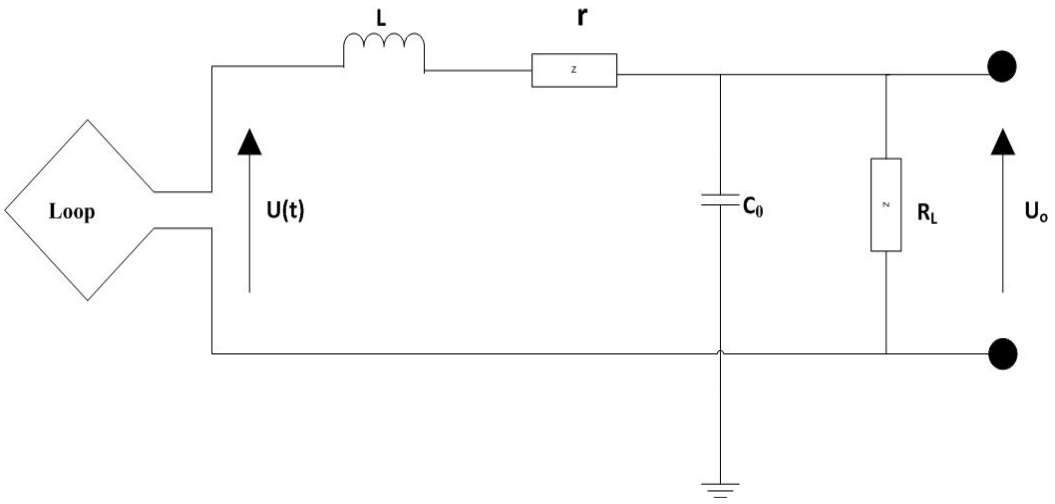

Fig. 3.2 Schematic diagram of the magnetic field antenna used in ILD

The light detectors used in ILD were 4 silicon photo-detectors with a response time of 0.45~0.95 microseconds. They were sensitive to light emission of lightning as far as 80 km, similar to those used by [Guo and Krider, 1983]. They found that average peak radiance of return stroke is from 6×10^5 W/m to 1×10^6 W/m.

The data file format was in wvf. A Matlab script program was developed to draw out those data. The Matlab script program developed was able to recognize the CG flash and find out the position of peak value of the electromagnetic field. For a given return stroke event, 2047 points before the peak value and 6144 points after the peak value were picked out in each channel, i.e, a total number of 8192 data points were picked

out, which is integer power of 2. These points were picked out with an interval of 20. As a result, the 8192 data points covered a time range of 16 ms, since the original data sample rate was 10 Mega Samples/s. The 8192 data points covering a time range of 16 ms is equivalent to a data filter rate of 500500 Samples/s.

Shown in Figure 3.3 are the optical and electromagnetic signals of one negative return stroke observed by the ILD.

It was found that the light signals had significant delay in time when compare to the electric and magnetic signals, as seen in Fig. 3.3. This could be explained with the idea by [Chen et al., 1990]. They inferred that current propagation front along the channel is characterized by the initial front of channel electron avalanche, whose propagation speed is more or less 1/3 of the speed of light in average. Since the light signal was emitted from the heated channel behind the current front and the electric signal was caused by the current, it is reasonable that light signals have a delay.

In general, the source direction (azimuth) is defined as an angle clockwise from the north. Electric fields are used to distinguish between negative and positive strokes. For a negative stroke, the magnetic field output of east–west loop is proportional to the sine of source azimuth and that of north–south loop is proportional to the cosine of source azimuth. A positive stroke only needs to add 180° to the result as for a negative one. For the stroke in Fig. 3.3, the ratio of peak amplitude of the magnetic field in

east–west loop and that in north–south loop gave a result of 167.2° in azimuth. In calculation of the azimuth, at least five data points around the peak of the magnetic field waveform were picked out and their mean value was used as the peak amplitude to eliminate random errors due to data readings.

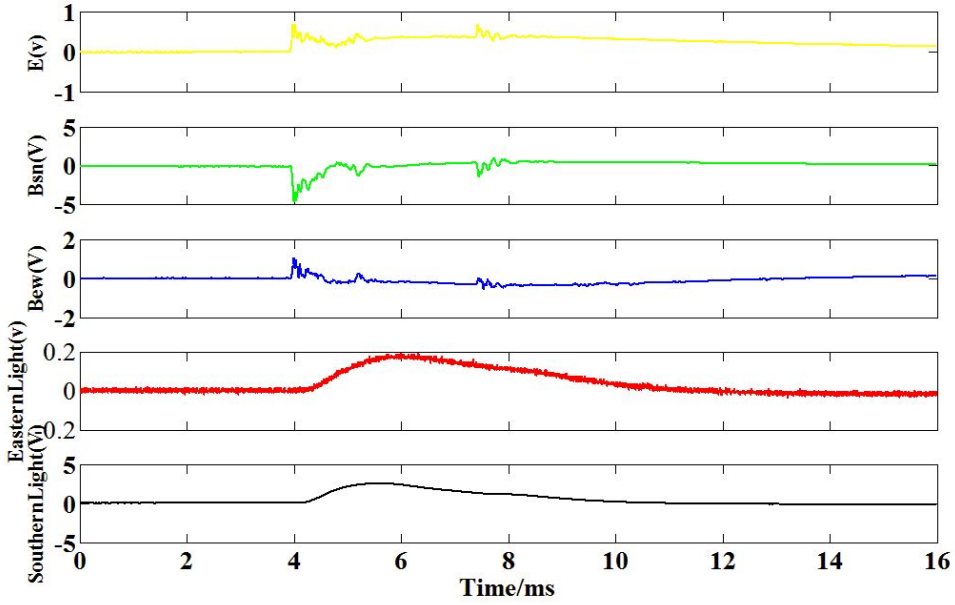

Fig. 3.3 Optical and electromagnetic signals observed by the ILD for a negative return stroke occurred at 19:19:02, 12 Aug., 2005. Upper to down: electric field (*E*), magnetic field in south-north loop (*Bsn*) and that in east-west loop (*Bew*), and light signal from the east and that from the south, respectively. Units are arbitrary

3.2 Properties of "site error" versus frequency

A DF operating at different frequency bands may introduce different "site error". A wideband DF is proved to be better than a narrowband one [Mach et al., 1986], but it is still subject to large "site error". To investigate how the "site error" varies with the

frequency, Fast Fourier Transformation (FFT) was performed for the outputs of north–south and east–west magnetic loops of the ILD. Only those frequencies fewer than 250 kHz have been displayed here due to lower sample rate at 500500 Hz when filter the data. The source azimuth versus the frequency was then obtained based on the ratios of the spectra of the magnetic signals in the two vertical loops (frequency domain analysis).

Shown in Fig. 3.4 is the result of source azimuth versus frequency, obtained by frequency domain analysis, for the same return stroke in Fig. 3.3. It is noted that the source azimuth varies significantly with the frequency, characterized by some sharp mono-polar and bi-polar pulses superposed on a relative flat curve. The range of variation of the azimuth is from 146° to 177°, with a mean value of 167.2°, the same as that determined by the peak amplitude of the magnetic field waveforms in time domain.

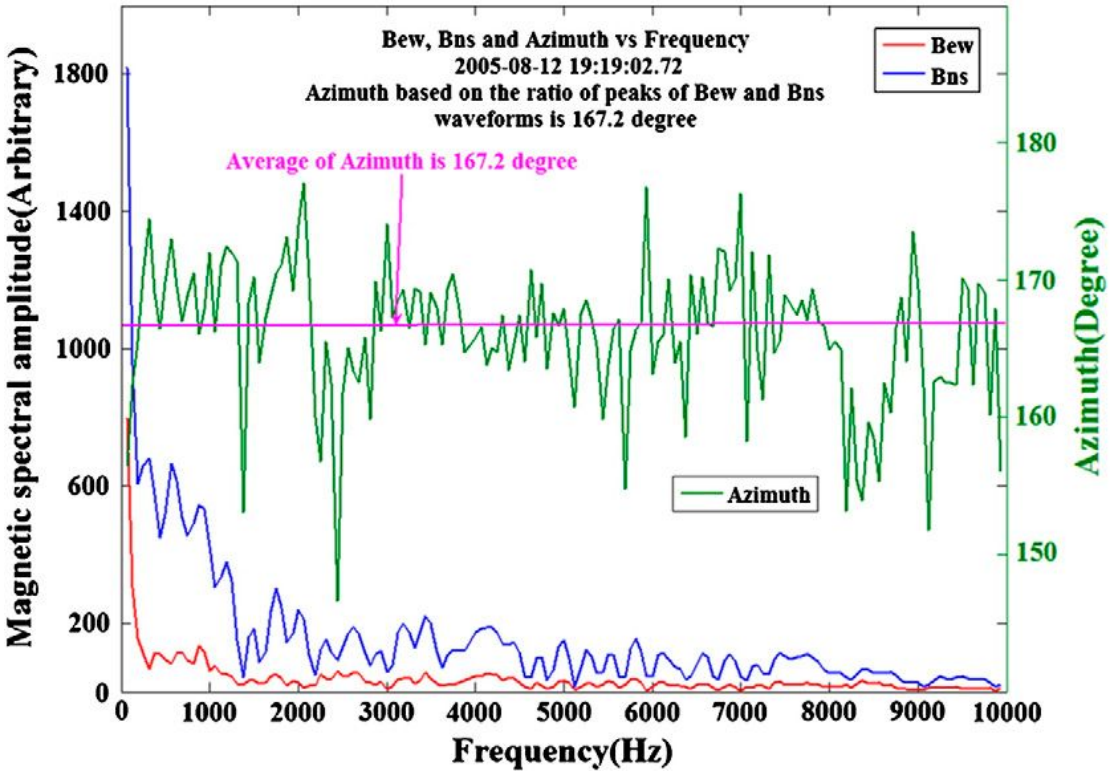

Fig. 3.4 The source azimuths versus frequencies based on ratios of spectra of *Bew* and *Bns*, with a mean azimuth of 167.2°, for the same stroke shown in Fig. 3.3. The azimuth based on the ratio of peaks of *Bew* and *Bns* waveforms is 167.2°

As shown in Chapter 2, the "site error" of a DF will not vary so much against the time if the surrounding structures will not change. Deduced from this property of the "site error", there should be some features in common in the result of source azimuth versus frequency among different lightning strokes detected by the same DF. To find out these common features, more lightning strokes are analyzed and some of the results are given in Figs. 3.5, 3.6 and 3.7 respectively. It is noted that there are always some bipolar pulses that appeared around the 2 kHz, 4 kHz, 6 kHz and 9 kHz in these figures but with different amplitude. According to the model presented later in chapter 4, a bipolar pulse around a certain frequency is linked to a magnetic-dipole-like

structure nearby the DF site. As long as this magnetic-dipole-like structure keeps no change, the source azimuth versus frequency for different lightning stroke will show a bipolar variation around the same frequency linked to that structure but with different amplitude. If the angle between the lightning source azimuth and the normal of a magnetic dipole gets very small, the influence of this magnetic dipole will be very small. That is why some bipolar pulses get small and some get large in these figures.

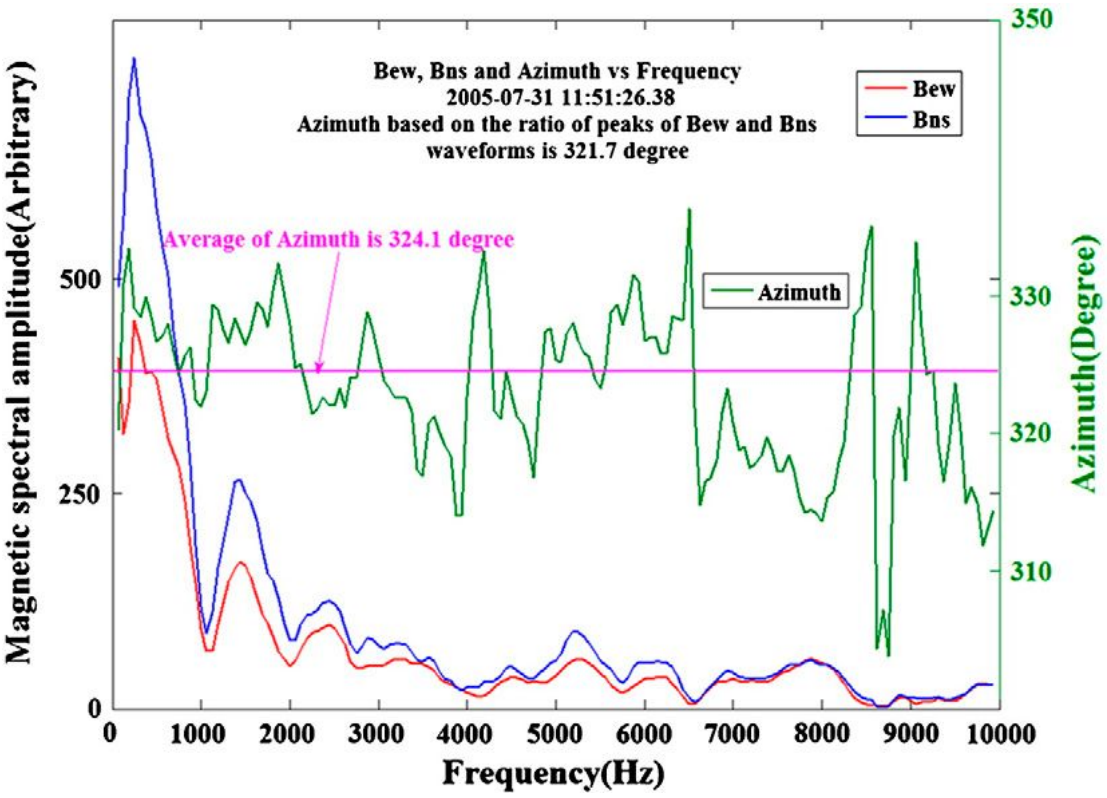

Fig. 3.5 Similar to Fig. 3.4 but for a lightning stroke at 11:51:26.38 on 31 July, 2005. The mean azimuth is 324.1°, while the azimuth based on the ratio of peaks of *Bew* and *Bns* waveforms is 321.7°

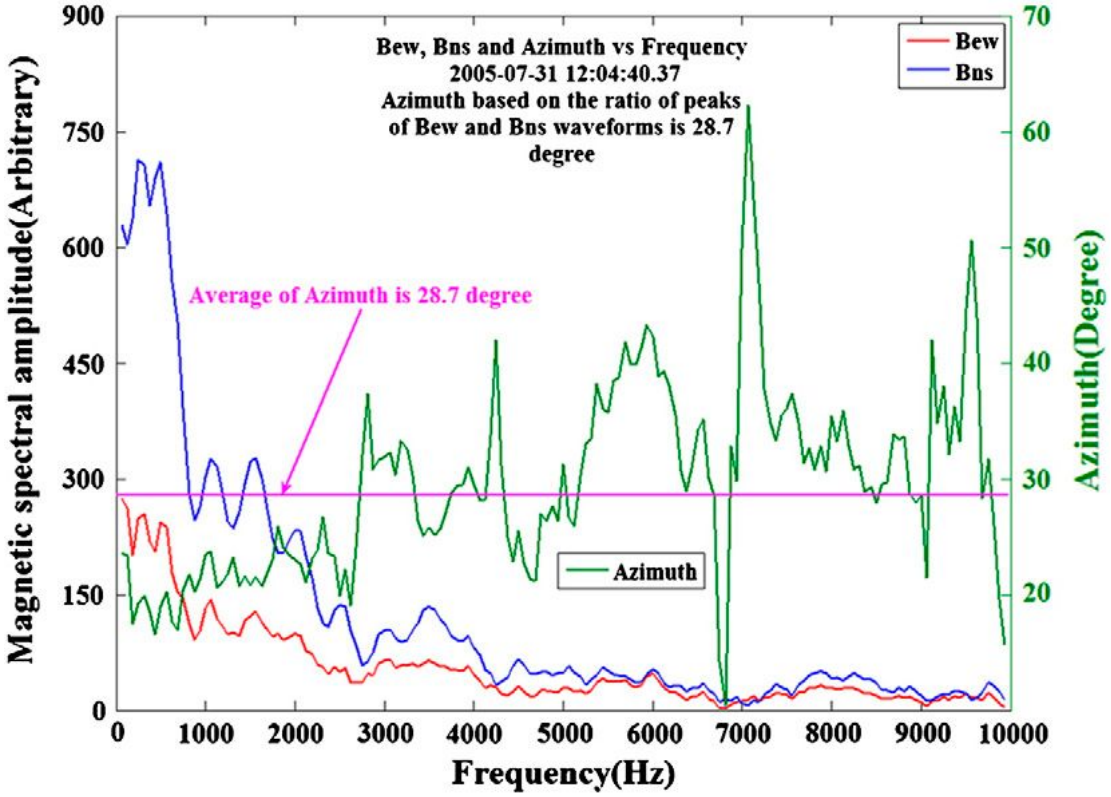

Fig. 3.6 Similar to Fig. 3.4 but for a lightning stroke at 12:04:40.37 on 31 July, 2005. The mean azimuth is 28.7°, while the azimuth based on the ratio of peaks of *Bew* and *Bns* waveforms is the same

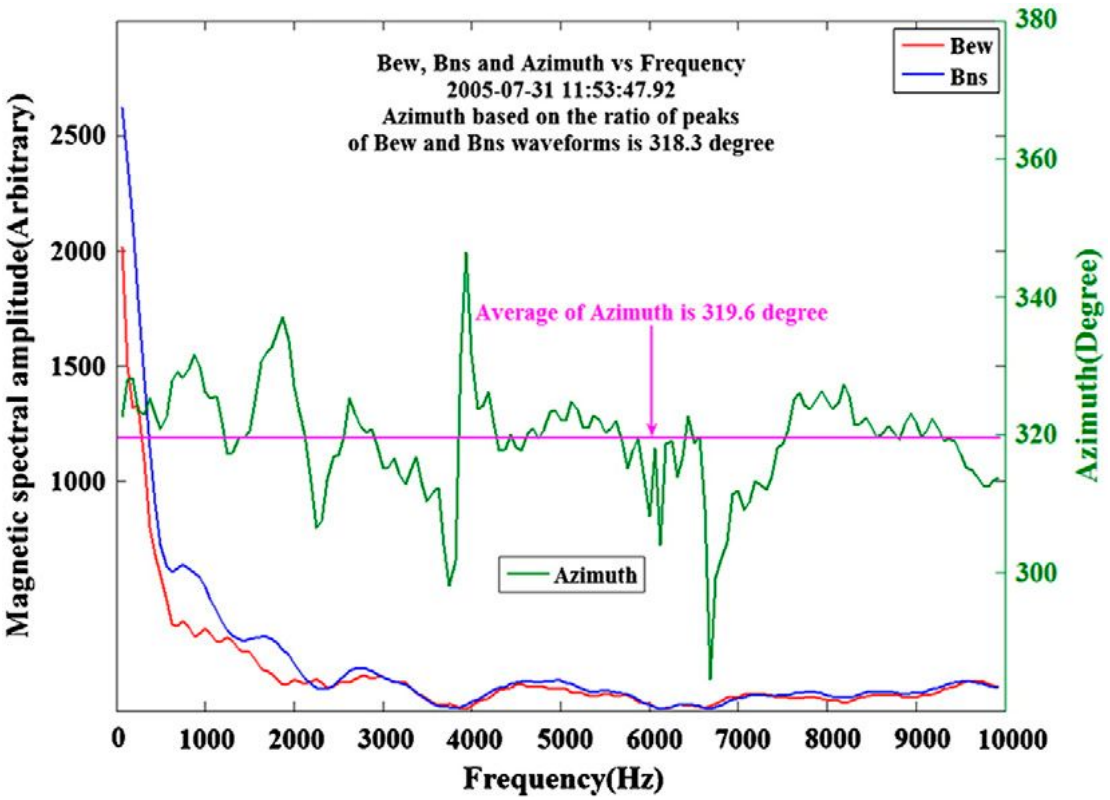

Fig. 3.7 Similar to Fig. 3.4 but for a lightning stroke occurred at 11:53:47.92 on 31 July of 2005. The mean azimuth is 319.6°, while the azimuth based on the ratio of peaks of *Bew* and *Bns* waveforms is 318.3°

3.3 Conclusion

The lightning-produced electric and magnetic fields recorded by ILD (a broadband DF system) in bands of 100 Hz to 250 kHz were analyzed to examine the dependency of estimated lightning source direction on the lightning signal frequency. Attentions were mainly paid on the magnetic direction finder technique. Besides the peak values of the magnetic fields from the two orthogonal vertical magnetic loop antenna, the

amplitude of these magnetic fields in frequency domain were also calculated and analyzed. It was found that the azimuths determined at different frequency were not the same. The source azimuth for a given lightning stroke appeared as a function of frequency with small mono-polar and large bi-polar impulses superposed on a relative flat curve.

Chapter 4

Interpretation and modeling of “site error” properties

Chen presented a simple electromagnetic dipole model for “site error” due to dipole radiations nearby a DF. This model could well explain the azimuth properties of “site error” [Chen et al., 1993]. The “site error” has odd cycles and dual cycles with respect to the source azimuth. In order to interpret the “site error” properties in frequency domain which have been described in Chapter 3, an improved electromagnetic dipole model has been proposed.

4.1 Models description

It is believed that the “site error” is due to reflections and re-excitations of incident lightning signals by structures and terrain elevations surrounding the DF site. These nearby structures can be decomposed into different electric and magnetic dipoles since the wavelengths we are interested in are much larger than their sizes.

For a lightning stroke with a magnetic field density of B (in tesla), let $B\sin\theta$ and $B\cos\theta$ present its incident magnetic signal density at a DF's east–west and north–south loops respectively, θ (in degree) represents its true azimuth to the DF's north, and *Bew*

and *Bns* represent its disturbed magnetic signal density received on the DF's east–west and north–south loops respectively.

For a magnetic dipole (i.e., a vertical loop-wise conductive object that is faced to a direction at angle β to north and is located at a close distance r (in meter) to a DF at azimuth φ, with an effective loop area s (in square meter), an equivalent resistance R (in ohm), a capacity C (in farad) and an inductance L (in henry)), it can be excited by the lightning magnetic field B and emits additional magnetic field ΔB to the DF.

As illustrated in Fig. 4.1, according to Faraday's Law and Ohm's Law, the current I (in ampere) on the magnetic dipole excited by the lightning stroke magnetic signal B at a frequency ω (in radian per second) can be expressed as:

$$I = \frac{jsB\omega \sin(\theta - \beta)}{R + j(\omega L - 1/\omega C)} \tag{4.1}$$

According to magnetic dipole (ring current) radiation theory (Fig. 4.1), the additional magnetic fields emitted by the magnetic dipole to the DF at the azimuth φ, in radial and angular directions respectively, are:

$$H_r = \frac{2Is}{4\pi}\left(\frac{1}{r^3} + j\frac{k}{r^2}\right)\cos\alpha e^{-jkr} \tag{4.2}$$

$$H_\alpha = \frac{Is}{4\pi}\left(\frac{1}{r^3} + j\frac{k}{r^2} - \frac{k^2}{r}\right)\sin\alpha e^{-jkr} \tag{4.3}$$

where, k is the wave number, $\alpha = (\beta - \varphi)$ is the normal angle of the magnetic dipole respected to the DF, and r is the radial distance from the dipole to the DF. Here is the derivation of equation 4.2 and 4.3. the electric field in radial and angular directions respectively, are:

$$E_r = \frac{2Idlk^3 \cos\theta}{4\pi\omega\varepsilon}\left(\frac{1}{k^2 r^2} - \frac{1}{(kr)^3}\right)e^{-jkr} \qquad (4.2.1)$$

$$E_\theta = \frac{Idlk^3 \sin\theta}{4\pi\omega\varepsilon}\left(\frac{j}{kr} + \frac{1}{(kr)^2} - \frac{j}{(kr)^3}\right)e^{-jkr} \qquad (4.3.1)$$

According to the duality of Maxwell equation, magnetic source equation could come from electric source equation. $E \to H$, $\varepsilon \to \mu$, $\mu \to \varepsilon$, $J \to J_m$, here $I_m dl = \mu j\omega Is$, with all these relationship, equation (4.2.1), (4.3.1) become equation (4.2) and (4.3). Because θ represents the original lightning source in this thesis, it was replaced by α to denote the angular direction.

Suppose there are several magnetic dipoles distributed around the DF, then the total additional magnetic fields emitted by those magnetic dipoles to the DF, in east–west ($\Delta B_{EW\text{-}M}$) and north–south ($\Delta B_{NS\text{-}M}$) loops respectively, are:

$$\begin{aligned}\Delta B_{EW-M} &= -\mu_0 \sum_i \cos\varphi_i \frac{2I_i s_i}{4\pi}\left(\frac{1}{r^3} + j\frac{k}{r^2}\right)\cos(\beta_i - \varphi_i) \\ &-\mu_0 \sum_i \sin\varphi_i \frac{I_i s_i}{4\pi}\left(\frac{1}{r^3} + j\frac{k}{r^2} - \frac{k^2}{r}\right)\sin(\beta_i - \varphi_i)\end{aligned} \qquad (4.4)$$

$$\Delta B_{NS-M} = \mu_0 \sum_i \sin\varphi_i \frac{2I_i s_i}{4\pi}\left(\frac{1}{r^3} + j\frac{k}{r^2}\right)\cos(\beta_i - \varphi_i)$$
$$-\mu_0 \sum_i \cos\varphi_i \frac{I_i s_i}{4\pi}\left(\frac{1}{r^3} + j\frac{k}{r^2} - \frac{k^2}{r}\right)\sin(\beta_i - \varphi_i) \qquad (4.5)$$

where subscript "*i*" stands for the *i*th magnetic dipole and μ_0 is the free space permeability.

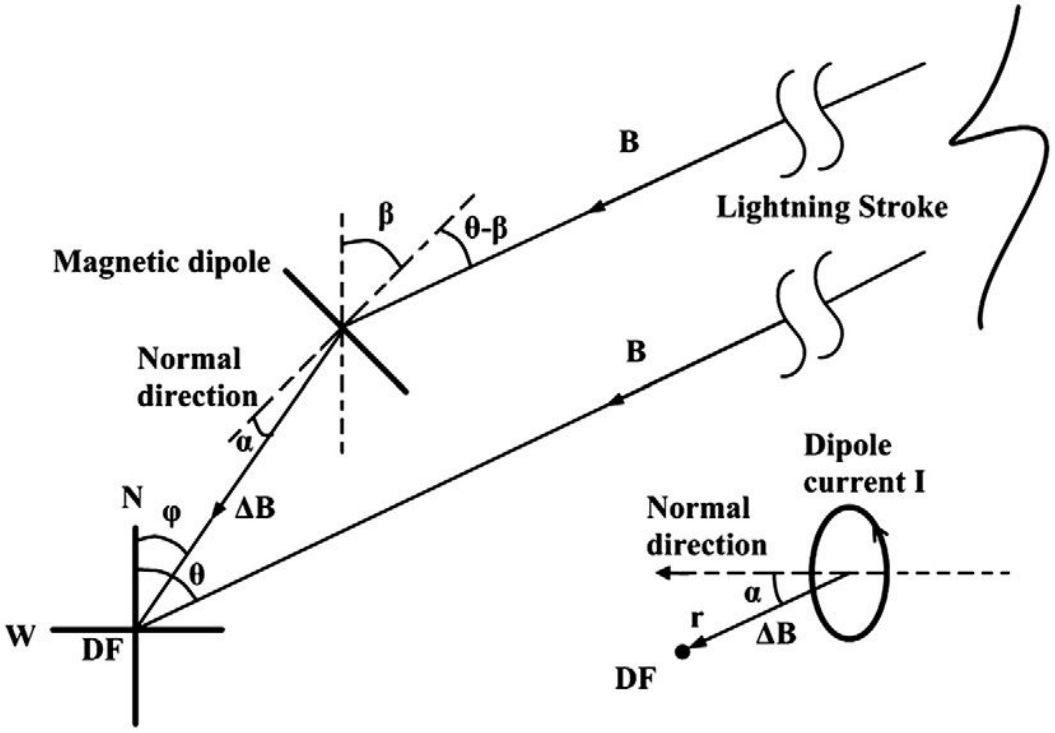

Fig. 4.1 Illustrations of a magnetic dipole excited by lightning magnetic field *B* and emission of extra magnetic field *ΔB* to a nearby DF

For an electrical dipole (i.e., a vertical pole-wise conductive object located at a close distance *r'* to the DF at azimuth η with an effective length *l* and an equivalent resistance *R'*, a capacity *C'* and an inductance *L'*), it can be excited by the lightning vertical electric field *E* (in volt per meter) and emits additional magnetic field *ΔB* to

the DF.

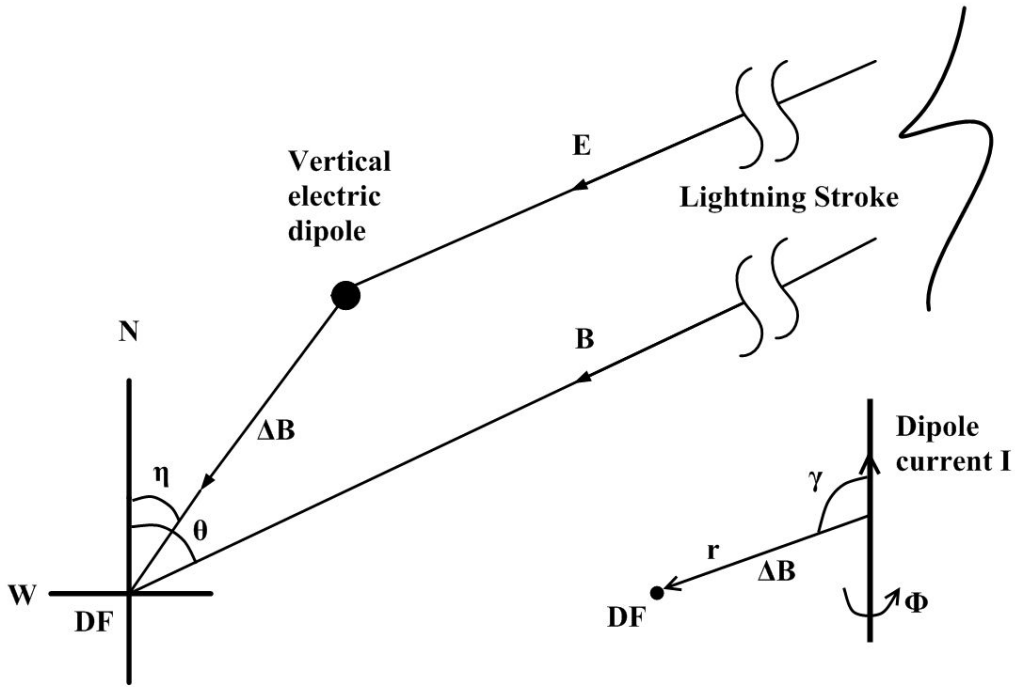

Fig. 4.2 Illustrations of a vertical electric dipole excited by lightning vertical electric field *E* and emission of extra magnetic field *ΔB* to a nearby DF

As illustrated in Fig. 4.2, for a lightning stroke with a magnetic field density of *B* (which is set to 1 Tesla afterward for simplicity), the current excited by its vertical electric field *E* on the electric dipole is given by

$$I = \frac{cBl}{R' + j(\omega L' - 1/\omega C')} \qquad (4.6)$$

where *c* (in meter per second) is the speed of light and *E*=*cB*. This is a simplified approach. The impedance in denominator of equation 4.6 including all those coupled

capacitances and inductances with earth.

According to electric dipole radiation theory (Fig. 4.2), the additional magnetic field generated by the electric dipole to the DF at the azimuth η, in angular direction, is:

$$H_{\phi} = \frac{Il}{4\pi}(\frac{1}{r^2} + j\frac{k}{r})\sin\gamma e^{-jkr} \qquad (4.7)$$

where, γ is the direction angle of the electrical dipole referred to the DF (which is assumed to be 90°) and r is the distance from the electric dipole to the DF. Suppose there are several electric dipoles distributed around the DF, then the total additional magnetic fields emitted by these electric dipoles to the DF, in east–west ($\Delta B_{EW\text{-}E}$) and north–south ($\Delta B_{NS\text{-}E}$) loops respectively, are:

$$\Delta B_{EW-E} = \sum_i \frac{\mu_0 c l_i^2}{4\pi} \times (\frac{1}{r^2} + j\frac{k}{r}) \times (\frac{1}{R_i^{'} + j(\omega L_i^{'} - 1/\omega C_i^{'})})\sin\eta_i \qquad (4.8)$$

$$\Delta B_{NS-E} = \sum_i \frac{\mu_0 c l_i^2}{4\pi} \times (\frac{1}{r^2} + j\frac{k}{r}) \times (\frac{1}{R_i^{'} + j(\omega L_i^{'} - 1/\omega C_i^{'})})\cos\eta_i \qquad (4.9)$$

where subscript "*i*" stands for the *i*th electric dipole.

Taking account that these dipoles are very close to the DF, their radiation components (i.e., the term*1/r*) and phase-shifts (i.e., the term *jkr*) can be ignored. Then, the total

magnetic fields received at the two loops of the DF at frequency ω are:

$$B_{EW} = \sin\theta + \Delta B_{EW-M} + \Delta B_{EW-E}$$

$$B_{EW} = \sin\theta - \mu_0 \sum_i \frac{2s_i^2}{4\pi} \cos\varphi_i \cos(\beta_i - \varphi_i) \sin(\theta - \beta_i) \times \frac{j\omega}{r^3} \times \left(\frac{1}{R_i + j(\omega L_i - 1/\omega C_i)}\right)$$

$$-\mu_0 \sum_i \frac{s_i^2}{4\pi} \sin\varphi_i \sin(\beta_i - \varphi_i) \sin(\theta - \beta_i) \times \frac{j\omega}{r^3} \times \left(\frac{1}{R_i + j(\omega L_i - 1/\omega C_i)}\right)$$

$$+\mu_0 \sum_i \frac{cl_i^2}{4\pi} \sin\eta_i \times \frac{1}{r^2} \times \left(\frac{1}{R_i^{'} + j(\omega L_i^{'} - 1/\omega C_i^{'})}\right) \qquad (4.10)$$

and

$$B_{NS} = \cos\theta + \Delta B_{NS-M} + \Delta B_{NS-E}$$

$$B_{NS} = \cos\theta + \mu_0 \sum_i \frac{2s_i^2}{4\pi} \sin\varphi_i \cos(\beta_i - \varphi_i) \sin(\theta - \beta_i) \times \frac{j\omega}{r^3} \times \left(\frac{1}{R_i + j(\omega L_i - 1/\omega C_i)}\right)$$

$$-\mu_0 \sum_i \frac{s_i^2}{4\pi} \cos\varphi_i \sin(\beta_i - \varphi_i) \sin(\theta - \beta_i) \times \frac{j\omega}{r^3} \times \left(\frac{1}{R_i + j(\omega L_i - 1/\omega C_i)}\right)$$

$$+\mu_0 \sum_i \frac{cl_i^2}{4\pi} \cos\eta_i \times \frac{1}{r^2} \times \left(\frac{1}{R_i^{'} + j(\omega L_i^{'} - 1/\omega C_i^{'})}\right) \qquad (4.11)$$

where, $sin\theta$ and $cos\theta$ are the original incident lightning magnetic fields in the east–west and north–south loops respectively. The source azimuth with "site error" is then given by,

$$\tan(\theta + \delta\theta) = B_{EW} / B_{NS} \qquad (4.12)$$

In practice, conducting objects that may form magnetic loops themselves or with the ground can be viewed as magnetic dipoles to a DF. Those objects include overhead lines, fences, buried cables, and buildings with steel frames. Conducting objects such as trees, various communication antenna and vertical poles are typical electric dipoles to a DF. Depending on surrounding environments, the slopes of ground near a DF may have the effects of both electric and magnetic dipoles.

4.2 Modeling results – frequency domain

With presumed parameters for electric and magnetic dipoles, variations of source azimuth with errors versus frequency can be simulated by Eqs. (4.10) to (4.12).

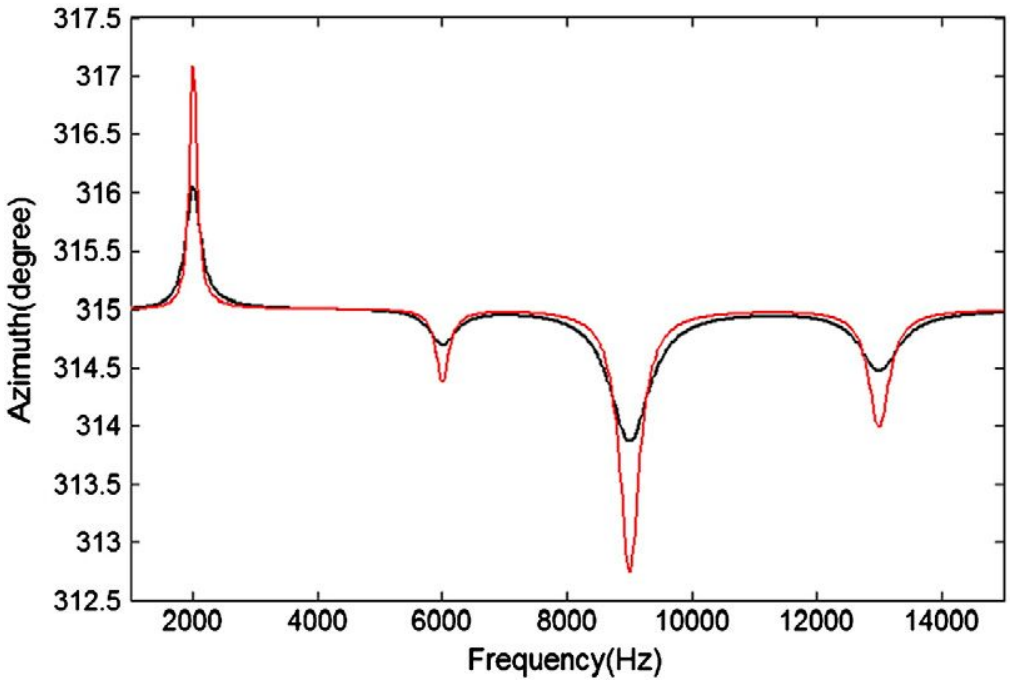

Fig. 4.3 Azimuth/“site error” versus frequency simulated with 4 presumed electric

dipoles nearby a DF for a source azimuth of 315°. Red line (larger amplitude) is for dipoles with smaller resistances and black line (smaller amplitude) is for dipoles with larger resistances

Shown in Fig. 4.3 is a simulation result with an assumed lightning source azimuth of 315° and 4 presumed electric dipoles located at close distance and at the north, east, south and west directions to the DF respectively. By choosing different *R'*, *C'* and *L'*, the resonant frequency of the four electric dipoles is set to 2, 6, 9 and 13 kHz respectively. Their parameters are shown in the Table 4.1. The result shows that an electric-dipole-wise structure may add a mono-polar impulsive "site error" to the true source azimuth, as shown in the figure. The amplitude, polarity and resonant frequency of the mono-polar impulse depend on the physical and electric parameters of the corresponding structure.

Table 4.1 Parameters of four electric dipoles

Electric dipole parameters	First	Second	Third	Fourth
Distance to DF (meter)	50m	50m	50m	50m
Resistance (ohm)	2 1	4 2	6 3	8 4
Inductance (H)	1/90	1/800	1/800	1/600
Capacitance (F)	1/(1.75e5)	1/(1.77e6)	1/(3.99e6)	1/(1.11e7)
Length (meter)	5.77	8.16	10	11.55
Azimuth to DF (radian)	π/8	5*π/6	1.3*π	1.6*π

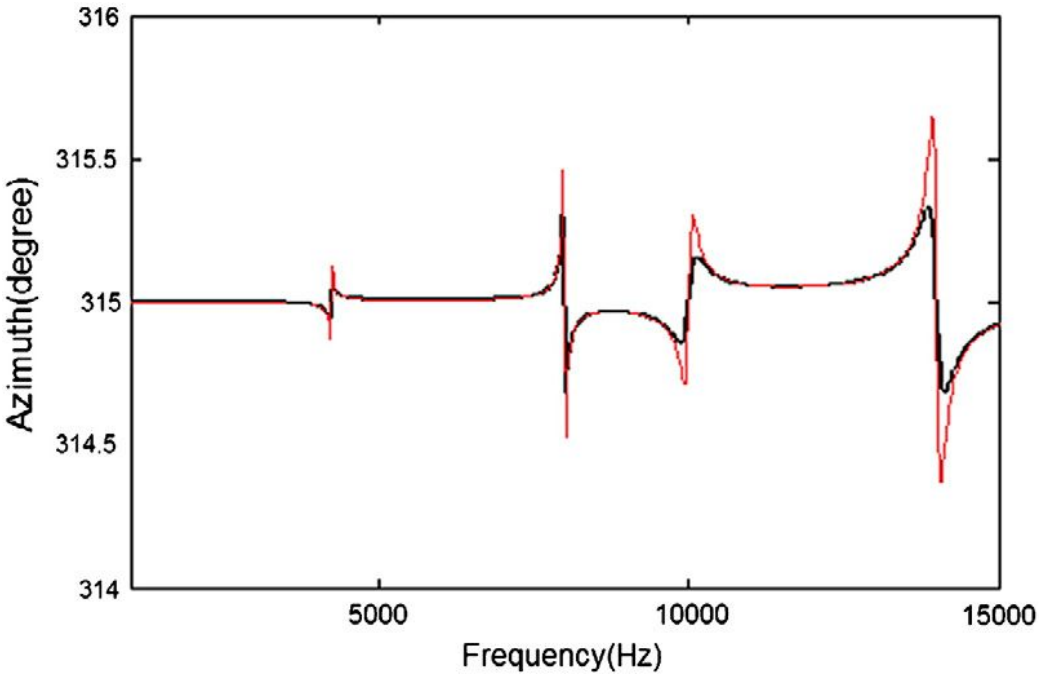

Fig. 4.4 Azimuth/"site error" versus frequency simulated with 4 presumed magnetic dipoles nearby a DF for a source azimuth of 315°. Red line (larger amplitude) is for dipoles with smaller resistances and black line (smaller amplitude) is for dipoles with larger resistances

Shown in Fig. 4.4 is a simulation result with an assumed source azimuth of 315° but with 4 presumed magnetic dipoles located at close distance and at north, east, south and west directions to the DF respectively. The resonant frequency of the four magnetic dipoles is set to 4, 8, 10 and 14 kHz respectively, by setting different values for *R*, *C* and *L*. Their parameters are shown in Table 4.2. The result shows that a magnetic-dipole-wise structure may cause a bi-polar impulsive "site error" to the true source azimuth, as shown in the figure. The amplitude and resonant frequency of the bi-polar impulse are determined by the position and electric parameters of the structure.

Table 4.2 Parameters of four magnetic dipoles

Magnetic dipole parameters	First	Second	Third	Fourth
Distance to DF (meter)	50	50	50	50
Resistance (ohm)	0.4 0.2	0.4 0.2	1.8 0.9	1.8 0.9
Inductance (H)	1/800	1/700	1/900	1/900
Capacitance (F)	1.12e-6	2.77e-7	2.28e-7	1.16e-7
Radius (meter)	8.43	10.03	11.09	11.92
Azimuth to DF (radian)	π/6	2*π/3	1.1*π	1.6*π
Face direction (radian)	1	1	1	1

Shown in Fig. 4.5 is the simulation result for the source azimuth of 315° but with the 4 presumed electric dipoles as in Fig. 4.3 in combination with the 4 presumed

magnetic dipoles as in Fig. 4.4. Those mono-polar changes are due to electric dipoles and those bi-polar ones are due to magnetic dipoles. The result can well explain the features of "site error" in frequency domain shown in Figs. 3.4, 3.5, 3.6 and 3.7. Meanwhile, the small mono-polar and large bi-polar pulses in Figs. 3.4, 3.5, 3.6 and 3.7 may mean that the magnetic dipole re-radiation dominated the "site error" of the ILD. In addition, if there are only two or three dipoles, the mono-polar or bi-polar pulses would become two or three respectively.

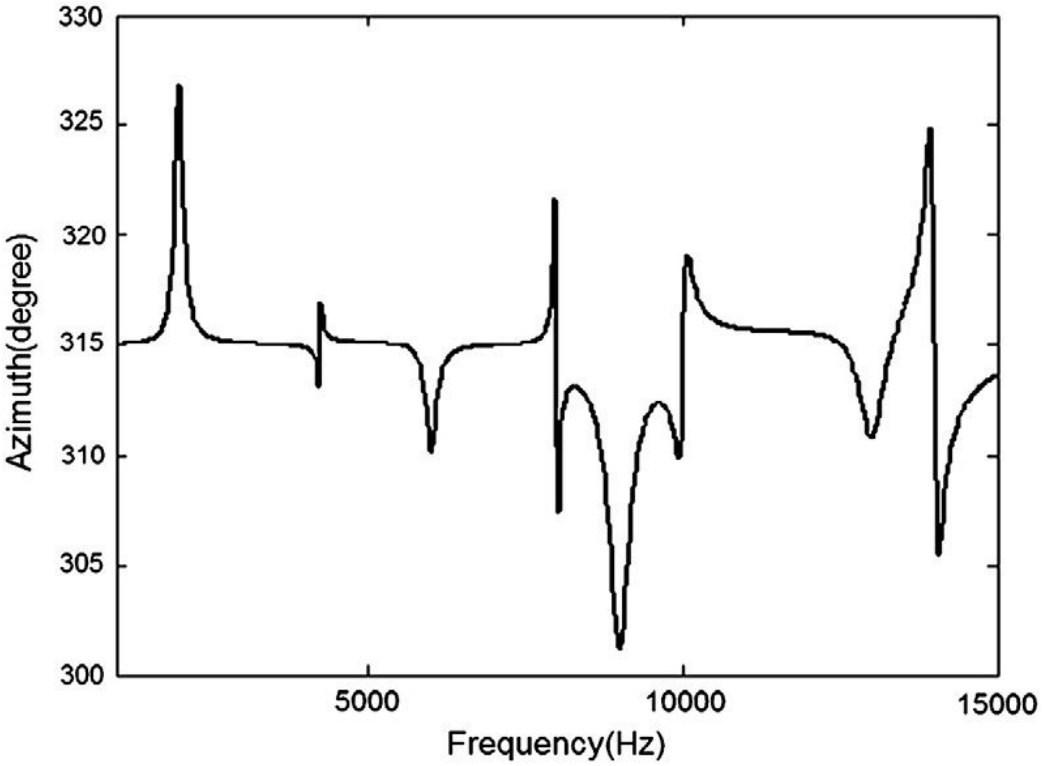

Fig. 4.5 Azimuth/"site error" versus frequency simulated with presumed 4 electric dipoles and 4 magnetic dipoles for a source azimuth of 315°

4.3 Modeling results – azimuthal domain

Eqs. (4.10), (4.11) and (4.12) can be used to simulate the feature of "site error"

against source azimuth as well. For a given electric dipole and a given magnetic dipole at a given frequency, Eqs. (4.10) and (4.11) can be simplified as,

$$B_{EW} = \sin\theta + A_1 \sin(\theta - \beta) + D_1 \qquad (4.13)$$

$$B_{NS} = \cos\theta + A_2 \sin(\theta - \beta) + D_2 \qquad (4.14)$$

where, A_1 and A_2 are two coefficients related to a magnetic dipole, and D_1 and D_2 are two coefficients related to an electric dipole. All of them are supposed theoretically to be smaller than 1 with no units. The incident magnetic field B is set to 1 Tesla for simplicity.

For an electric dipole, taking account of that the D_1 and D_2 as well as the "site error" are a small value, Eqs. (4.12), (4.13) and (4.14) together give,

$$\sin(\delta\theta) \approx D_1 \cos\theta - D_2 \sin\theta - \frac{(D_1^2 - D_2^2)}{2} \sin(2\theta) - D_1 D_2 \cos(2\theta) \qquad (4.15)$$

in the right of Eq. (4.15), the first two terms are much larger than the last two terms because D_1 and D_2 are much smaller than 1. The "site error" will appear as a function of the source azimuth in a sinusoidal waveform with a dominant period of 360°. Fig.4.6 is a simulation result with Eq. (4.15) for an electric dipole with $D_1 = 0.1$ and $D_2 = 0.2$. In case that both D_1 and D_2 are larger say 0.5, Eq. (4.15) may also produce significant component with a period of 180° in the "site error" curve.

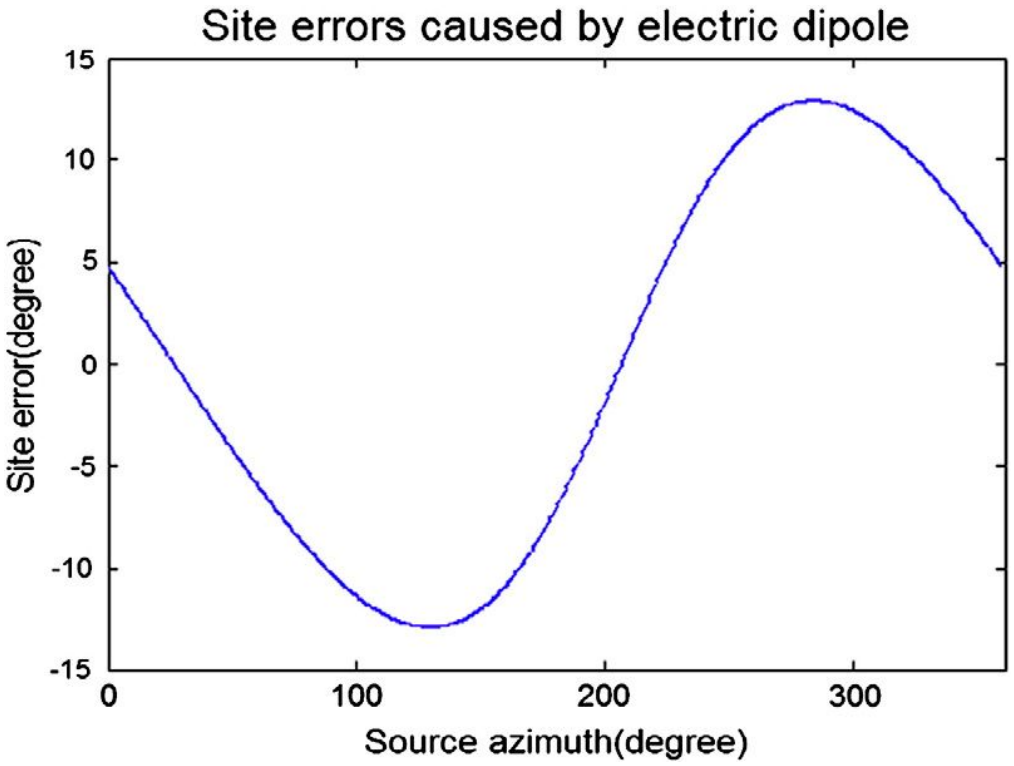

Fig. 4.6 Simulated "site error" versus source azimuth for an electric dipole with Eq. (4.15)

Similarly, for a magnetic dipole Eqs. (4.12), (4.13) and (4.14) give,

$$\sin(\delta\theta) = A_1 \cos\theta \sin(\theta-\beta) - A_2 \sin\theta \sin(\theta-\beta)$$

$$-\frac{A_1^2 - A_2^2}{2}\sin(2\theta)\sin^2(\theta-\beta) - A_1 A_2 \sin^2(\theta-\beta)\cos(2\theta) \qquad (4.16)$$

in the right of Eq. (4.16), the first two terms are dominant. The "site error" will appear as a function of source azimuth in a sinusoidal waveform with a dominant period of 180°. Fig. 4.7 is a simulation result with Eq. (4.16) for a magnetic dipole with β=20°,

$A_1 = 0.1$ and $A_2 = 0.02$. When both A_1 and A_2 are relatively larger, Eq. (4.16) may also yield significant component with a period of 45° in the "site error" curve.

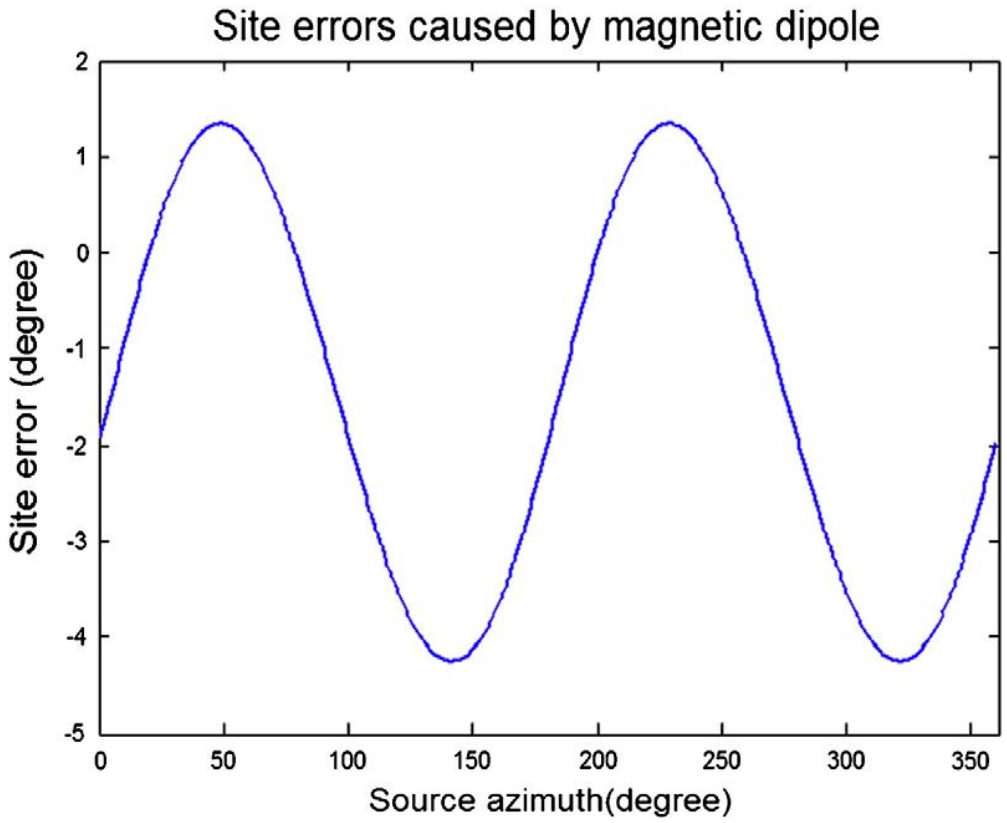

Fig. 4.7 Simulated "site error" versus source azimuth for a magnetic dipole with Eq. (4.16)

As shown in Figs. 4.6 and 4.7, the one-cycle changes of the "site error" are due to electric dipoles while the dual-cycle changes are due to the magnetic dipoles. These results can well explain the observed results shown in Figs. 2.6 and 2.7 in Chapter 2. Meanwhile, dominant dual-cycle sinusoidal structure of Figs. 2.6 and 2.7 may mean that the magnetic dipole re-radiation is the main factor causing the "site error" for these DFs.

4.4 Optimal approaches for “site error” corrections

In Chapter 2, possible approaches for site error estimations and corrections for a multi-station LLN were listed and discussed. It shows that the “site error” as a function of the source azimuth for individual sensors can be found based on appropriate statistics of historical lightning data of the LLN concerned [Chen et al., 1991]. As long as a DF's site environment has no changes, its “site error” will keep no changes. Therefore, the “site error” obtained by using historical data may be used for future “site error” corrections. However such approaches are not real-time ones and are not applicable to a stand-along DF.

In Chapter 3, the property of “site error” in the frequency domain was investigated based on lightning magnetic fields recorded by a single DF (the ILD). It shows that the source azimuth for a given lightning stroke appears as a function of frequency with small mono-polar and large bi-polar impulses superposed on a relative flat curve. Besides, theoretical modeling of the “site error” shows that the large bi-polar impulse is due to DF's nearby magnetic-loop - like conducting objects, while the small mono-polar impulse is due to DF's nearby electric-pole-like conducting objects.

Based on all above analyses, following three measures are proposed which can minimize the “site error” in real-time, especially for a stand along DF:

a) It is better to design a DF with broad bandwidth, say 100 Hz to 200 kHz as the ILD. Many existing DFs operate only at a bandwidth of 1 kHz to 30 kHz.

b) If possible, the optimal source azimuth should be determined by averaging the azimuths in frequency domain in a broad frequency range, especially when the magnetic dipole is the main cause for the "site error". Such an averaging process can significantly mitigate the bi-polar impulse type errors. Further more, suppose there are no electric and magnetic dipoles around the observer antenna, i.e. "site error" does not exist, the azimuth versus frequency would be a straight horizontal line. The horizontal line also means a direct DC signal from another point of view. Mono-polar and bipolar superpose on this straight line can be viewed as non-DC signals. A typical low-pass wave filter is able to erase these high frequency components easily. In fact only the DC component of that signal sequence is needed. According to the definition of Discrete Fourier Transform, DC component of a signal sequence is just the mean value of these data [Chen, 2008].

c) In case that the electric dipole contributes a lot to the "site error", the above averaging process cannot eliminate the mono-polar impulse type errors. In such a case, the optimal source azimuth may be obtained by curve fitting typical mono-polar or bi-polar impulses appearing in the source azimuth curve in frequency domain with the model in Chapter 4.1.

As a first example, we take the ILD and the lightning stroke in Figs. 3.3 and 3.4 to demonstrate how the above three measures can help to minimize the "site error" for a stand along DF. The source azimuth based on the ratio of optical signals in the photo-detectors of the ILD for the stroke is 168.8° (light: South/East=2.55/0.50333, in Fig. 3.3), which can be seen as the "true" azimuth. The source azimuth based on the ratio of magnetic field peaks in time domain (in broadband) in the two loops of the ILD for the stroke is 167.2°, which is very close to the 168.8°. This indicates that the ILD as a DF with a broad bandwidth (100 Hz to 200 kHz) may give the source azimuth with high accuracy. On the other hand, when the source azimuth versus frequency is examined (Fig. 3.4), it varies from 146 to 177°. This indicates that any DF operating at a narrow frequency band may introduce significant "site error". However, when the average of the source azimuths in frequency domain in Fig. 3.4 is taken, it gives a value of 167.2°, which is again very close to the 168.8°. This indicates that averaging process of the azimuths in frequency domain for a DF may give the source azimuth with high accuracy. Furthermore, the source azimuth may be obtained by curving fitting of the source azimuths in frequency domain with the electromagnetic dipole model in Chapter 4.1, especially when the electric dipole dominates the "site error". Fig. 4.8 shows a curve fitting of three typical mono-polar impulses in frequency range from 9.5 kHz to 12.5 kHz of Fig. 3.4. With 3 presumed electric dipoles, the model fitting gives a source azimuth of 167.4°, which is much closer to the 168.8°.

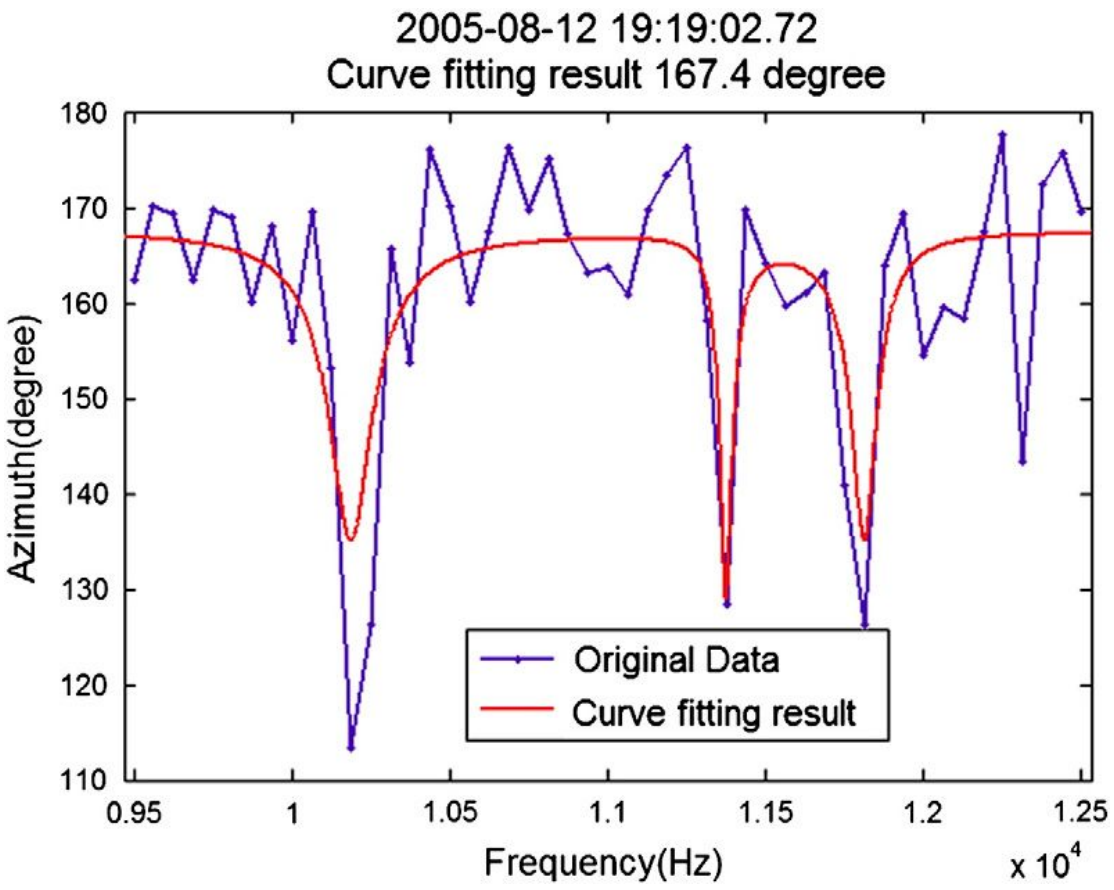

Fig. 4.8 Model fitting of the azimuth curve in Fig. 3.4 in the frequency range of 9.5 to 12.5 kHz with 3 presumed electric dipoles

Here is a second example. A lightning return stroke event occurred at 19:20:49.93 on 12 Aug., 2005. Its optical and electromagnetic signals observed by the ILD are shown in Fig. 4.9. The source azimuth based on the ratio of optical signals in the photo-detectors of the ILD for the stroke is 158.9° (light: South/East=3.67/1.41, in Fig.4.9). The source azimuth based on the ratio of magnetic field peaks in time domain (in broadband) in the two loops of the ILD for the stroke is 160°. When the source azimuth versus frequency is examined (Fig. 4.10), it varies from 136 to 175°. Fig. 4.11 shows a curve fitting of two typical mono-polar impulses in frequency range

from 5 kHz to 6 kHz. With 2 presumed electric dipoles, the model fitting gives a source azimuth of 160.3°.

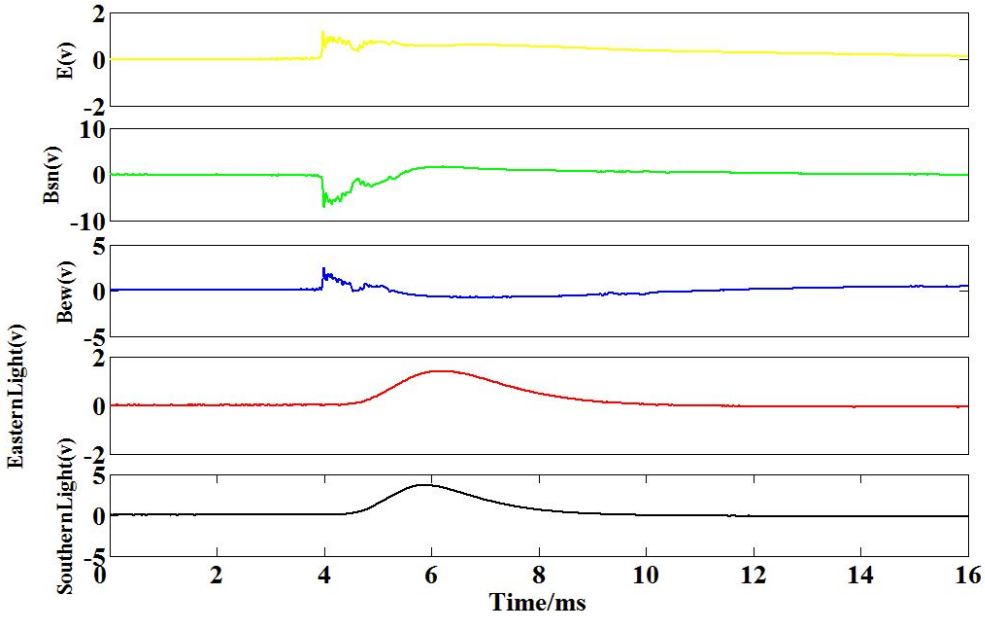

Fig. 4.9 Optical and electromagnetic signals observed by the ILD for a negative return stroke occurred at 19:20:49, 12 Aug., 2005. Upper to down: electric field (*E*), magnetic field in south–north loop (*Bsn*) and that in east–west loop (*Bew*), and light signal from the east and that from the south, respectively. Units are arbitrary

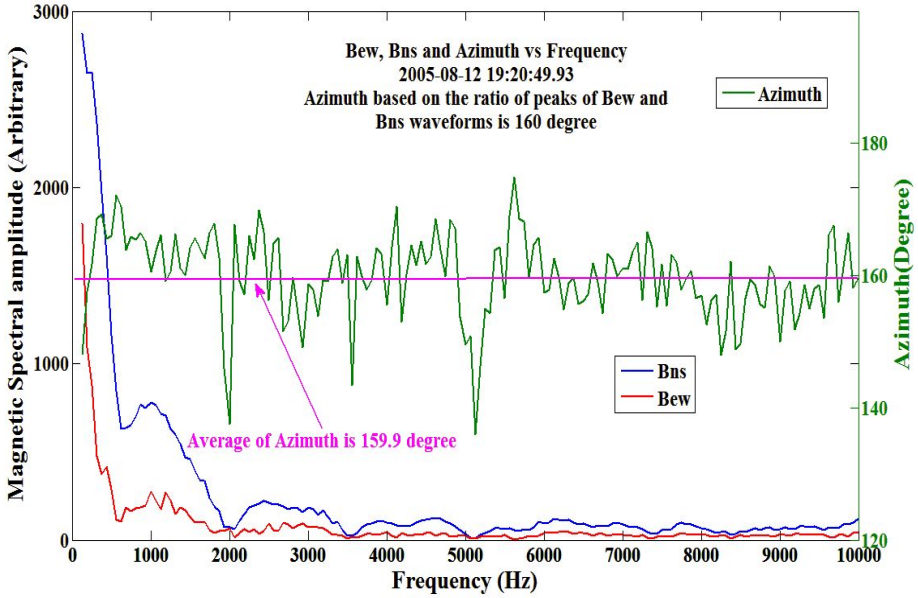

Fig. 4.10 Source azimuths versus frequencies based on ratios of spectra of *Bew* and *Bns*, with a mean azimuth of 159.9°, for the same stroke shown in Fig. 4.9. The azimuth based on the ratio of peaks of *Bew* and *Bns* waveforms is 160°

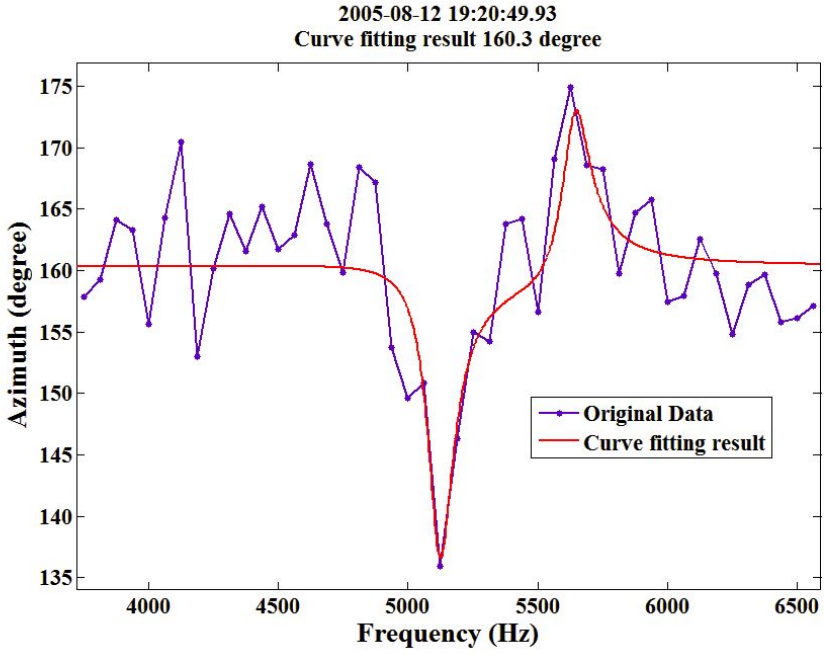

Fig. 4.11 Model fitting of the azimuth curve in Fig. 4.10 in the frequency range of 5 to 6 kHz with 2 presumed electric dipoles

Another example was recorded at 12:04:11.35 on 13 Aug., 2005. Its optical and electromagnetic signals observed by the ILD are shown in Fig. 4.12. The source azimuth based on the ratio of magnetic field peaks in time domain (in broadband) in the two loops of the ILD for the stroke is 297° (Fig. 4.13). Fig. 4.14 shows a curve fitting of one typical bi-polar impulse and one mono-polar impulse in frequency range from 1.6 kHz to 2.2 kHz. The model fitting gives a source azimuth of 297.3°.

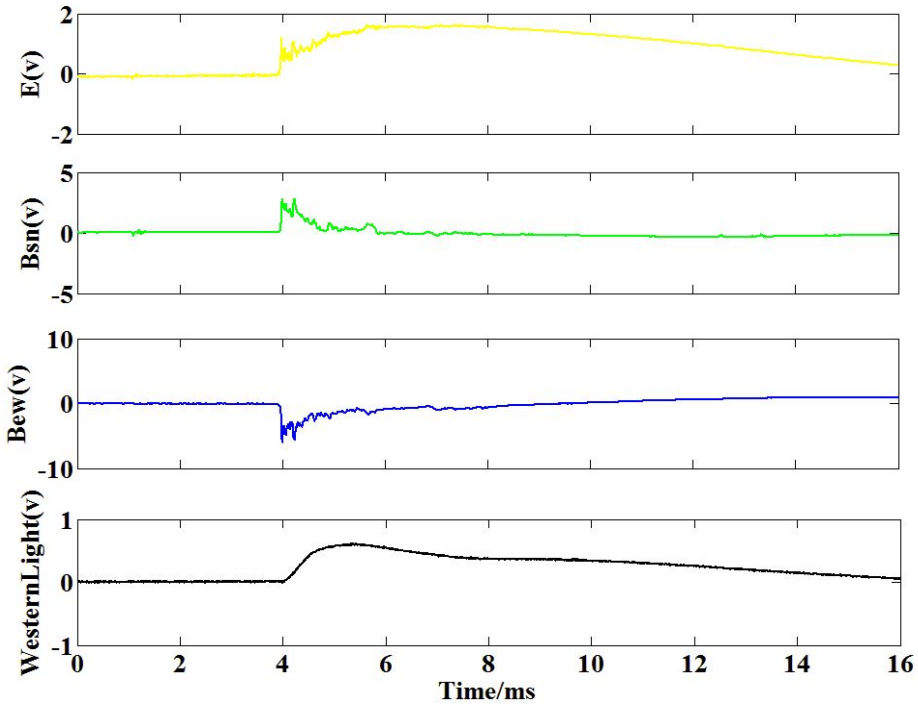

Fig. 4.12 Optical and electromagnetic signals observed by the ILD for a negative return stroke occurred at 12:04:11, 13 Aug., 2005. Upper to down: electric field (*E*), magnetic field in south–north loop (*Bsn*) and that in east–west loop (*Bew*), and light signal from the west, respectively. Units are arbitrary

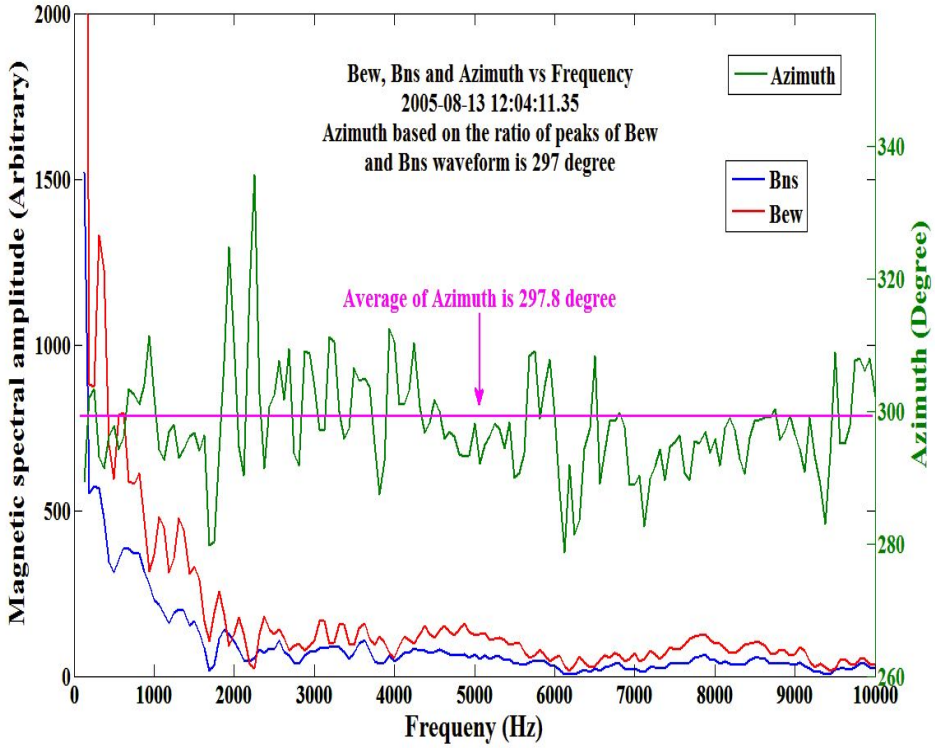

Fig. 4.13 The source azimuths versus frequencies based on ratios of spectra of *Bew* and *Bns*, with a mean azimuth of 297.8°, for the same stroke shown in Fig. 4.12. The azimuth based on the ratio of peaks of *Bew* and *Bns* waveforms is 297°

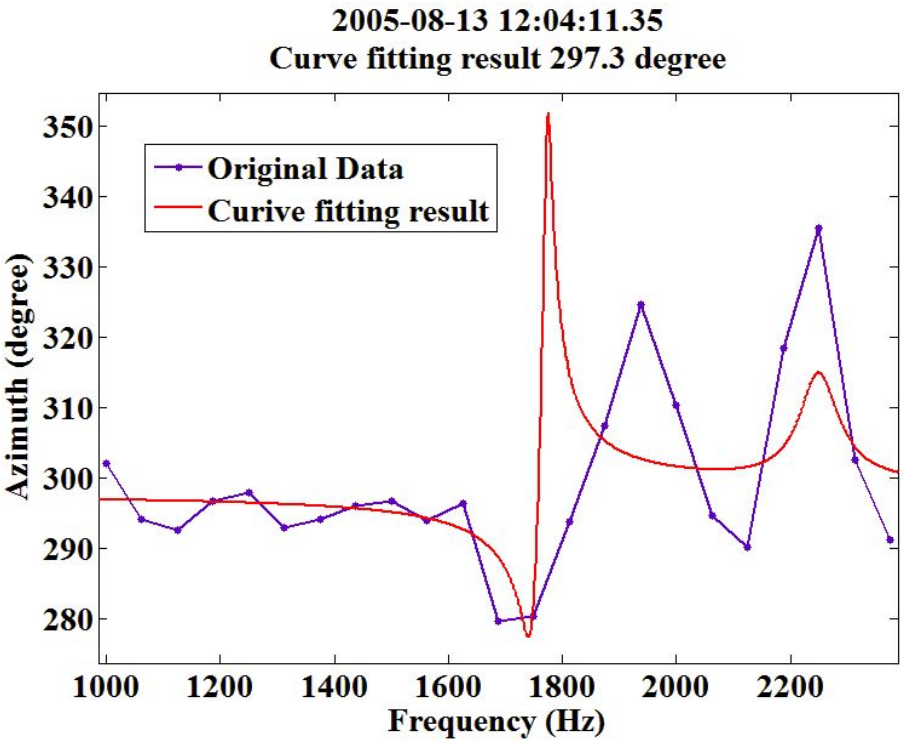

Fig. 4.14 Model fitting of the azimuth curve in Fig. 4.13 in the frequency range of 1.6 to 2.2 kHz with 2 presumed dipoles

In practice, averaging the azimuths in frequency domain in a broad frequency range will be much better, since sometimes the curve fitting method may not converge.

4.5 Conclusion

Theoretical interpretation and modeling of the "site error" have been attempted based on an electromagnetic dipole model. Simulations with the model show that the mono-polar impulsive fluctuations of the "site error" in frequency domain are due to the reflection of lightning incident signals by the "electric-dipole-wise" structures nearby a DF, while the bi-polar ones are due to the "magnetic-dipole-wise" structures.

Simulations also show that an “electric-dipole-wise” structure causes a “site error” as a function of source azimuth with a dominant period of 360°, while a “magnetic-dipole-wise” one causes a “site error” as a function of source azimuth with a dominant period of 180°. Furthermore, alternative approaches for obtaining the true source azimuth for a return stroke based on a single-station DF observation were discussed.

Chapter 5

A practical approach for “site error” corrections of TOA/DF LLN

5.1 Description of the approach

5.1.1 Background

The most of existing wide-area LLN in the world are using DF/TOA combined technique. For a lightning stroke detected by 4 or more sensors, the stroke is located by TOA technique. For a stroke detected by less than 4 sensors, the stroke is located by DF/TOA mixed approach. The highest detection efficiency of a single sensor in a 25 DF/TOA regional LLN in China is no more than about 80% [Chen et al., 2011]. This means that the DE of 4-sensor based TOA approach is no more than about 40%. A large number of lightning stroke were captured by only three or two sensors in the regional LLN. They were located based DF/TOA mixed approach with “site error” remained. Therefore, corrections of “site error” of DF/TOA sensors are practically still necessary.

5.1.2 Basic idea

Although both of TOA and DF techniques are not immune to errors, they have irrelevant causes of errors. The "site error" of a DF sensor is mainly caused by the sensor nearby structures, such as buildings, power lines and cables, and by variation in the surrounding terrain. The accuracy of time synchronization and the terrain properties such as ground roughness and conductivity may affect the accuracy of a TOA system. Honma attempted to correct the influence of terrain elevation on TOA systems and achieved a location accuracy of 270 m [Honma et al., 2011]. Although TOA has lower DE, it is still able to correct DF's "site error" since it has higher location accuracy when compared with that of DF. For instance, with an error of less than 500 m for a source-to-sensor distance of more than 30 km, the azimuthal error is just less than 1 degree.

In a LLN with DF/TOA technique, each sensor records both the lightning signal arrival time and the lightning source direction. For a lightning stroke detected by 4 or more sensors, the azimuths resulted from the TOA method would be different with those reported from the DF method. The azimuth differences between these two methods can be viewed as the "site error" of corresponding DF. This ideal does not change the definition of "site error", it is statistical analysis and evolution using redundant data. Furthermore, the location results of TOA algorithm have been filtered to make sure that they have relatively high accuracy. The filter algorithm can be seen in section 5.2.2. The pattern of "site error" versus azimuth for each sensor in a LLN would come out when enough number of lightning strokes are detected by the LLN.

Then the pattern of "site error" could be used to correct each sensor's azimuth error, hence to improve the accuracy of lightning locations.

5.2 Results of "site error" for a TOA/DF LLN in China

5.2.1 The LLN and its lightning data

The above idea has been examined with a regional LLN in Yunnan, China. The Yunnan LLN is composed of 25 sensors, with 23 within Yunnan Province and 2 in Guangxi Province in southwest China (Fig. 5.1). All the 25 sensors are based TOA/DF combined technique and are able to locate strokes in CG flashes. These 25 sensors were manufactured by the Center for Space Science and Applied Research, Chinese Academy of Sciences. Each sensor records the date, arrival time, azimuth, E strength, H strength, and peak time etc. At least 2 sensors are needed to locate a lightning stroke and at most 4 sensors are used. The two sensors in Guangxi Province recorded very few events due to some unknown reasons so their data haven't been processed.

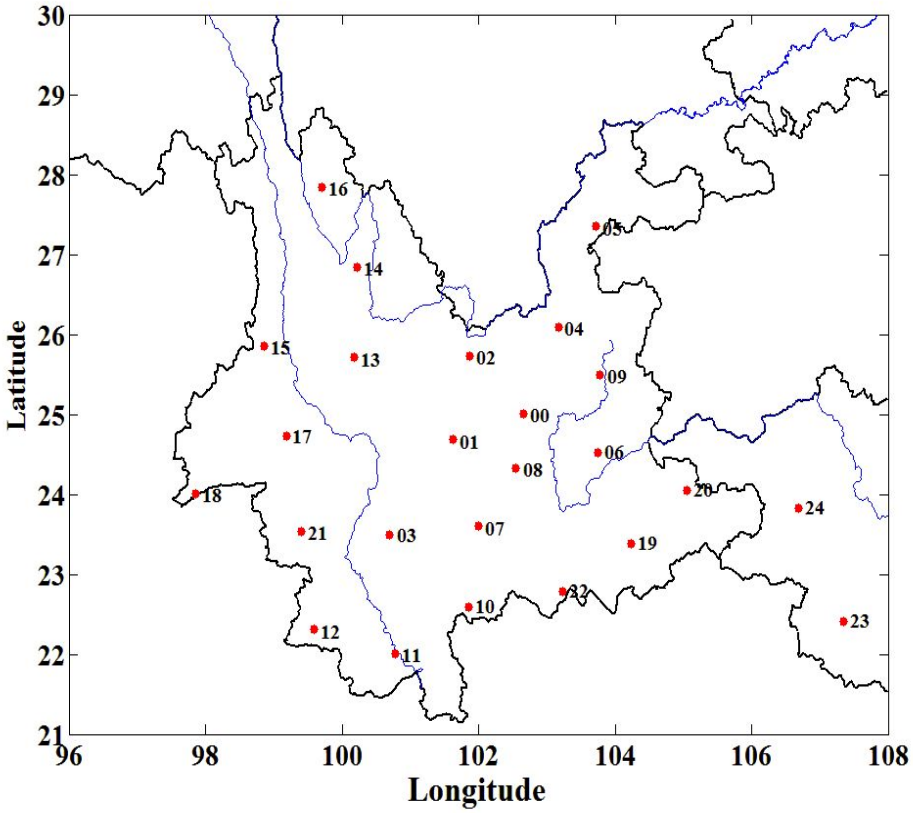

Fig. 5.1 The LLN with 25 DF/TOA type sensors in Yunnan Province in southwest China

In 2008, about 1,063,786 lightning return strokes in total were recorded by the Yunnan LLN. Among those, about 474,510 strokes were located by 4-sensors TOA algorithm, 334,890 strokes by 2-sensors DF/TOA mixed algorithm and the remaining by 3-sensors DF/TOA mixed algorithm.

5.2.2 “Site error” pattern obtained

The spatial and seasonal patterns of “site error” for individual sensors were found by means of comparisons of locations of lightning strokes detected by at least 4 sensors between DF and TOA algorithm.

For example, for a lightning stroke occurred at time 20:41:22 on 04 Aug., 2008, it was detected by sensors No.01, No. 03, No. 08 and No. 13 with the signal arrival times and DF azimuths as shown in Table 5.1. The stroke location determined by using TOA algorithm was (Longitude101.8478E, Latitude 23.9250N). This TOA location in turn gave an azimuth of 67.96 degree to sensor No. 03 (TOA azimuth in Table 5.1). The 3.5 degree deviation between the DF azimuth and TOA azimuth was then counted as the “site error” of sensor No.03 for the stroke at that azimuth and distance. The “site error” patterns for sensor No.03 came out when such an approach was applied to a huge number of eligible lightning strokes occurred surrounding the sensor at different azimuths and distances.

Table 5.1 Details of ae lightning stroke detected by 4 sensors in Yunnan LLN at 20h41m22 on 04 Aug., 2008

Sensor	Arrival time (second)	DF azimuth	TOA azimuth	Site error
No.01	22.2819291	159.07	---	--
No.03	22.2820573	64.43	67.96	3.5
No.08	22.2819188	236.02	--	--
No.13	22.2825050	136.09	--	--

To make sure that the lightning stroke being used for “site error” estimation has high location accuracy, data screening was done. For a stroke detected by more than 4 sensors, arrival times were adopted to check which 4 sensors had contributed to the stroke location determination. The event occurring time was extrapolated according to the signal arrival time and source distance to each sensor. The group of 4 sensors which resulted in a minimum standard deviation in event time estimation when compared with other group combinations was picked out for “site error” estimation. Only those strokes that had a TOA location accuracy of less than 500 m were used.

Shown in Fig. 5.2 are the patterns of “site error” versus source azimuth for sensor No.3 for various source-sensor distance ranges. The horizontal axis represents source azimuth given by 4-sensor TOA algorithm and the vertical axis represents the “site error” at corresponding azimuth. For the source-sensor distance range of 30-50 km, it was found that the “site error” could be as large as 15 degrees with a mean value of about 3.6 degree. The plots of the “site error” show a variation of dual cycles against the source azimuth, which is very consistent with that in literature as shown in Fig.2.2. There is a similarity in the variation pattern between the “site error” for the distance range of 30-50 km and those for 50-100 km and 100-200 km. This suggests that the “site error” is insensitive to source-sensor distances.

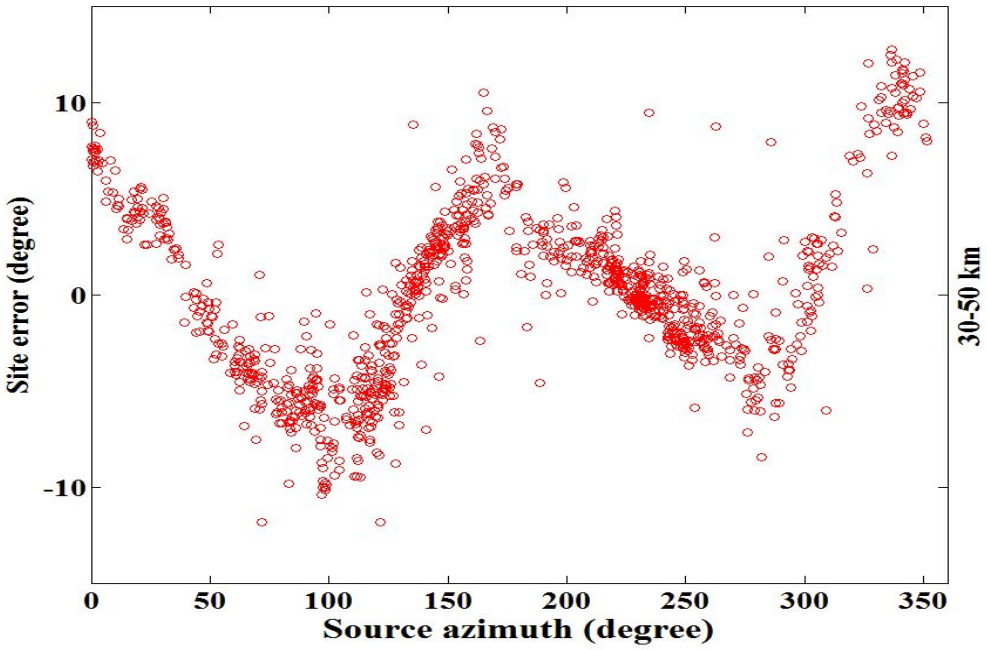

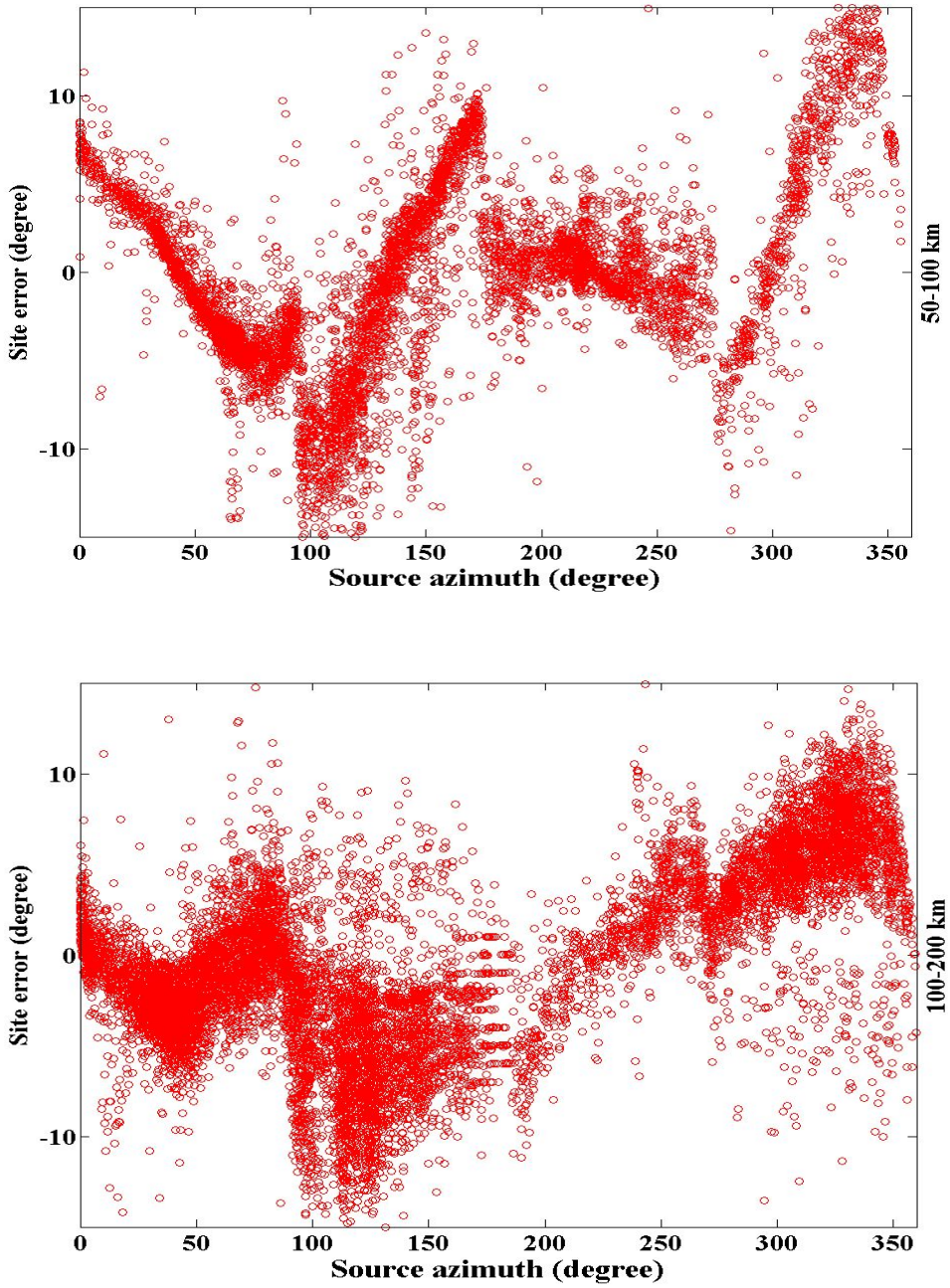

Fig. 5.2 The patterns of "site error" versus source azimuth for sensor No.3 for distance ranges of 30-50 km, 50-100 km and 100-200 km respectively

Shown in Fig. 5.3 and Fig. 5.4 are the "site error" patterns for sensors No. 1 and No.12 respectively. These results show that the "site error" pattern of a sensor does not change so much against the source distance. This supports the theory that the "site

error" is caused by DF's nearby objects and insensitive to distance.

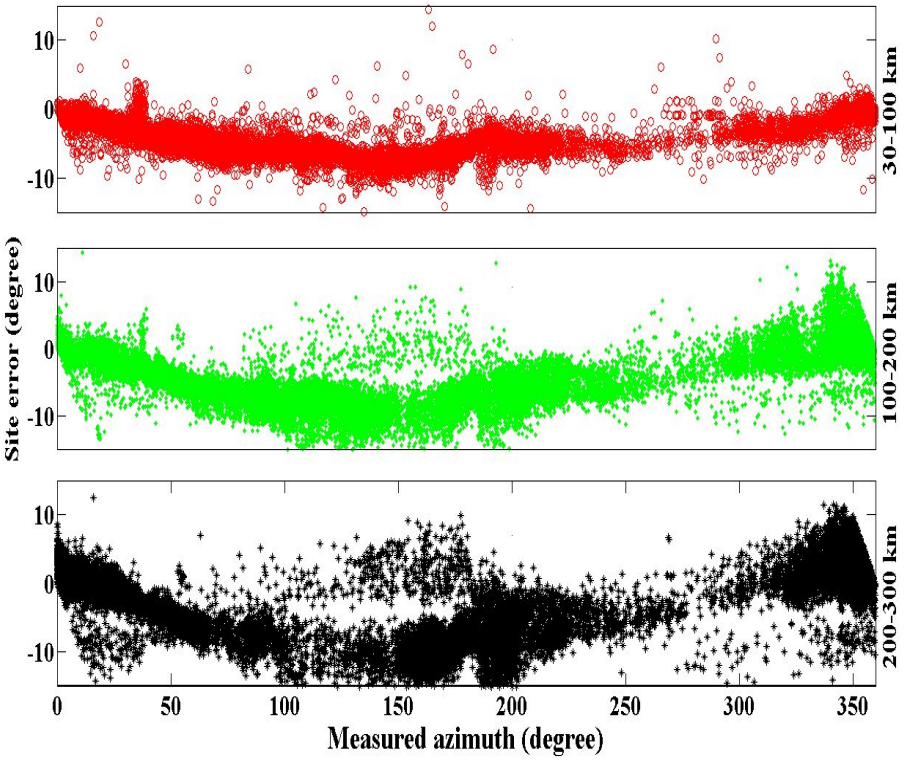

Fig. 5.3 The patterns of "site error" versus source azimuth for sensor No.1 for various distance ranges

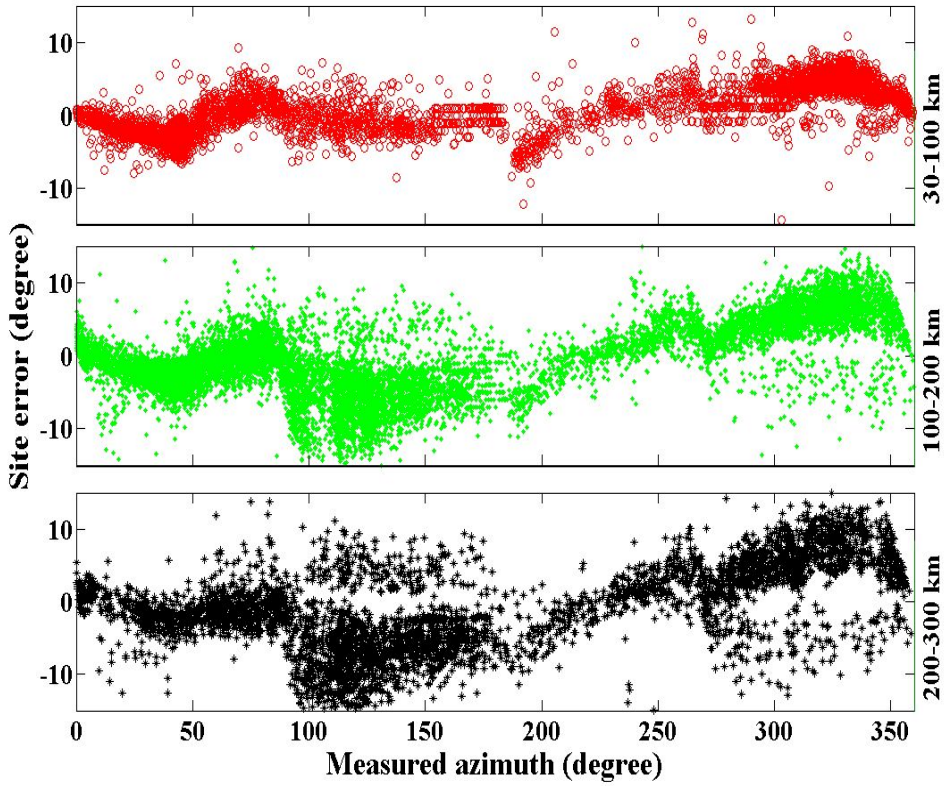

Fig. 5.4 The patterns of "site error" versus source azimuth for sensor No.12 for various distance ranges

In order to examine the time stability of "site error", the "site error" against seasons was discussed for sensor No. 3 as shown in Fig. 5.5. In the figure, the upper panel is the "site error" obtained using the data from January to June and the lower panel is that obtained using the data from July to December in 2008. Both plots have the similar trend and amplitude. The only difference is that lower panel has more data points because there were more lightning activities in the summer season. Similarity of "site error" between separated time periods is committed to the idea that "site error" is stable as long as the sensor installation environment has no changes. This fact gives a clue for improvements of lightning location accuracy by "site error"

correction. It is believed that the "site error" pattern of a given sensor will be duplicated from year to year if the site environment has no changes. All one needs to do is to get the "site error" pattern for each sensor with existing data and apply it for error correction for further observations.

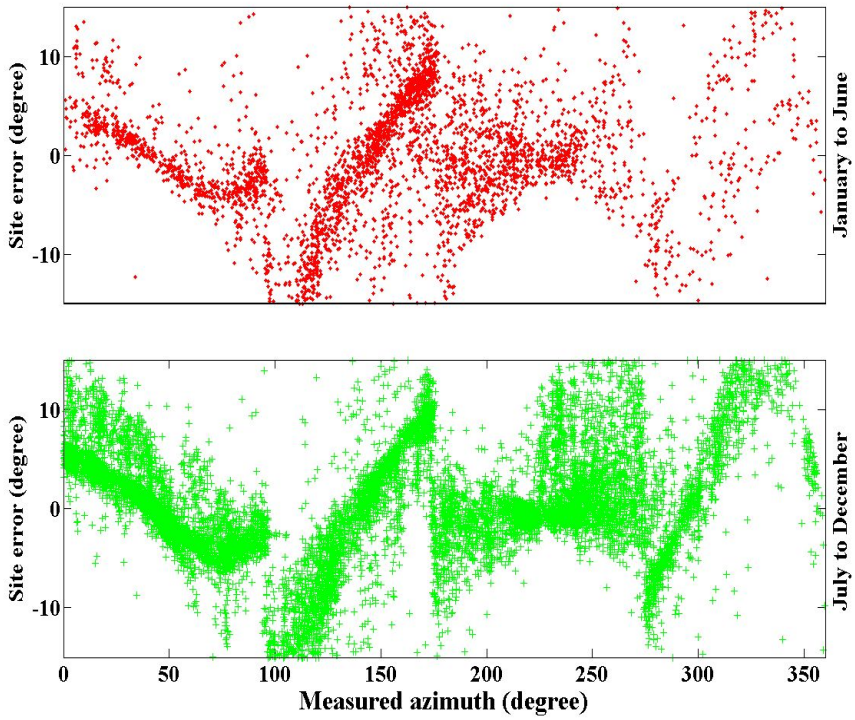

Fig. 5.5 Seasonal variation of the pattern of "site error" versus source azimuth for sensor No.3 for the distance range of 100-200 km

5.3 Statistics of lightning data with and without "site error" corrections

According to statistics on the Yunnan regional LLN in 2008, only 44.6% of lightning stroke were detected by four or more sensors simultaneously and therefore were

located by using the TOA algorithm. The left were affected by the “site error” more or less since they were located by using 2- or 3-sensor algorithm.

As mentioned in section 5.1.2, once the “site error” pattern is obtained, it can be incorporated into 2-senor sensor location algorithm to improve the location accuracy.

5.3.1 “Site error” correction procedure

Although “site error” is insensitive to distance, the random error of “site error” patterns may increase with distance, as the lightning signal strength decreases with distance. On the contrary, at small distance (less than 30 km), four-station TOA location error could not be ignored and it will make the “site error” pattern blurred. As shown in Fig. 5.6, the “site error” pattern is not very clear at distance less than 30 km.

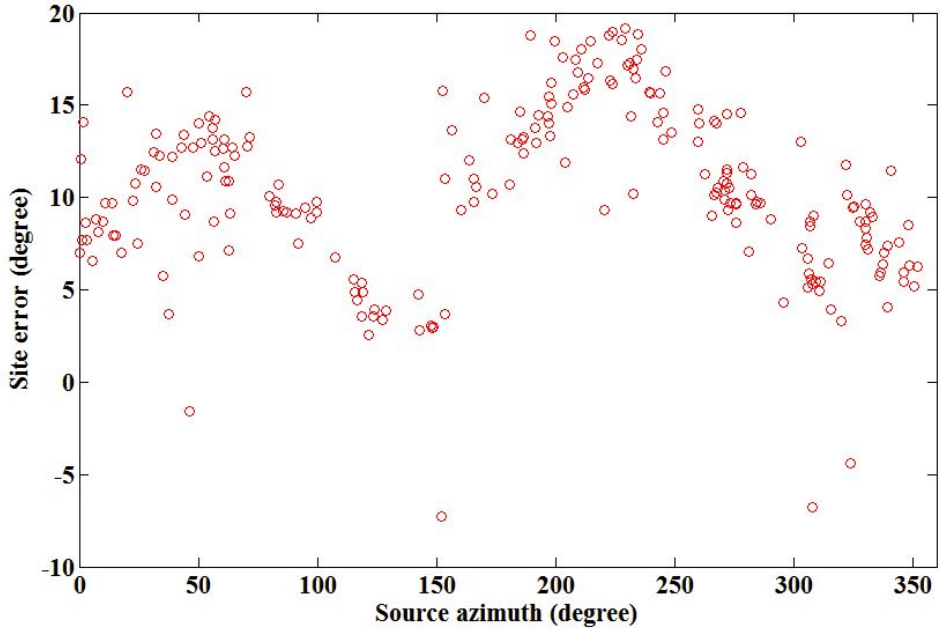

Fig. 5.6 “Site error” pattern of sensor No.13 obtained for distance range less than 30 km

In order to minimize the influence caused by random error and large angle error at small distance, “site error" pattern in moderate distance was adopted to make correction. A vivid “site error” pattern is just the first step. It should be converted into a quantitative “site error” versus detected azimuth curve. A specific procedure for getting such a “site error” versus detected azimuth curve is proposed as following:

Step 1: Plot the “site error” pattern for a moderate distance range (say 30-50 km, as shown in Fig. 5.7). Horizontal axis is the azimuth decided by four-station TOA algorithm, i.e. the true source azimuth. Vertical axis represents the “site error” at corresponding source azimuth. Positive value means clockwise displacement of single-station-detected azimuth to the four-station TOA azimuth.

Step 2: Tick out some data points which have obvious faults manually.

Step 3: Calculate the average value of "site error" at an interval of some certain degrees in azimuth. At present study, the interval in azimuth is 5 degrees. Because most of the "site error" is less than 20 degrees, a 5 degree interval in azimuth introduces only 0.5 degree error at most. Then the "site error" versus source azimuth curve can be plotted, as shown in Fig. 5.8 by the dot-line.

Step 4: However, the curve obtained in *Step 3* is not intuitive enough to make a correction since the source azimuth is unknown. The "site error" versus source azimuth curve needs to be converted into single-station-detected azimuth domain by using the sum of "site error" and corresponding source azimuth as the horizontal axis, as shown in Fig. 5.8 by the solid-line.

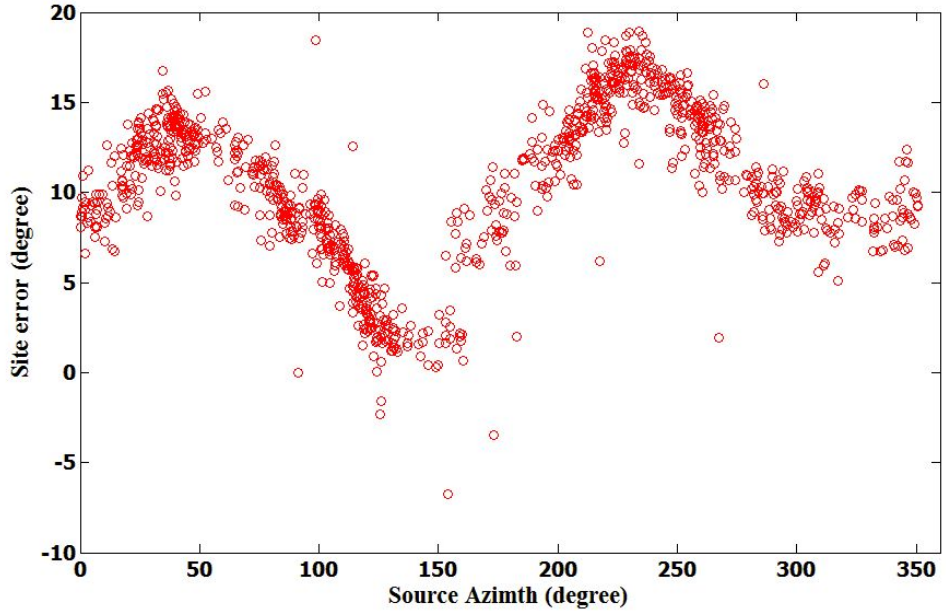

Fig. 5.7 The patterns of "site error" versus source azimuth for sensor No.13 within a distance range from 30 to 50 km

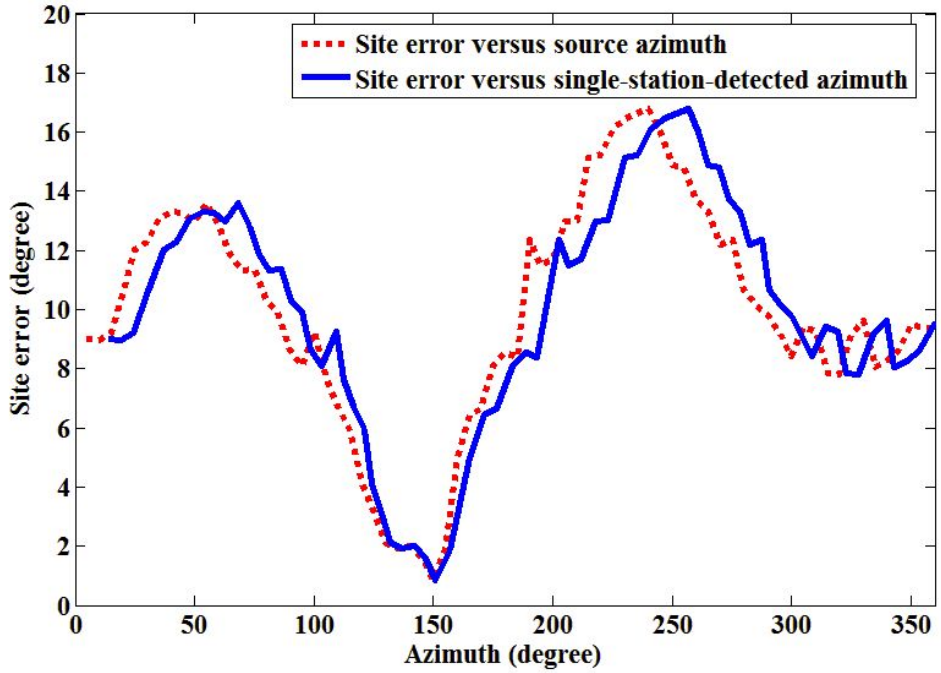

Fig. 5.8 The "site error" versus source azimuth curve (dot-line) and it has been converted into single-station-detected azimuth domain (solid-line)

As an example, Figs. 5.7 and 5.8 show the pattern of "site error" correction curve obtained based on the above procedure for sensor No.13. Once a lightning signal is detected by sensor No. 13, it has an original detected azimuth. This original detected azimuth's corresponding "site error" can be found from Fig. 5.8. Subtracting the "site error" from the original detected azimuth gives the true source azimuth. In practice, such "site error" data, as shown in Fig. 5.8, are discrete. To ensure that every detected azimuth has its corresponding "site error" value, an interpolation function can be employed to produce values between the discrete data points.

With a similar procedure to Fig. 5.8 for sensor No. 13, the curves of "site error" versus detected azimuth for all other sensors in the Yunnan LLN have been generated. The thing left is how to use these "site error" curves for error corrections.

In general, for lightning locations given by the four- or three-station algorithm that is TOA technique dominant, "site error" correction process does no more helps in improving their location accuracy. However, for lightning locations given by the two-station algorithm that is DF technique dominant, they usually have poor location accuracy and the "site error" correction process is necessary to them. A specific procedure for "site error" correction for a lightning location given by the two-station algorithm is described in following:

Step 1: Get the detected azimuths and arrival times of the stroke signal at the two sensors by which the stroke is detected.

Step 2: The difference in the arrival time between the two sensors will fix a hyperbola on ground surface.

Step 3: The two detected azimuths with corresponding "site error" corrections will produce two corrected azimuths that are with higher accuracy than the detected ones. Each corrected azimuth produces a radial line that intersects with the hyperbola in *Step 2* at a point on ground. The mid-point on the hyperbola between the two intersection points is then viewed as the corrected lightning stroke location.

5.3.2 Demonstration of "site error" correction

To demonstrate the significance of "site error" corrections, some case studies have been done.

Fig. 5.9 shows the comparison between some 4-sensor located strokes and 2-sensor located strokes with and without "site error" corrections, for lightning strokes detected in one hour period during a thunderstorm on 19 July of 2008, in Yunnan LLN. In the figure, red stars denote 4-sensor located strokes for reference and green stars and cyan stars denote the same 2-sensor located strokes without and with "site error" correction respectively. It can be seen that the strokes located by 2-sensor algorithm with "site error" corrections (cyan stars) are more centralized and closer to those strokes located by 4-sensor algorithm (red stars), when comparing with those 2-sensor located strokes without "site error" corrections (green stars).

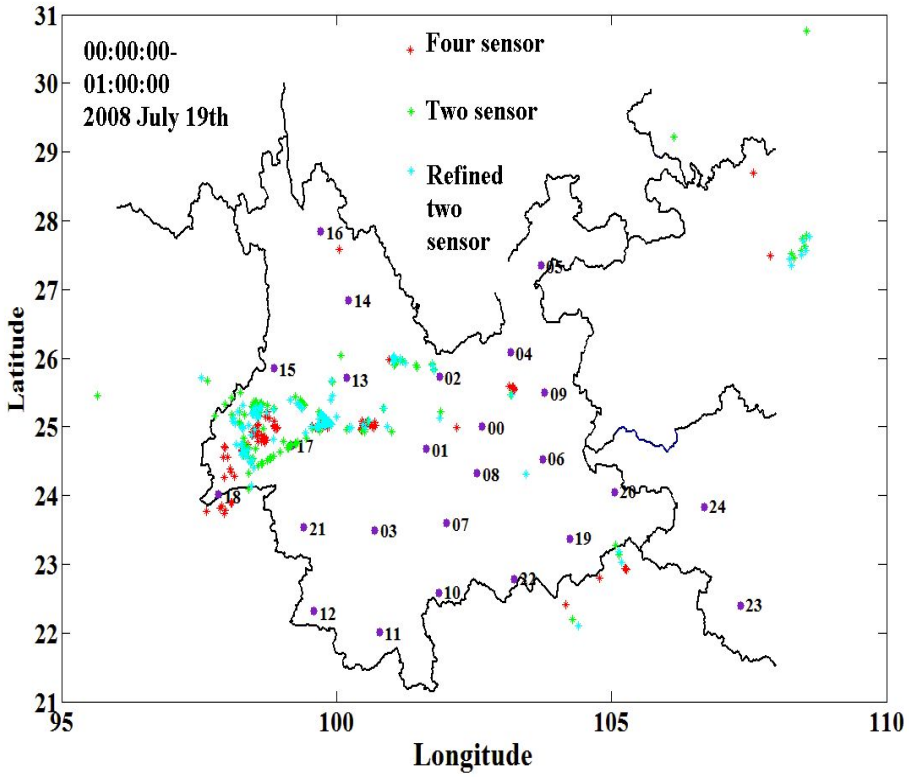

Fig. 5.9 Comparison of lightning strokes located by 2-sensor algorithm before (green stars) and after (cyan stars) "site error" corrections, with those strokes located by 4-sensor algorithm as reference, for lightning strokes during one hour period in a thunderstorm on 19 July of 2008, in Yunnan LLN

Fig. 5.10 is a comparison as Fig. 5.9 but for lightning strokes detected from 12:00:00 to 12:10:00 on 24 June, 2008. Sensors' locations and background map were hidden from sight in the figure for simplicity. Strokes were grouped into three groups according to their spatial distribution. Each group has been marked by a black box. The effect of "site error" correction will become more obvious by representing strokes in same color in a box as one mark. For instance, all red circles in first box of Fig.5.10 were represented by one red circle at the gravity center of all these red circles. So do

the green and cyan ones. The result is shown in Fig. 5.11. It can be seen from these figures that locating results of two-sensor after correction are quite different from those without correction, and the former ones are more close to that of four-sensor than the later ones.

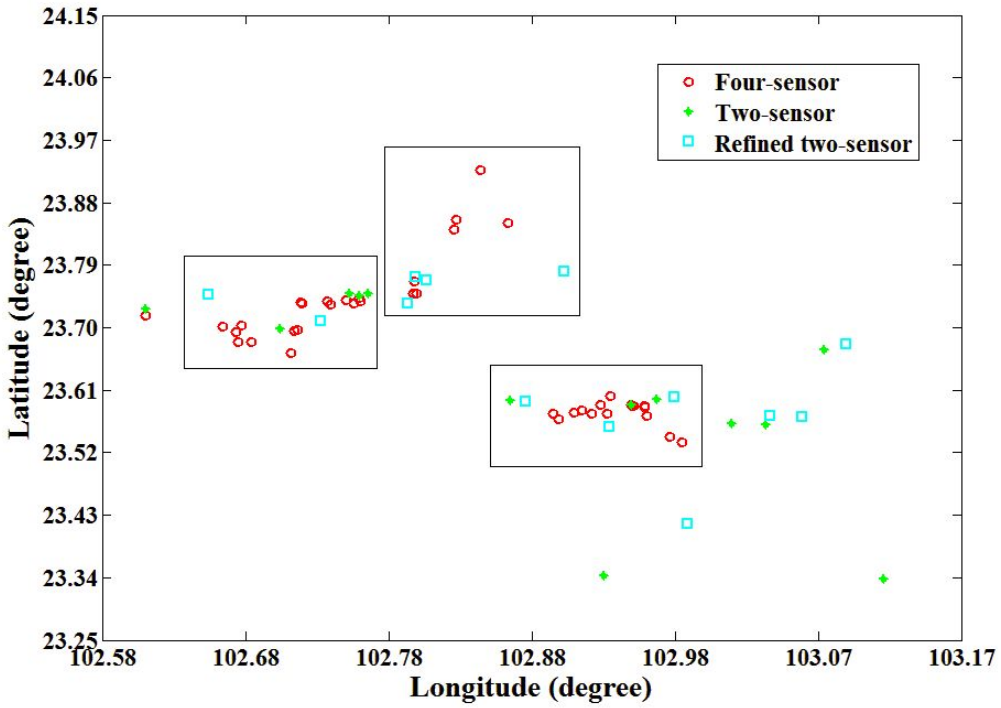

Fig. 5.10 A comparison similar to Fig. 5.9 but for lightning strokes from 12:00:00 to 12:10:00 in a thunderstorm on 24 June, 2008, in Yunnan LLN

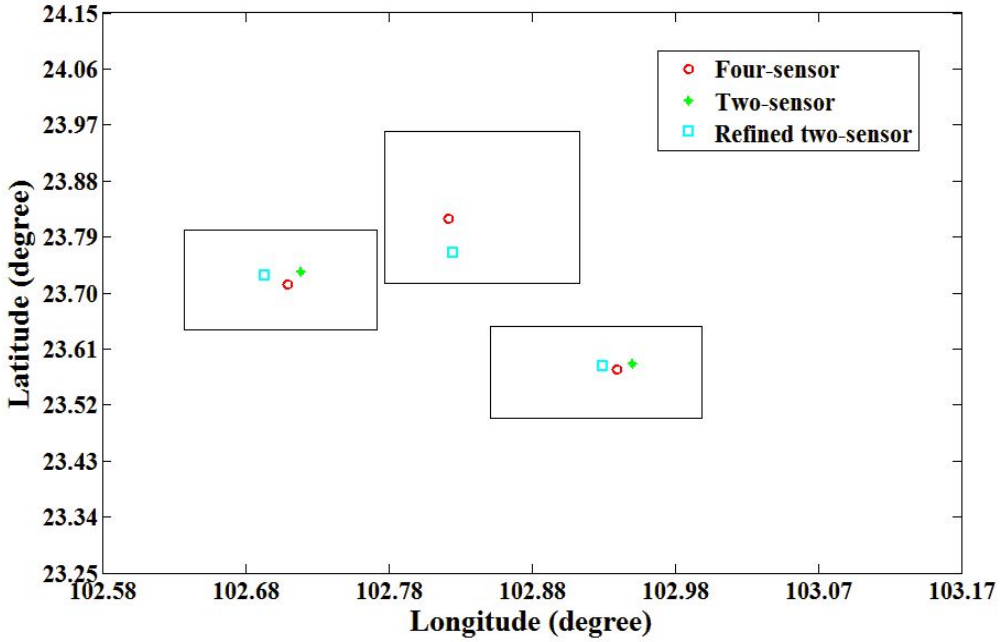

Fig. 5.11 A centralized version of Fig. 5.10 for clarity of the effect of "site error" correction

Shown in Fig. 5.12 and Fig. 5.13 are two other comparisons similar to that shown in Figs. 5.10 & 5. 11, but for lightning strokes detected from 13:00:00 to 13:10:00 and from 13:10:00 to 13:20:00 respectively, also on 24 June, 2008, in Yunnan LLN. All these comparisons show that the "site error" corrections do make the locating results of two-sensor algorithm improved significantly.

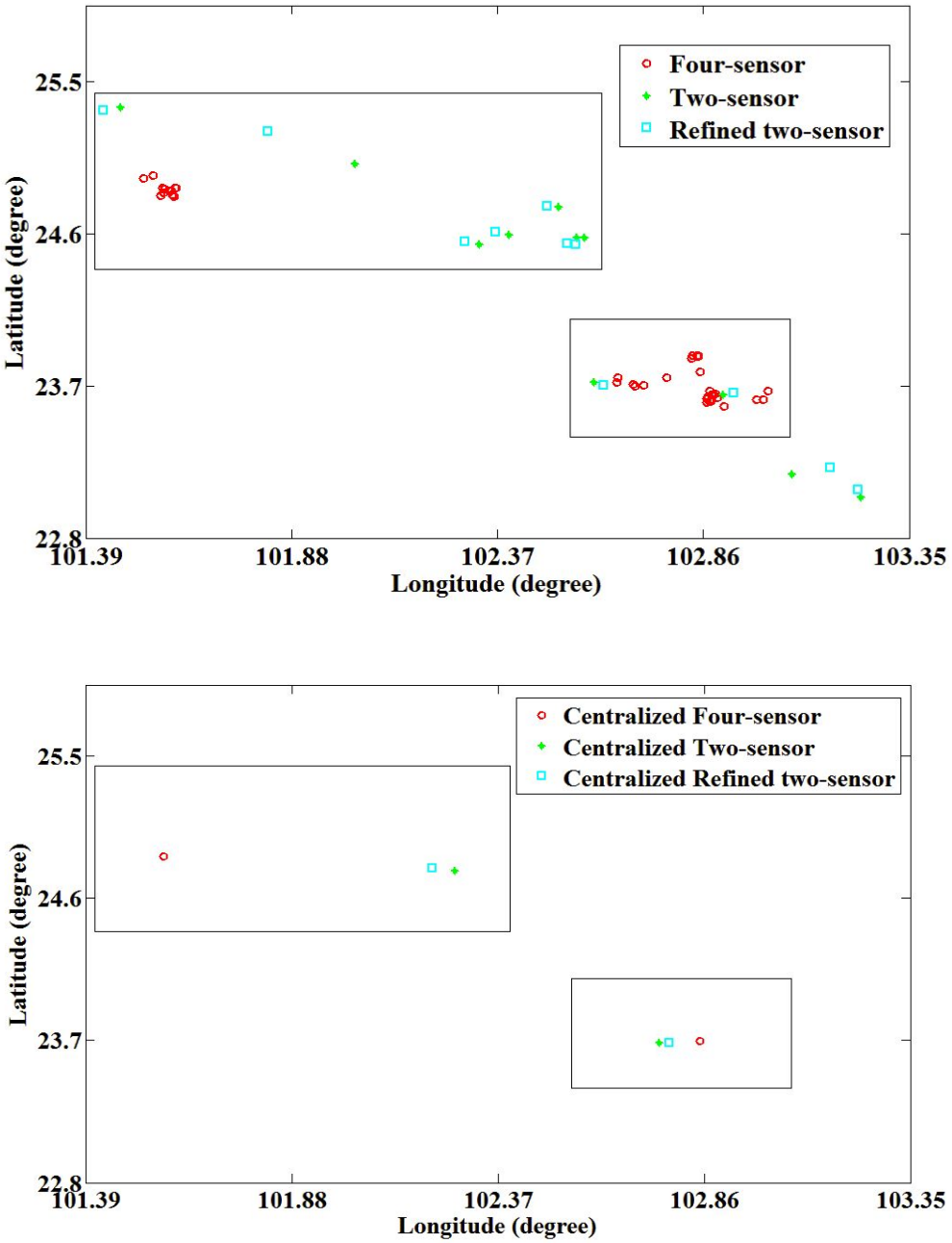

Fig. 5.12 A similar comparison to Figs. 5.10 & 5.11 respectively, but for lightning strokes from 13:00:00 to 13:10:00 in a thunderstorm on 24 June, 2008. Cyan squares (with corrections) are more close to red circles than green crosses (no corrections)

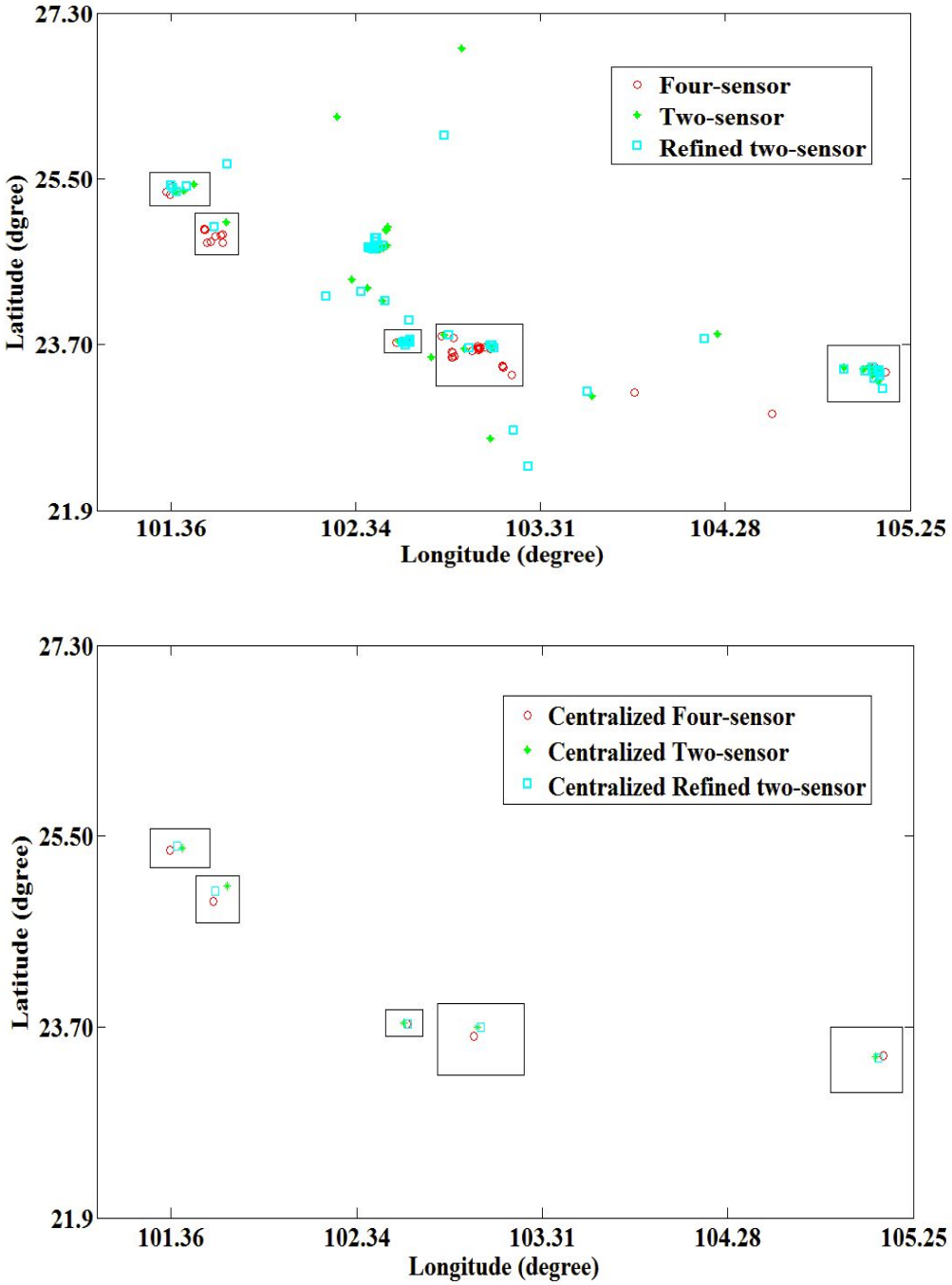

Fig. 5.13 A similar comparison to Fig. 5.12, but for lightning strokes from 13:10:00 to 13:20:00 in a thunderstorm on 24 June, 2008.

5.3.3 Statistics of lightning data with and without "site error" corrections

With the improvement of two sensors location results, it becomes possible to dig out more information from the historical LLN data. Thanks to the research works done by others, the properties of subsequent strokes have appeared. Some of them will be addressed in this part based on statistics of LLN data with and without "site error" corrected.

In general, a cloud-to-ground flash could have several large current pulse stages which are called return strokes. To count how many return strokes occurred within a flash, optical observation or electric field review are mainly utilized. First return stroke and subsequent return stroke are different at their signature feature of electric field. Uman has made a brief summary [Uman, 1987]. As shown in Fig. 5.14, the main difference lies in the time separation between leader and stroke. Subsequent return stroke is featured with a shorter slow front. It also goes cross zero time line earlier than first return stroke. In [Cooray and Perez, 1994], the antenna system has a response time of 0.2 microseconds and its decay time constant was 200 milliseconds. They found that the average number of strokes per flash was 3.4, and the percentage of single-stroke flashes was 18%. In certain places of China similar measuring equipment has been built with a sampling frequency of 1 MHz. The results showed that the average number of strokes per flash was 3.76 and the percentage of

single-stroke flashes was 39.8% [Qie et al., 2001]. Rakov adopted high temporal-resolution optical observations. He gave a result that the average number of strokes per flash was 4.1 and 17% of the flashes had no subsequent stroke [Rakov et al., 1994]. Unlike those single-station observations, number of stroke per flash given by LLN would become smaller [Rodger and Russell, 2002]. After modification of algorithm, per 2.3 strokes could be counted in a flash by U. S. National Lightning Detection Network. One of the reasons is that LLN has certain threshold for recording a stroke event. If a lightning signal was not strong enough, it could not be detected by at least two sensors.

Although the statistical results of inter-stroke interval given by different persons at different places have small discrepancy, the mean time separation between strokes would less than 100 ms and the maximum value should no larger than 500 ms. Table 5.2 shows the average inter-stroke time interval between return strokes. In this chapter, the Yunnan LLN data package gives a value of 76 ms, which is a little larger than the results of Cooray and Qie.

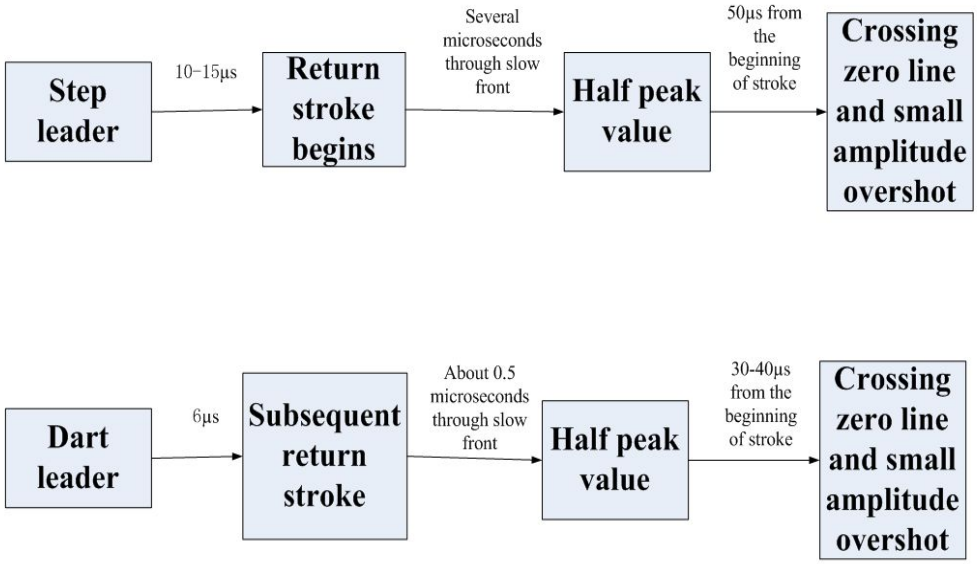

Fig. 5.14 Comparison of first return stroke and subsequent return stroke

Table 5.2 List of time interval between successive return strokes within one flash

Data source	Arithmetic mean of time interval (ms)
Cooray and Perez, 1994	65
Qie et al., 2001	64.3
Yunnan LLN data in 2008	76

Some properties on strokes were presented by [Christina et al., 2009]. Only the estimated peak current and distribution of new-ground-contacts by stroke order are

concerned here. In this paper, average peak current of strokes creating new ground terminations is -21.1 kA which is larger than that of strokes remained in previous channel. Mean peak current of subsequent strokes remaining in a preexisting channel is -11.9 kA. Second return stroke has strong tendency to create a new channel, the percentage is 59%. However, when it comes to high order stroke, it almost remained in the preexisting channel. When stroke order is higher than 5, only 5% of them will create a new ground termination. In [Rakov et al., 1994], the probability of creating a new termination has become zero when stroke order is larger than 4.

Specific features of lightning subsequent return stroke would have some variations at different literatures since their observation methods, areas and weather conditions are different. In addition, it is debatable when people define or confirm a "flash". U. S. National Lightning Detection Network has adopted a multiplicity algorithm described in [Cummins et al., 1998]. All strokes within a flash have a spatial restriction of 10 km and their time window is 1 s. Time interval of two continuous strokes should be less than 0.5 s. Rodger put forward an improved algorithm to group subsequent strokes into flashes. He extended time window from 1 to 2 s. The most special point in his algorithm is that spatial restriction reduces linearly with the passage of time. When time is zero, spatial window is 20 km. When time reaches 2 s the spatial window becomes 0 km. This algorithm also removed the limitation on time separation between strokes. It makes the average flash multiplicity increased from 2.1 to 2.3 [Rodger and Russell, 2002].

In order to investigating the properties of return strokes in Yunnan LLN and the effect of “site error” correction, the strokes recorded in data package should be grouped into flashes. A newly grouping algorithm was developed. In this algorithm, each flash should occur within 1 s and time separation between every two successive strokes cannot exceed 200 ms. As mentioned before, high order strokes almost remained in previous channel, so another criterion is that high order strokes (larger than four) should be very close to each other, but subjected to limited location accuracy of the LLN

With the Yunnan LLN data in 2008, 3966 flashes that have at least 5 subsequent return strokes per flash were first selected for statistical analysis. All these flashes have a spatial restriction of 10 km per flash and all strokes were decided by four-station algorithm. High order strokes spatial distribution has connection with the network location accuracy. Fig. 5.15 shows the inter stroke separation distribution within one flash. It is obvious that high order strokes are more concentrated and most of them scattered within a 500 m hoop. Bear this in mind, the 3966 flashes were filtered by the criterion that the 4th and 5th strokes should stay with each other no more than 500 m since the accuracy of most modern DF/TOA LLN is around 500 m.

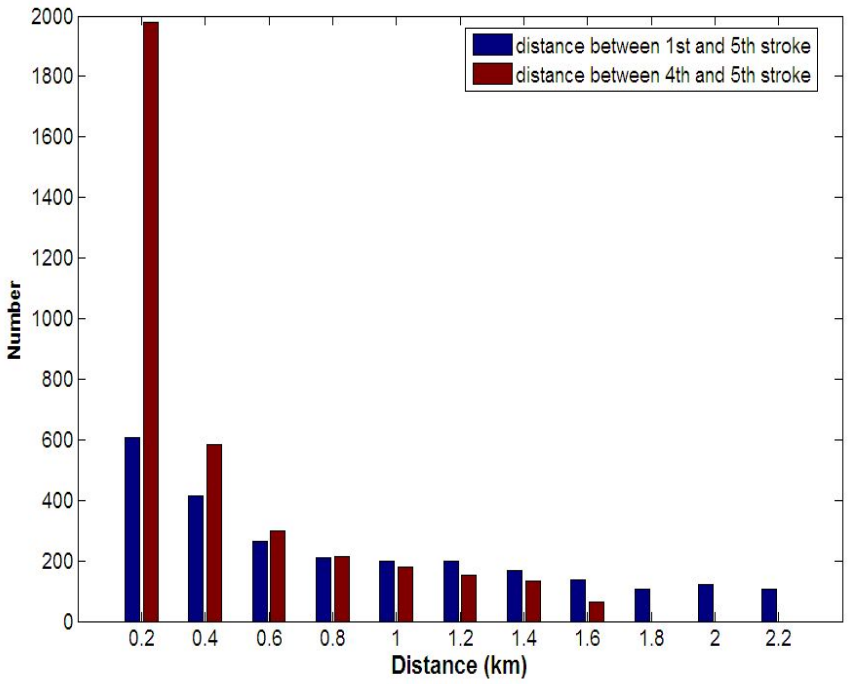

Fig. 5.15 Flash number distributions against the distance separation in ground contact between 1st and 5th stroke and that between 4th and 5th stroke in a flash. The 0.2 on the horizontal axis denotes the number of flashes whose inter stroke distance is less than 0.2 km, and so on. Total flash number is 3966.

After the above mentioned filtering, the residual 2532 flashes have become a group of flashes with the least misclassification. This algorithm makes sure that all strokes belong to their corresponding flashes. It inevitably lost certain information of those flashes whose strokes number is less than 5, however, the flashes picked out were able to reveal enough information and this action is so conservative that no misleading data would be coupled. Fig. 5.16 is the distribution of flash number against distance separation between strokes in a flash for the flashes after filtering. It shows that the number of flashes decreases with the inter stroke distance increases. The average

distance between 4th and 5th stroke is 0.15 km and the average distance between 1st and 5th stroke is 1.53 km.

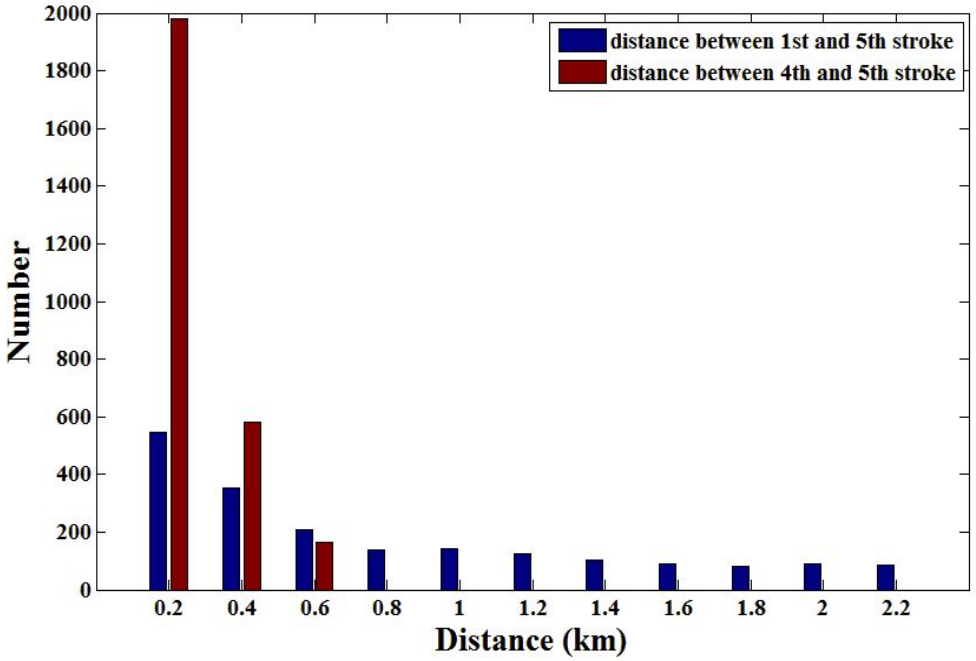

Fig. 5.16 Distribution of flash number against inter stroke distance for flashes whose distance between the 4th and 5th stroke is less than 500 m. All strokes were located by four-station algorithm. Total flash number is 2532.

When it comes to those flashes that were located by two-station algorithm, the filtering rules need some revisions. The two-station results involved "site error" so they had a lower accuracy. Here is the grouping algorithm for two-station located flashes. Within 1 s at least 5 strokes should occur and the time separation between two successive strokes should less than 200 ms. The distance between the 4th and 5th strokes should less than 900 m due to random errors, assuming that they have similar "site error" since they are supposed to have the same location (channel). After

filtering, 1532 flashes have remained. The statistical results are shown in upper panel in Fig. 5.17. The average distance between the 4th and 5th stroke is 0.36 km and the average distance between the 1st and 5th stroke is 3.23 km for these 1532 flashes.

Since two-station results were affected by "site error" and the error can be corrected based on four-station results, the 1532 flashes were reprocessed by eliminating the "site error" using the method stated in previous sections. The results after "site error" correction are shown in the lower panel in Fig. 5.17. The reprocessed data leads to an obvious decreasing in the distance between strokes of a flash. Mean value of distance between the 4th and 5th stroke become to 0.35 km and that between the 1st and 5th stroke become to 2.8 km. "Site error" elimination does little affection on high order strokes separation distance because high order strokes stay together and the azimuth correction would make same influence on these strokes. Therefore, only the variations in the distribution of flash number against distance separation between the 1st and 5th stroke before and after "site error" corrections s have been shown in Fig. 5.17. As seen from the figure, for the data with "site error" correction (lower panel in Fig. 5.17), the number of flashes has an obvious tendency of decrease with the increase of the distance between the 1st and 5th strokes, which is more close to the tendency of those four-station results (Fig. 5.16) than the data with no "site error" correction (upper panel in Fig. 5.17). This implies that the "site error" correction indeed improved the location accuracy of those flashes located with two-station algorithm.

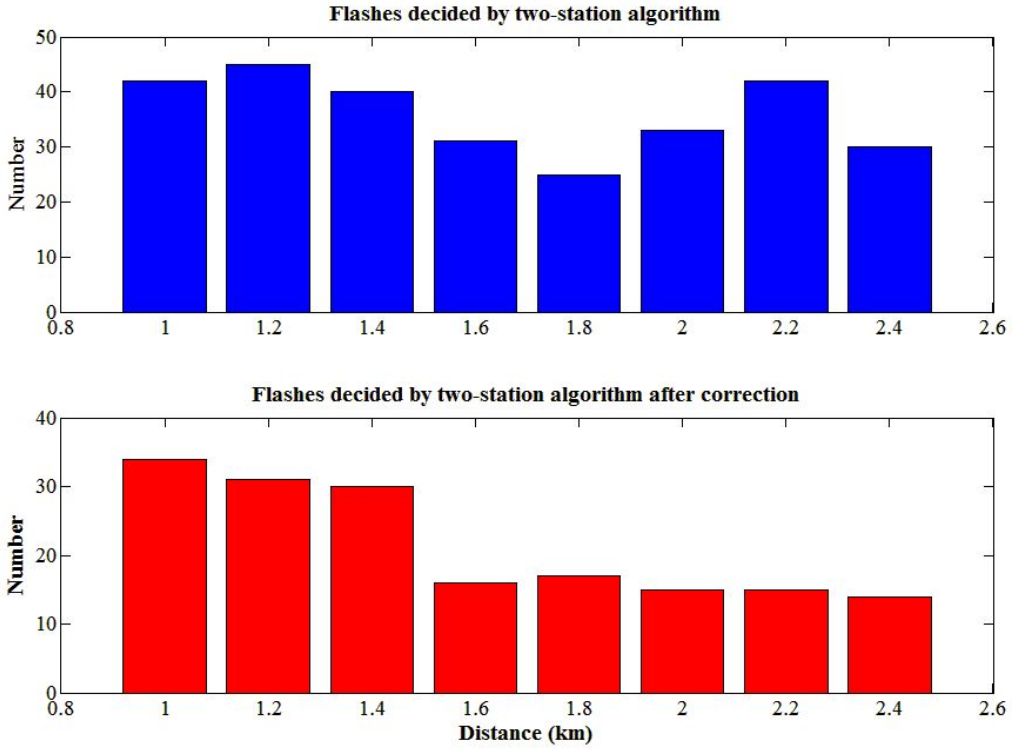

Fig. 5.17 Flash number distribution against the distance between the 1st and 5th stroke for flashes located by two-station algorithm with and without "site error" corrections. Upper panel: without corrections, lower panel: with corrections.

The data package also contained lightning strength. It is convenient to investigate the probability of subsequent return stroke creating a new channel and its relationship with the lightning strength. Since four-station results have an accuracy of 500 m for a single stroke, if the 5th stroke in a flash is far away from the 1st stroke in the flash than 1000 m, this flash would be classified as having more than one ground contacts. Lightning strength of a flash is taken as the mean value of the strength of its 1st, 4th and 5th strokes. Table 5.3 shows the strength distribution of the 2532 flashes located by four-station algorithm versus the probability of producing a new ground contact

within a flash. Larger magnitude of lightning strength (mean stroke peak current in kA) is corresponding to a larger probability of producing a new ground contact.

Table 5.3 Probability of creating a new ground contact versus flash strength (mean stroke peak current in kA)

Flash strength distribution (kA)	Probability of creating a new ground contact
25-50	43%
50-100	53%
100-200	70%

5.4 Conclusion

This chapter proposed a method for "site error" estimation and corrections for DF/TOA type LLN. "Site error" of a DF/TOA sensor in azimuth domain was studied by comparing the source direction found with the DF technique with that found with the TOA technique. About one million lightning strokes recorded by the Yunnan LLN in 2008 were used for this study. The patterns of "site error" versus source azimuth for individual sensors found are in well consistence with previous observation and theory. The "site error" versus source azimuth varied in either odd-cycle or dual-cycle form, or a superposition of both and it was insensitive to source-sensor distance. The results support the theory that "site error" are caused by sensor nearby electric-dipole-wise or

magnetic-dipole-wise objects. Both the theory in Chapter 4 and the results in this study support that the “site error” are stable against seasons as long as the site environment has no changes. It is these features that make the “site error” corrections practicable.

With the “site error” obtained, attempts of “site error” corrections were done. The results showed that a stroke location based DF algorithm with “site error” corrections was comparable with that based on TOA algorithm. Statistics of lightning data after “site error” correction also become more consistent with other people’s observation results. Number of flashes decreased with the distance between the 1st and 5th stroke in a flash increased. Larger magnitude of a flash strength is corresponding to a larger probability of producing a new ground contact.

Chapter 6

Experimental study of a single-station lightning locating technique with a broadband DF

6.1 Background

Comparing to a LLN a single-station lightning location system is easy to install, does not need precise time synchronization and lower maintenance costs. Its algorithm is useful for scientific research on specific lightning event such as the estimation of return stroke peak current. Besides research of thunderstorm distribution and lightning accident analysis, the realistic role of single-station lightning locating system is its lightning forecasting and warning. At present, power industries, civil aviation and tourist attractions are calling for lightning protecting and warning. A typical electric field mill is able to provide an advanced warning up to 5-8 minutes [Song et al., 2011]. Its working range is limited within a radius of 10 km. Fortunately, the single-station lightning locating technique is supposed to be sensitive to the lightning signal as far as 130 km. So it could offer more warning time than traditional electric field mill.

To a single-station location system, source-observer distance becomes the key issue. A single-station lightning locating approach usually involves a lightning source distance

finding method plus the DF technique. Since DF technique has been investigated in previous chapters and already gained high accuracy when broadband magnetic loop antenna was adopted, this chapter would focus on lightning source distance finding.

6.2 Existing single-station lightning locating techniques

There are many kinds of method to get the distance of lightning based on a single-station observation and most of them need to be improved further when compared to the sophisticated multi-station lightning locating techniques.

The simplest method to estimate the distance is based on the amplitude of lightning signal, which assumes that there is a fixed distribution pattern of lightning strengths in a thunderstorm and the amplitude of lightning signal in average decreases with distance [Horner, 1960]. The lightning locations given by this technique are the thunderstorm rough location rather than the lightning stroke location. Mardiana built a single-station lightning locating system based on this theory [Mardiana, 2007]. Developing and decaying of thunderstorms can be shown on real time map. It also serves as a lightning warning instrument.

Full wave method in waveguide is another approach to get the distance of lightning. The lightning-produced electromagnetic fields propagate in forms of ground wave and sky wave. The sky wave would be reflected between the ground and ionosphere. The

signal received by an antenna at ground is the superposition of those ground wave and sky wave with certain wavelengths which meet the waveguide boundary conditions. However, this theory is only valid for medium and short distance in the frequency bands from 3 to 30 kHz. From the view of wave line theory, some signal is just reflected by the ionosphere once, and others are reflected between the ground and ionosphere several times. The time differences between those signals are able to tell the distance of lightning source and the height of the ionosphere [Nagano et al., 2007]. The detecting range and accuracy of this technique highly depend on the diurnal change of the height of the ionosphere. The detecting range of this method is about a few hundred kilometers with accuracy of ten percent.

When it comes to large distance, Schumann Resonance has been investigated and it is an indicator of global lightning activities. Electromagnetic signal will form standing waves in the resonant cavity consisted of earth surface and ionosphere. They are featured by the superposition of background noise and strong extremely low frequency pulse signals. Schumann Resonance is a dominant mode when frequency is lower than 100 Hz [Volland, 1995]. Wait first proposed a mode theory on Schumann Resonance [Wait, 1962]. Nickolaenko and Hayakawa put forward a simplified formula based on Wait's theory and it can be extensively used [Nickolaenko and Hayakawa, 2002]. Location accuracy of this method by studying Schumann Resonance caused by strong lightning events is one hundred times larger than that of NLDN [Boccippio et al., 1998].

The concept of wave impedance was proposed by Kemp and Jone [Kemp and Jone, 1971], which is the ratio of electric and magnetic field amplitude. Korol and Nickolaenko investigated the pattern of wave impedance versus distance and found a routine for source-observer distance derivation. They also pointed out that reflection from ionosphere could be ignored within a short distance observation such as 50 km [Korol and Nickolaenko, 1993].

The phase difference between the electric field and magnetic field also contains the distance information. At low frequency and short distance the phase difference is -90 degree, when the frequency gets higher or distance gets increasing, the phase difference is close to 0 degree. This property has been utilized by [Shvets et al., 1997].

Lights with different wavelength travel at different speeds during the same medium. So does the signal emitted by lightning. The group speeds of ELF/VLF at different frequency are different. The time delay of signal on different frequency is able to tell the distance. A simple method based on delay time difference was described by Ramachandran. His location results have been tested and verified with World-Wide Lightning Location Network (WWLLN). Its working range is from 3000 to 16250 km with an average deviation of 4.7% within 3500 km [Ramachandran et al., 2007].

Another difference among different frequency is the group delay. It is defined as the

differential of phase versus frequency. However, this method is only valid for distance large than 1000 km with an accuracy of 100 km [Brundell et al., 2002].

6.3 Present single-station lightning location technique

6.3.1 Basic theory of present technique

The lightning return stroke channel can be viewed as a vertical electric dipole antenna standing on conductive plane, when both the frequency wavelength and the source-observer distance concerned are much longer than the lightning channel scale. Although the lightning stroke channel is usually several kilometers long, its effective length may be shorter than 1 km because the stroke current is found to attenuate significantly as it propagates from ground upwards. Meanwhile, after a few milliseconds, the lightning channel may extend into the cloud with horizontal movement of charge in clouds. So the lowest frequency free from much noise may be several hundred hertz. Based on all these aspects, the dipole model might be valid for lightning stroke at distances more than 5 km away and for frequency bands from 100Hz to more than 15 kHz. This is the basis of the present study.

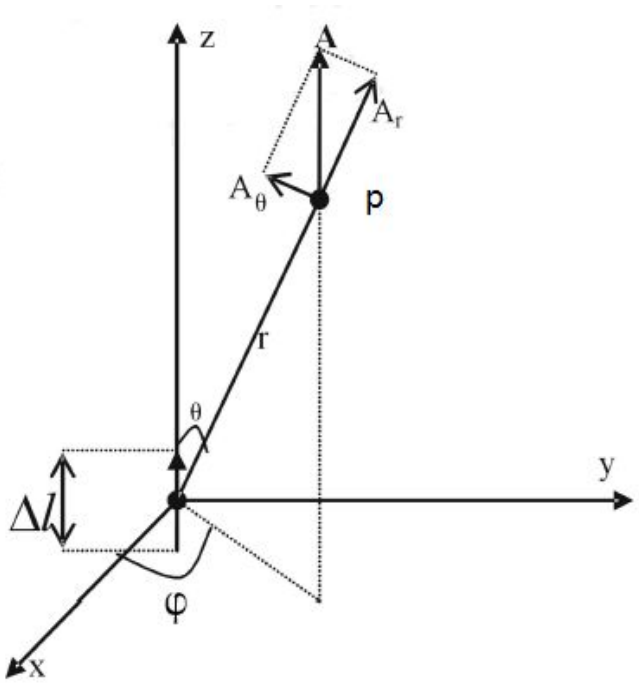

Fig. 6.1 Schematic diagram of an electric dipole in coordinate

Suppose the lightning current is *I* with a length of *dl* as shown in Figure 6.1. The current dipole is along *z* axis and at the origin point of the coordinate system. Then vector potential at point *P* in space is given by the formula:

$$A(r) = \frac{\mu}{4\pi}\int_{l} \frac{Idl\,\hat{a}_z}{r} e^{-jkr} = \hat{a}_z \frac{\mu}{4\pi} \bullet \frac{Idl}{r} e^{-jkr}.$$

here spherical coordinate is employed so that the vector potential is:

$$A = \hat{a}_r A_z \cos\theta - \hat{a}_\theta A_z \sin\theta \quad \text{and} \quad A_z = \frac{\mu}{4\pi} \bullet \frac{Idl}{r} e^{-jkr}.$$

with this, electromagnetic field at point *P* can be calculated as:

$$\hat{H} = \frac{1}{\mu}\nabla \times A = \frac{1}{\mu \bullet r^2 \sin\theta}\begin{vmatrix} \hat{a_r} & r\hat{a_\theta} & r\sin\theta\hat{a_\varphi} \\ \frac{\partial}{\partial r} & \frac{\partial}{\partial \theta} & \frac{\partial}{\partial \varphi} \\ A_z\cos\theta & -rA_z\sin\theta & 0 \end{vmatrix}$$, and

$\hat{E} = \frac{1}{j\omega\varepsilon}\nabla \times \hat{H}$ [Lu et al., 2006].

Since the observer antenna is at ground level, θ tends to be $\pi/2$. Only horizontal magnetic field and vertical electrical field would exist at the observer.

So for a dipole current Idl at radian frequency ω, the vertical electric field E_ω and horizontal magnetic field H_ω at distance r from the observer on ground are given by

$$E_\omega = \frac{Idlk^3}{4\pi\omega\varepsilon}[\frac{j}{kr} + \frac{1}{(kr)^2} - \frac{j}{(kr)^3}]e^{-jkr} \quad (6.1)$$

$$H_\omega = \frac{Idlk^2}{4\pi}[\frac{j}{kr} + \frac{1}{(kr)^2}]e^{-jkr} \quad (6.2)$$

where c is the speed of light.

Both the electric and magnetic fields attenuate with the growth of distance. The magnitude of either the electric or the magnetic fields cannot tell the distance because the current of lightning stroke is not a constant. However, the ratio of electric and magnetic fields no longer depends on the lightning current and it varies with source-observer distance.

$$|\frac{E_\omega}{H_\omega}| = G\sqrt{\frac{\mu_0}{\varepsilon_0}}\,|\frac{1}{kr} - \frac{1}{j+\frac{1}{kr}}| \qquad (6.3)$$

$$|\frac{E_\omega}{H_\omega}| \approx G\sqrt{\frac{\mu_0}{\varepsilon_0}} = A, \quad \text{for 60~120 kHz} \qquad (6.4)$$

where, G is a correction coefficient taking account of the difference in systematic gain between the measuring systems for the electric and magnetic fields. The term (*kr*) will be much larger than 1 at a moderate distance for high frequencies such as 60 ~ 120 kHz, and the ratio of electric and magnetic fields tends to be a constant (*A*) as shown by Eq. (6.4). On the contrary, the term (*kr*) will be much smaller than 1 at a moderate distance for low frequencies such as 100 Hz ~ 15 kHz, and the ratio of electric and magnetic fields tends to follow Eq. (6.5).

$$|\frac{E_\omega}{H_\omega}| \to \frac{A}{kr} + \delta = \frac{B}{f} + \delta, \qquad \text{for 100Hz ~15kHz} \qquad (6.5)$$

$$r = \frac{cA}{2\pi B} \qquad (6.6)$$

where, δ is a figure much smaller than 1. By curve fitting of Eq. (6.4) & (6.5) with the spectra of electric and magnetic fields observed, the *A* and *B* can be found, and then the source-observer distance is found. A specific algorithm for source-observer distance determination with Eqs. (6.5) and (6.6) is as following:

1) Record the (*E*) and (*H*) fields of a stroke at a single-station in VLF/LF bands simultaneously;

2) Get the spectra of ($E\omega$) and ($H\omega$) by Fast Fourier Transform, plot ($E\omega/H\omega$) versus frequency (f);

3) Fit the plots ($E\omega/H\omega$ *v.s* f) at high frequency bands (60~ 120 kHz) with Eq. (6.4) to get (A); this is for gain calibration between the electric and magnetic field measurements;

4) Fit the plots ($E\omega/H\omega$ *v.s* f) at low frequency bands (100 Hz ~ 15 kHz) with Eq. (6.5) to get B;

5) Get source-observer distance from (A) and (B) by Eq. (6.6).

The above approach has a precondition that the data acquisition system should cover the frequency bands from where ($kr<<1$) to where ($kr>>1$). For instance, for locating a lightning stroke at a distance up to 300 km, the lower frequency boundary of the system should be much less than 160 Hz, and that for locating a lightning stroke at a distance up to 150 km should be much less than 320 Hz, etc.

In fact, the Fast Fourier Transform of E and H fields also contain their phase differences. The Eq. (6.1) divided by Eq. (6.2) indicates the phase differences between electric and magnetic fields as:

$$\frac{E_\omega}{H_\omega} = \frac{-jk}{\varepsilon_0 \omega} \bullet \left(\frac{1}{kr} + \frac{j^2}{j + \frac{1}{kr}}\right) \qquad (6.7)$$

as shown in Eq. (6.7), the phase difference between E and H is closed to $-\pi/2$ when $kr<<1$ and the phase difference tends to 0 when $kr>>1$. In other words, the phase differences of different frequencies would vary within $-\pi/2$ to 0 for a certain distance. The curve of phase angle versus frequency is modulated by the distance. To derive the distance, there are two kinds of approaches. One is let the distance r become a parameter for curve fitting. Fit the experimental data with theoretical phase angle curve. The other one is based on single frequency point analysis. The experimental data contains phase angle of E/H information. Each frequency point is corresponding to a phase angle. The phase angle of a frequency in experimental data can be picked out and which distance at this frequency would have this phase angle can be found out in theory. Final result of the source distance should be based on combined consideration of several frequency points.

The influence of ground surface which is not a perfect conductor needs to be also investigated. Model of a vertical electric dipole over a stratified half-space is taken into account. This problem was firstly investigated by Sommerfeld [Sommerfeld, 1926]. He presented this model when they consider the propagation of radio waves along the ground surface. This model takes the earth as a homogeneous dissipative half-space. Although it does not consider the curvature of ground surface and the reflection of ionosphere, it is reasonable to make that kind of approximation when people focus on a short range of transmission. Wait summarized this problem and gave a comprehensive result in his book [Wait, 1962].

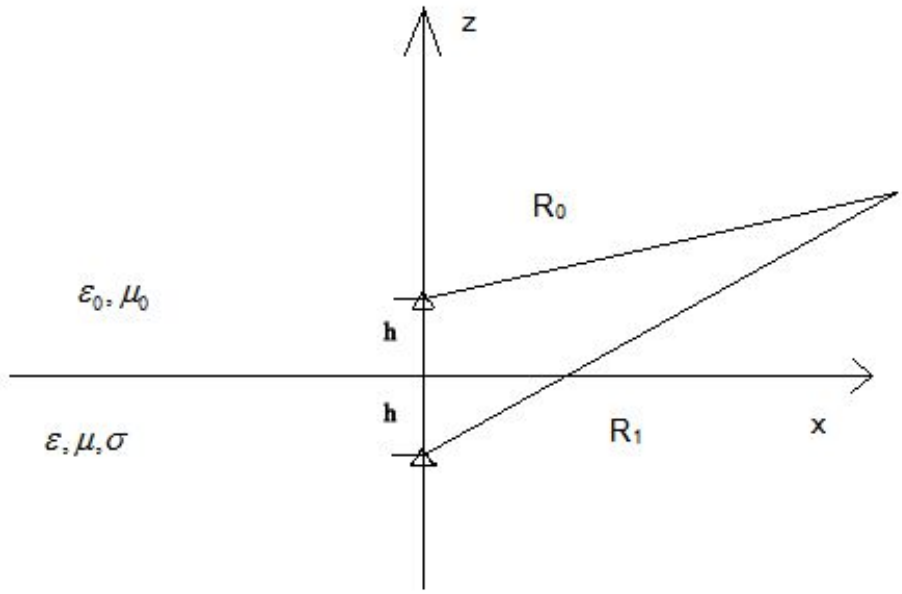

Fig. 6.2 Schematic diagram of a vertical electric dipole over a stratified half-space

As show in Fig. 6.2, the interface of air and ground is the plane *z=0*. A vertical electric dipole *Idl* is at the *z* axis with a distance of *h* from ground. Wait deduced the vector potential at those two half space. Here only the upper half-space is concerned and the vector potential at that space is

$$A_{z0} = \frac{\mu_0 Idl}{4\pi}[\frac{e^{-ik_0 R_0}}{R_0} + \frac{e^{-ik_0 R_1}}{R_1} - 2P] \qquad (6.8)$$

where, $P = \int_0^\infty \frac{(ik_0\lambda\Delta)e^{-u_0(h-z)}}{(u_0 + ik_0\Delta)u_0} J_0(\lambda\rho)d\lambda$,

$\Delta = \frac{\mu}{\sigma + i\omega\varepsilon}$, $u^2 = \lambda^2 + i\sigma\mu\omega - \varepsilon\mu\omega^2$, $\rho^2 = R_0^2 - (z+h)^2$, and

z is the height of observer and λ can be any value. Eq. (6.8) has its physical

interpretation. The first two terms mean the vector potential of the electric dipole and its mirror and the *2P* represents an amendment because the ground is non-perfect conductor. If the conductivity in Eq. (6.8) tends to be infinite, *2P* will tends to be zero and only the electric dipole and its mirror are left.

When calculate the electromagnetic field of such a vertical electric dipole, further simplify can be made. Gated wideband antenna is able to display only the initial ground wave portion of the VLF signals to avoid the non-vertical lightning channel sections' influence. So the height (*h*) of effective lightning stroke channel as an electric dipole can be set to zero. If the observer also at ground level ($z = h = 0$), the vector potential at the observer point becomes

$$A_{z0} = \frac{\mu_0 Idl}{2\pi} \frac{e^{-ik_0 R}}{R} F(p_e) \qquad (6.9)$$

where *R* is the distance between dipole source and observer, $P_e = \frac{-ik_0 R}{2}\Delta^2$, and F() is a function which is defined as $F(w) = 1 - i(\pi w)^{1/2} e^{-w} erfc(iw^{1/2})$.

Once the vector potential is appeared, electromagnetic fields could be obtained by the following formula

$B = \nabla \times A$ and $E = -i\frac{\nabla \times B}{\varepsilon\omega\mu}$.

it was found that with the growth of frequency, the *B* and *E* fields of a dipole over a

non-perfect conducting ground ($\sigma=0.001$) attenuate faster than that over a perfect conducting ground ($\sigma>>1$). A rough explanation for this phenomenon was given by [Guo, 1997]. According to Ohm's Law, current in a conductor is $J = \sigma E$. Maxwell's equations tell that $\varepsilon \nabla \bullet E = \rho$, so $\nabla \bullet J = \frac{\sigma}{\varepsilon}\rho$, if take charge conservation principle into account, a following equation comes out,

$$\frac{\partial \rho}{\partial t} = -\nabla \bullet J = -\frac{\sigma}{\varepsilon}\rho \qquad (6.10)$$

The charge density in a conductor is deduced by solving this differential equation as,

$$\rho(t) = \rho_0 e^{-\frac{\sigma}{\varepsilon}t} \qquad (6.11)$$

Eq. (6.11) means that when $\omega << \tau^{-1} = \frac{\sigma}{\varepsilon}$, the conductor can be viewed as a perfect conductor. If the frequency goes higher and the conductivity is not very large such as the dry ground, the soil may not be viewed as a perfect conductor. It means that there would be charge or energy dissipating inside the conductor.

Fortunately, the *E/H* versus frequency pattern almost not change no matter it is a perfect conducting ground or not. It is reasonable to ignore the existence of a non-perfect conductive ground surface when computing the source-observe distance based on Eq. (6.7). As shown in Fig. 6.3, for a certain distance (50 km in this figure), the amplitude of ratio of *E* and *H* decreases with frequency and then increases to a value very near 377.

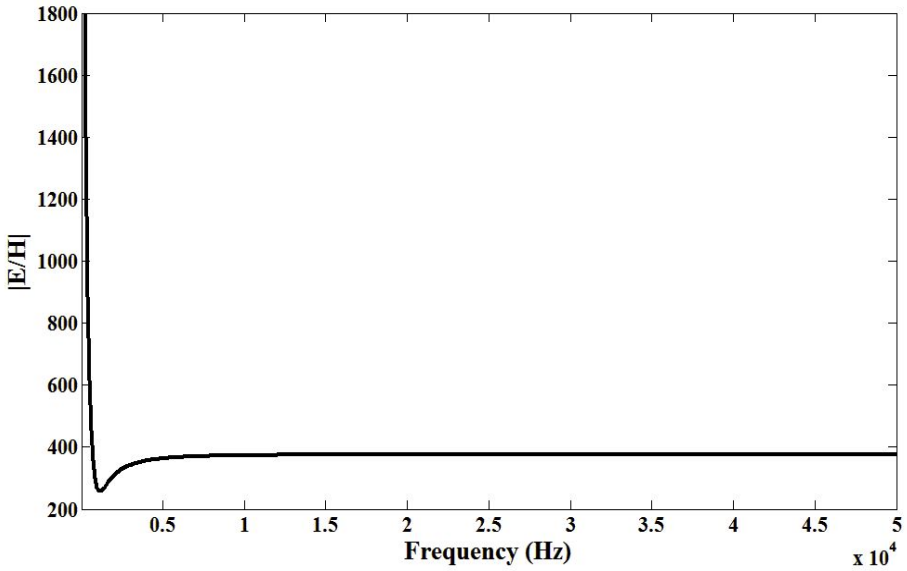

Fig. 6.3 A typical *E/H* versus frequency pattern for a distance r = 50 km in Eq. (6.7)

6.3.2 Validation of the present technique

With the data obtained by the ILD (Integrated Lightning Detecting system) (see Chapter 3 for details of the ILD), the above theory has been examined.

Fig.6.4 shows the electric and magnetic fields recorded simultaneously by the ILD for a close negative return stroke occurred at 11:45:32 on 13 August, 2005. Where (*E*) is the vertical electric field in frequency bands of 100 Hz to 1 MHz, (*Bsn*) the output of south-north magnetic loop and (*Bew*) the output of east-west magnetic loop in frequency bands of 100 Hz to 200 kHz, of the ILD. Positive value of the electric field indicates negative cloud to ground lightning stroke. Empirically, the waveforms of Fig.6.4 indicate that this return stroke is around 10 -20 km.

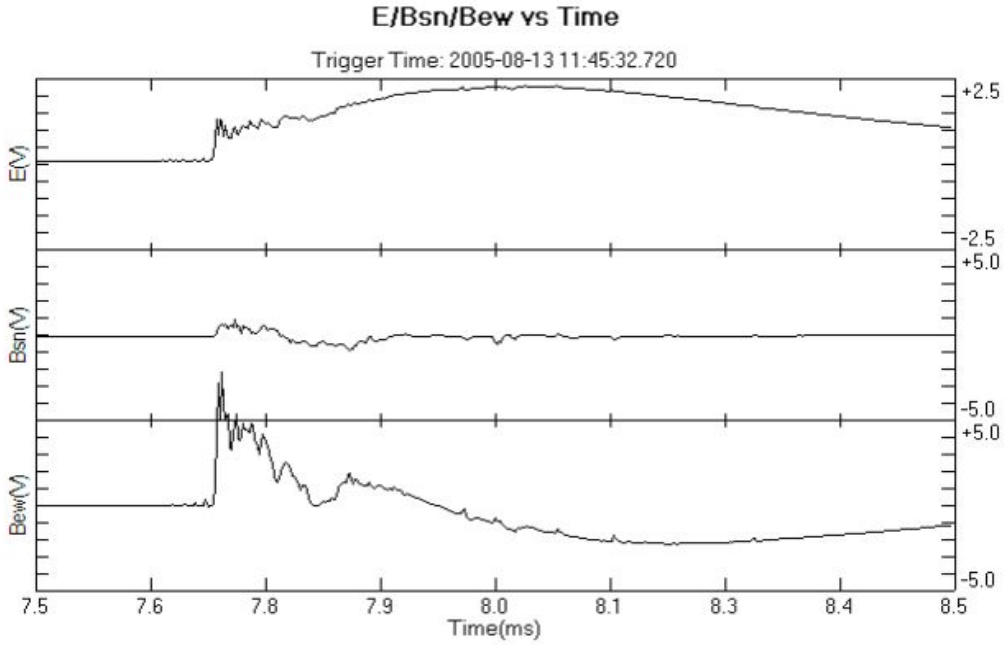

Fig. 6.4 Electric and magnetic fields measured for a return stroke occurred at 11:45:32 on 13 Aug., 2005. Where (*E*) is the vertical electric field in frequency bands of 100 Hz to 1 MHz, (*Bsn*) the output of south-north magnetic loop and (*Bew*) that of east-west magnetic loop in frequency bands of 100 Hz to 200 kHz, of the ILD

Fig. 6.5 is the spectra of the electric field, Fig. 6.6 is that of the magnetic field, and Fig. 6.7 is the ratio of spectra of the electric and magnetic fields, for the same return stroke shown in Fig. 6.4. The magnetic field spectra, therefore the *E/B* (or *E/H*) ratios, are calculated based on either the lager one or the combination of two magnetic field components (*Bsn* and *Bew*) in case.

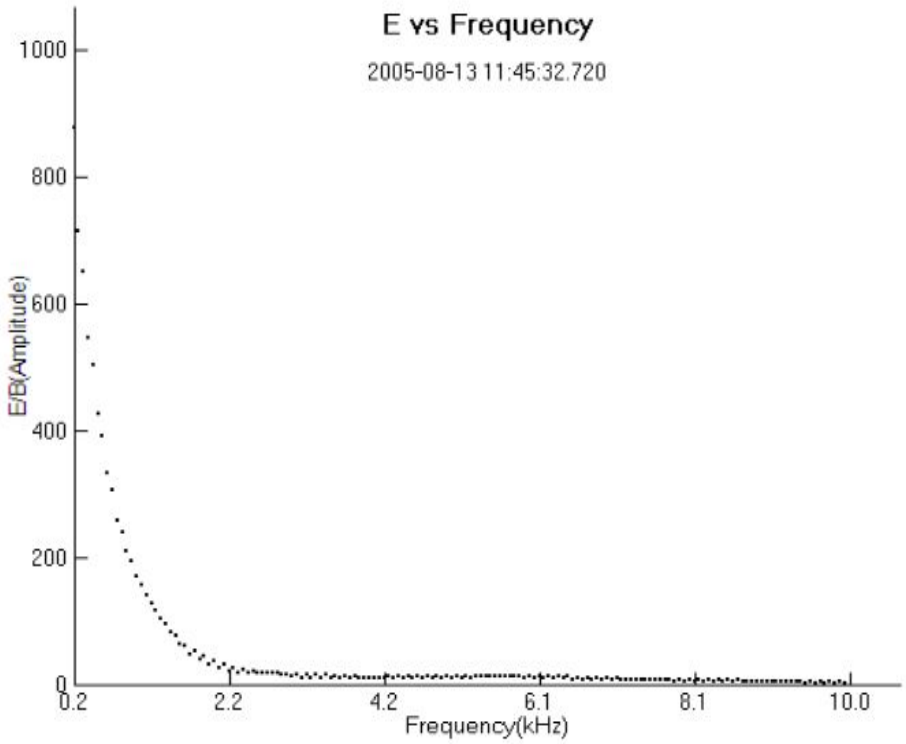

Fig. 6.5 Spectra of the electric field for the stroke shown in Fig. 6.4

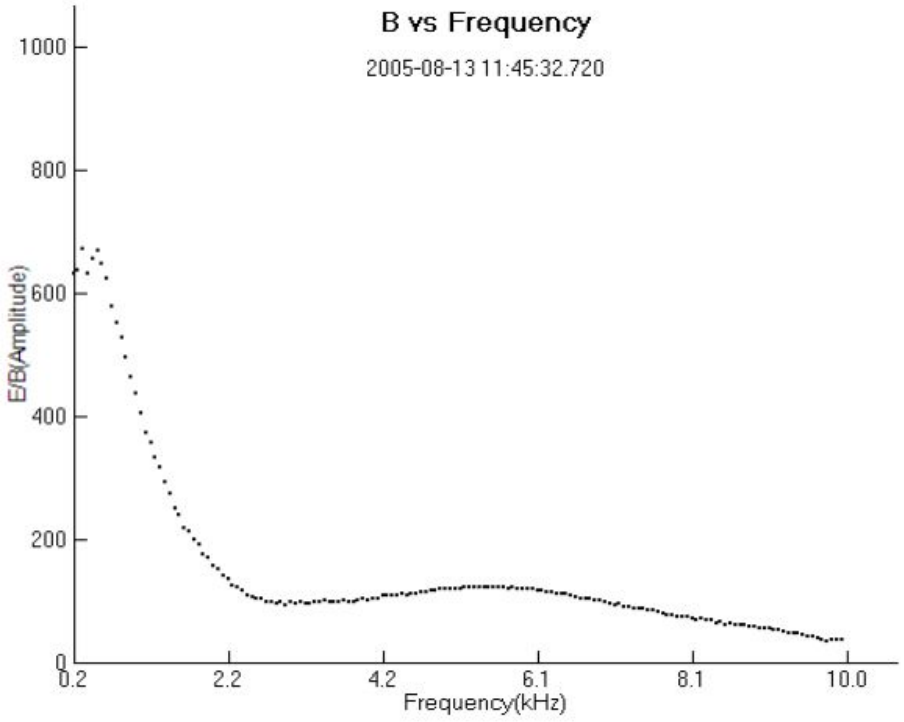

Fig. 6.6 Spectra of the magnetic field for the stroke shown in Fig. 6.4

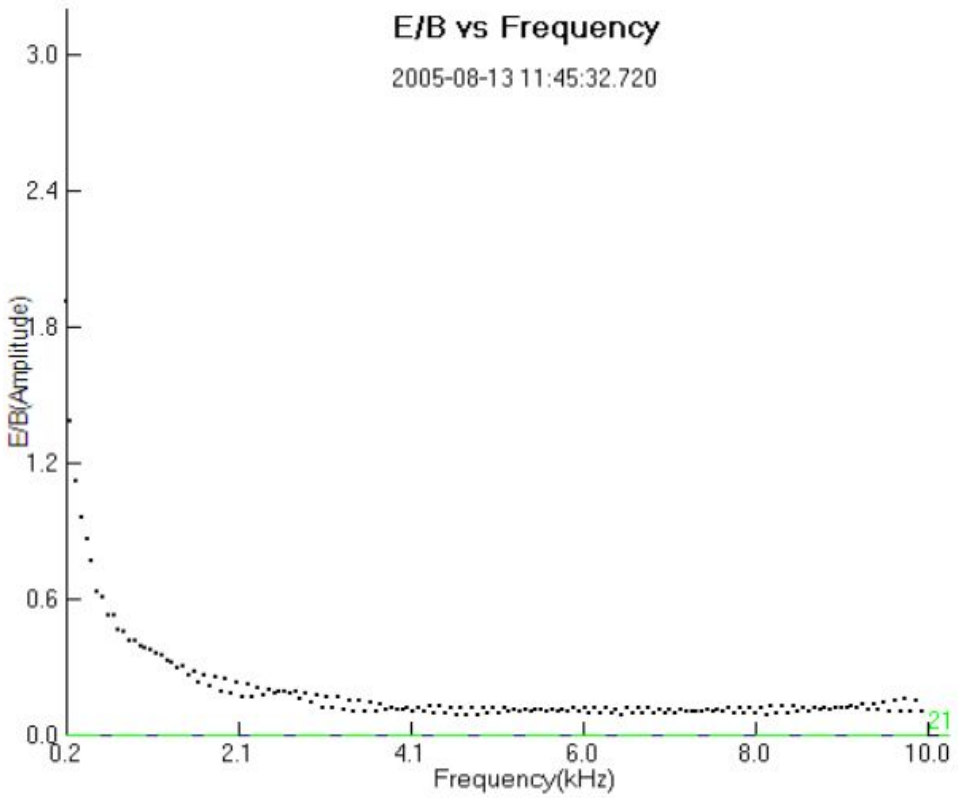

Fig. 6.7 Observed *E/B* (or *E/H*) ratio versus frequency for the stroke shown in Fig. 6.4

Fitting of Eq. (6.4) with (*E/B*) ratio in high frequency bands (say 61~102 kHz) gives coefficient (*A*). Fitting of Eq. (6.5) with (*E/B*) ratio in low frequency bands (say 122 Hz to 10 kHz) as shown in Fig. 6.8, gives coefficient (*B*).

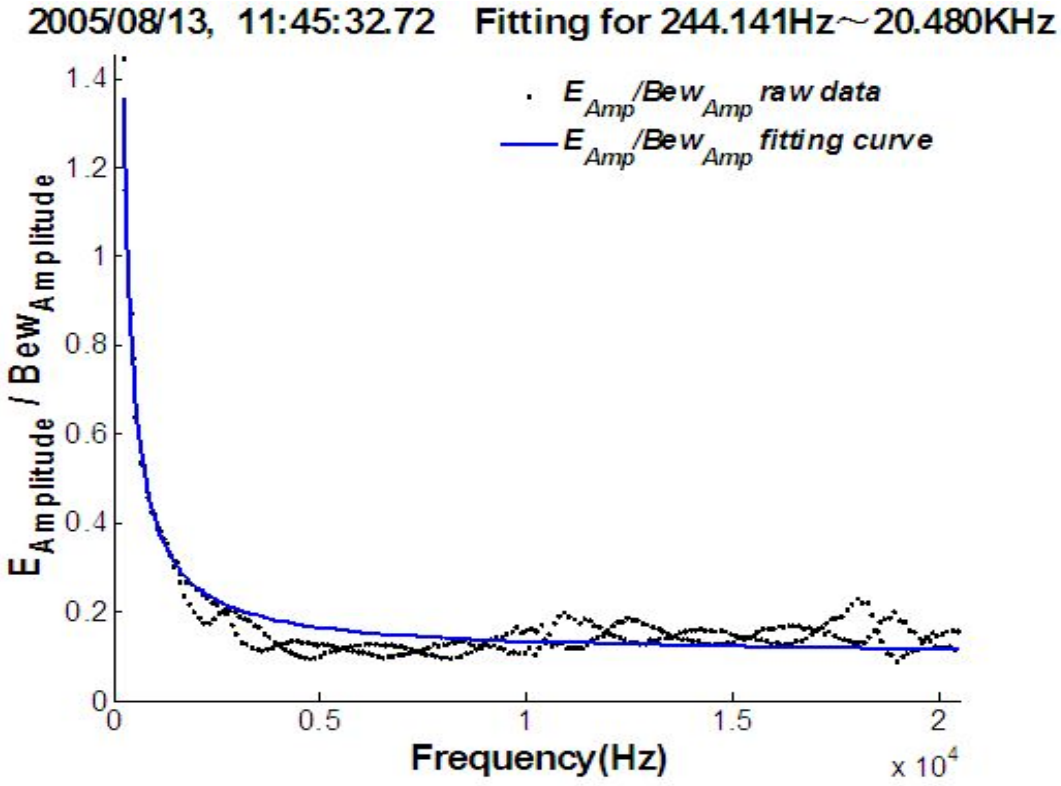

Fig. 6.8 Curve fitting of the *E/B* ratio with Eq. (6.5) for the stroke in Fig. 6.4

In practice, the range of frequency chosen for curve fitting would influence the results slightly. Estimations have been done for different frequency ranges and the results are shown in Table 6.1. The distance of the stroke found is in the range of 8.2 - 8.9 km, which is well consistent with the empirical value.

Table 6.1 Locating results for the stroke shown in Fig. 6.4

2005/08/13 11:45:32.72, Azimuth = 74.6°					
Low band (*f*)	**Coeff. *B***	***δ***	**High band (*f*)**	**Coeff. *A***	***r* (km)**
122Hz ~3kHz	872.76	-0.2206			8.2
122Hz ~6kHz	844.10	-0.1205	61 ~ 102 kHz	0.15	8.4
122Hz ~ 10kHz	821.85	-0.0618			8.7
122Hz ~15kHz	800.94	-0.0074			8.9

Figs. 6.9 and 6.10 show the measured electric and magnetic fields for two more return strokes occurred during the same storm as that in Fig. 6.4. Empirically, Fig. 6.9 seems to be the field waveforms of a return stroke at around 10-20 km, and Fig. 6.10 seems to be that of a return stroke at a distance more than about 30 km away. The locating results are shown in Tables 6.2 and 6.3, respectively. The return stroke distance found for Fig. 6.9 is in the range of 18.3 - 19.2 km and that for Fig. 6.10 is of 42.4 - 49.2 km. Both are well consistent with the empirical values. These three examples indicate that the proposed method can work well for close return strokes at least in the analyzed range of 10 - 50 km.

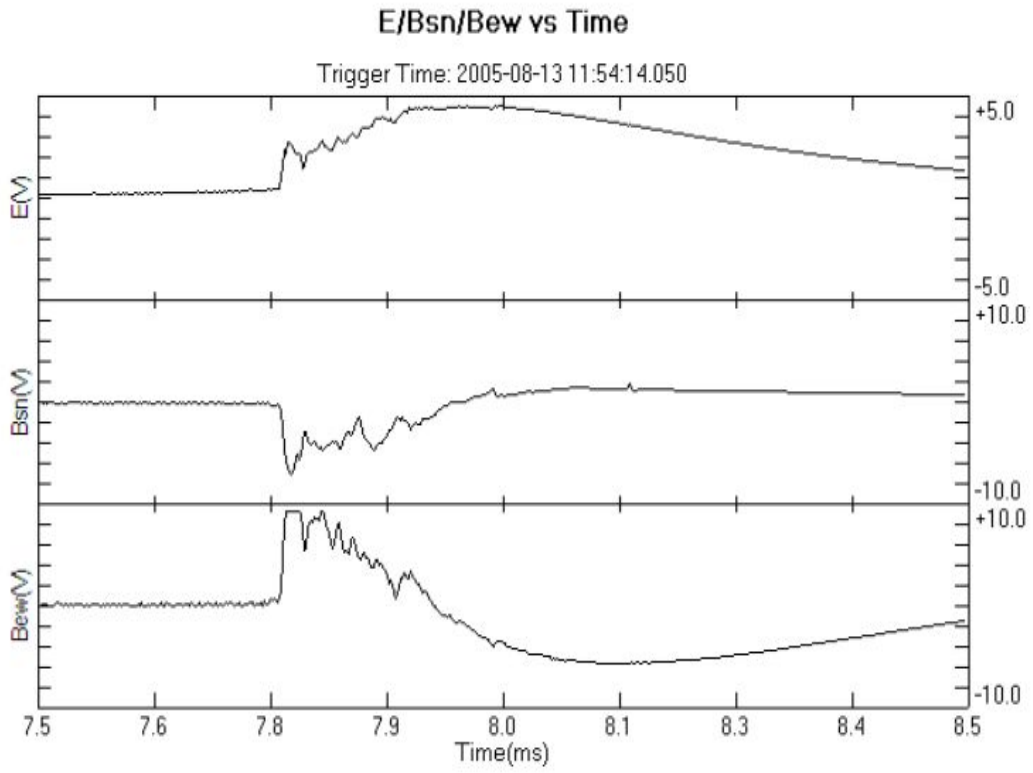

Fig. 6.9 Same as Fig. 6.4 but for a stroke occurred at 11:54:14, 13 Aug., 2005

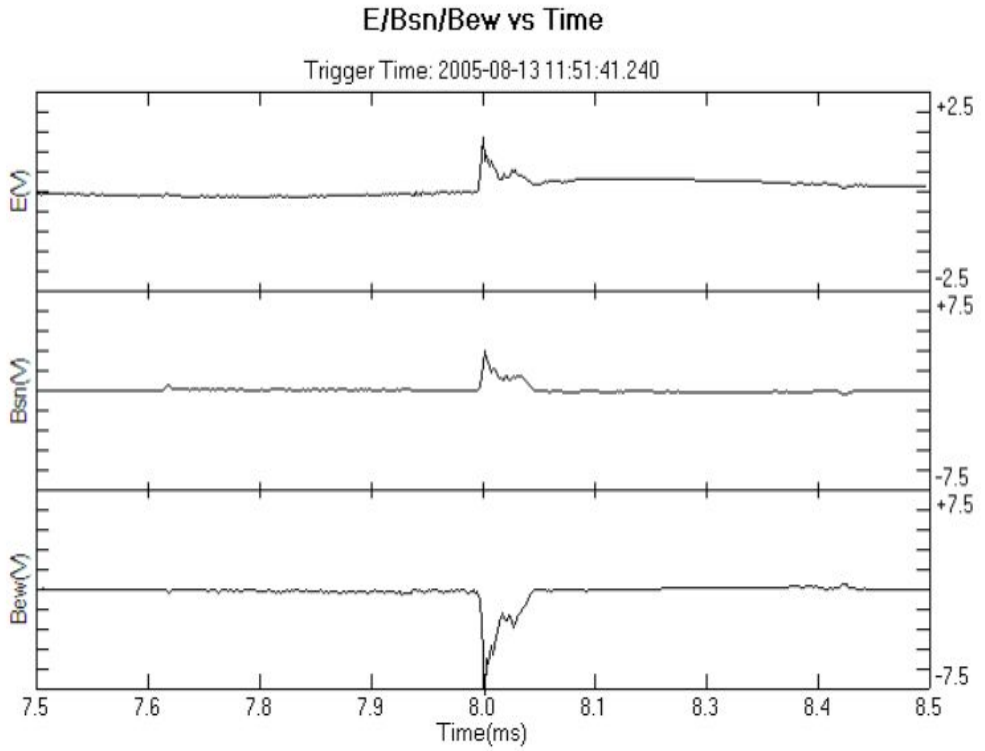

Fig. 6.10 Same as Fig. 6.4 but for a stroke occurred at 11:51:41, 13 Aug., 2005

Table 6.2 Locating results for the stroke shown in Fig. 6.9 (Azimuth 327.4°)

Low band (*f*)	**Coeff. *B***	δ	**High band (*f*)**	**Coeff. *A***	***r* (km)**
122Hz ~3kHz	460.65	0.0157			18.3
122Hz ~6kHz	462.92	0.0077	61~ 102 kHz	0.18	18.2
122Hz~10kHz	453.27	0.0350			18.6
122Hz ~15kHz	438.84	0.0725			19.2

Table 6.3 Locating results for the stroke shown in Fig. 6.10 (Azimuth 157.8°)

Low band (*f*)	**Coeff. *B***	***δ***	**High band (*f*)**	**Coeff. *A***	***r* (km)**
122 Hz ~3 kHz	141.32	0.1964			49.2
122 Hz ~6 kHz	162.07	0.1262	61 ~102 kHz	0.15	42.9
122 Hz~10 kHz	164.11	0.1202			42.4
122 Hz ~15 kHz	163.47	0.1218			42.6

In Section 6.3.1, the phase difference algorithm was also introduced with Eq. (6.7). Following is an example for validation of the relationship between *E/H* phase difference and source distance with the ILD data. A lightning flash occurred at 12:42:16.27, on 22 April, 2010 was captured by the ILD. Fig 6.11 shows its original data.

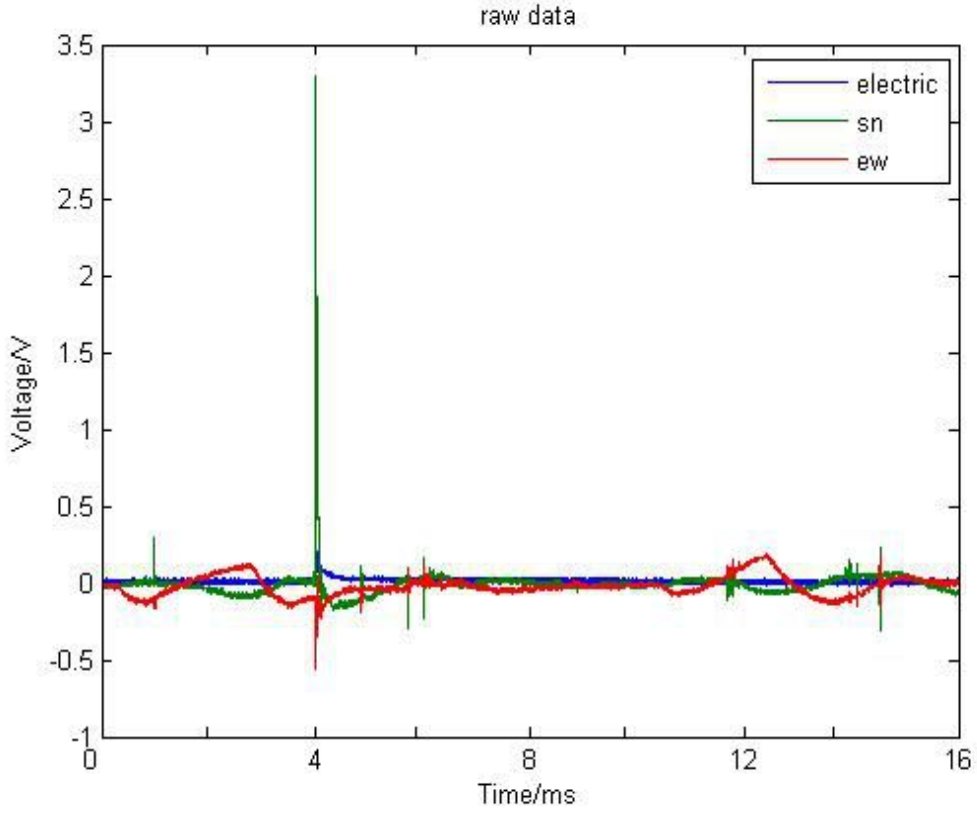

Fig. 6.11 Original data for a lightning stroke occurred at 12:42:16.27, on 22 April, 2010. The "sn" indicates the magnetic field from south-north loop, "ew" indicates the magnetic field from east-west loop and "electric" indicates the *E*-field

This is a negative cloud to ground flash. All the three groups of data have been fast Fourier transformed to get their frequency spectra (Fig. 6.12). Two channels (SN and EW) have recorded the magnetic field. The final *H*-field spectra are based on the combination of two channels' spectra $H_\omega = \sqrt{H_{sn\omega}^2 + H_{ew\omega}^2}$.

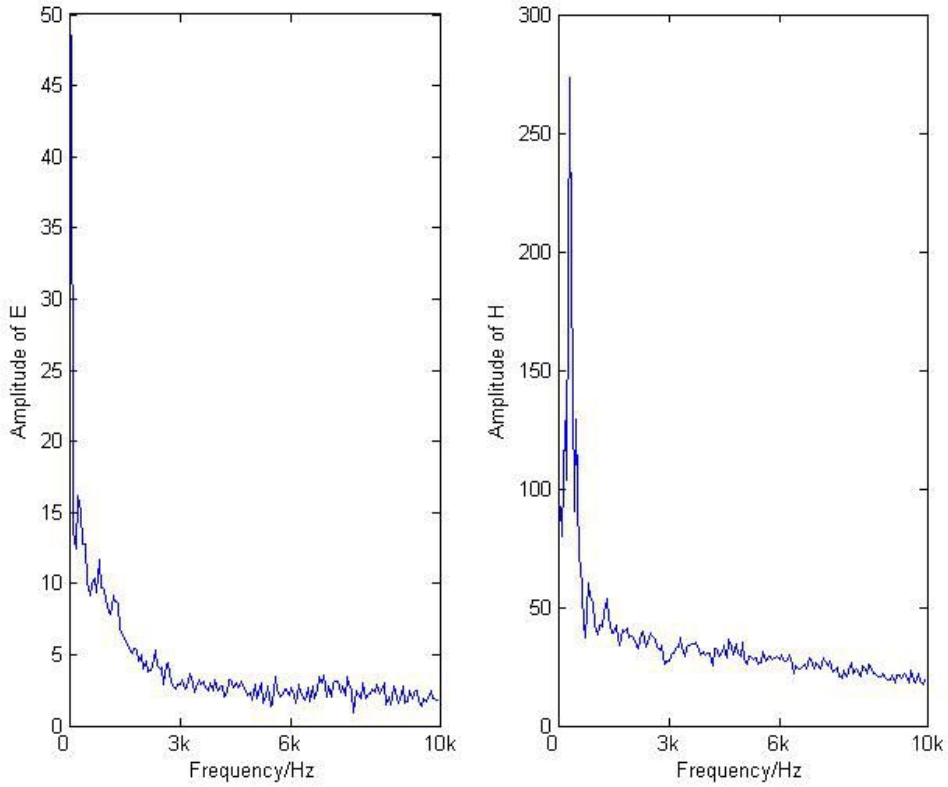

Fig. 6.12 Spectra of the electric (*E*) and magnetic (*H*) fields for the lightning return stroke shown in Fig. 6.11

Then the *E/H* versus frequency pattern is obtained as shown in Fig. 6.13. It is very similar to Fig. 6.3. This indicates that the experiment data has covered the essential frequency range with a same gain.

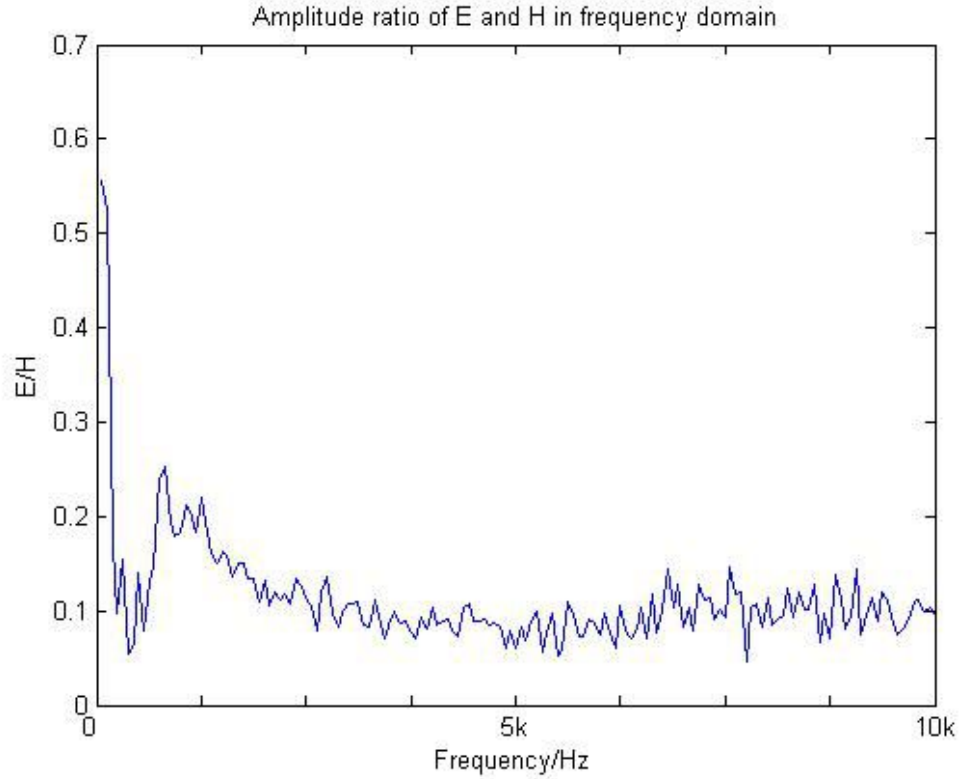

Fig. 6.13 Ratio of *E/H* versus frequency for the return stroke in Fig. 6.11

Fast Fourier Transform of time domain signal not only gives out the amplitude spectra but also the phases. The phase differences between *E* and *H* versus different frequencies for the same stroke in Fig. 6.11 has been plotted and shown in Fig. 6.14.

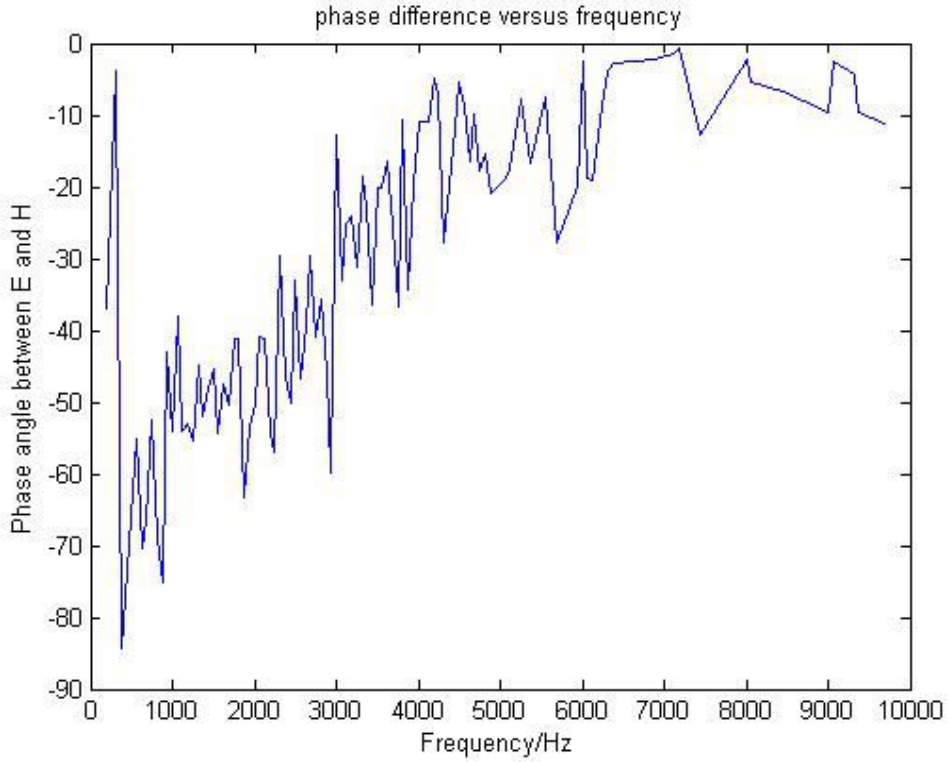

Fig. 6.14 Phase differences between *E* and *H* versus frequency for the same lightning stroke in Fig. 6.11

Set the range of lightning source as a variable parameter and fit the pattern in Fig. 6.14 with theoretical curve. Fig 6.15 is the curve fitting results and the lightning stroke distance (*r*) determined is 21.8 km.

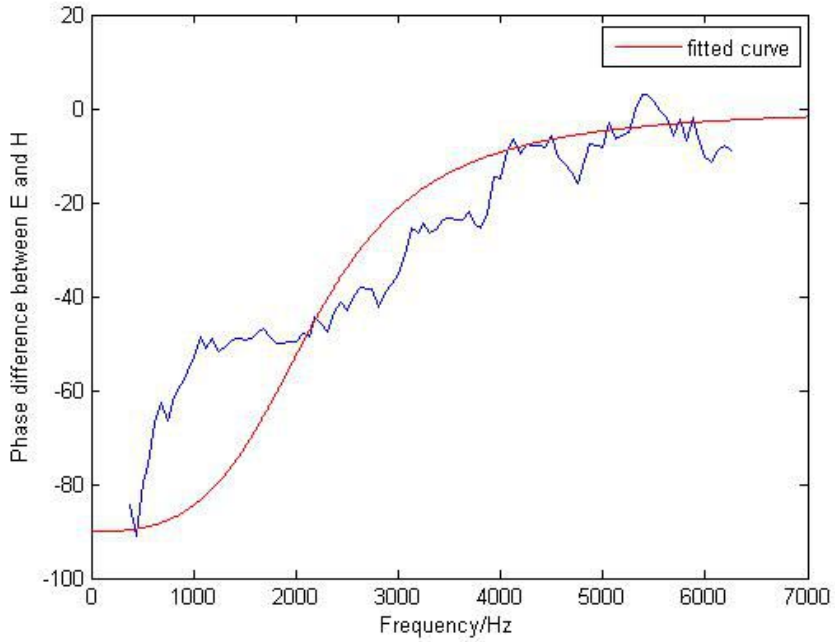

Fig. 6.15 Curve fitting result of the *E/H* phase difference versus frequency pattern for the stroke in Fig. 6.11. Red line represents the theoretical curve for r =21.8 km

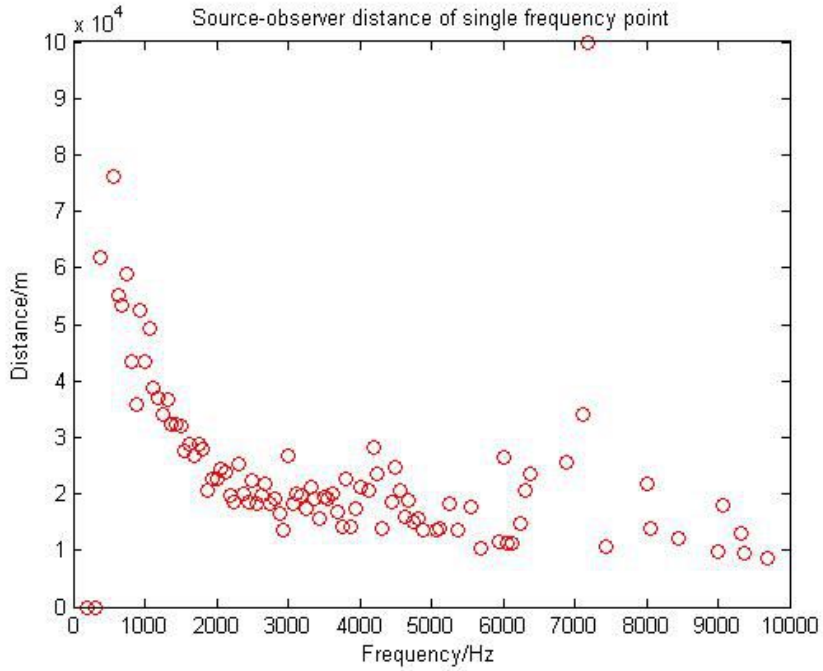

Fig. 6.16 Source distances determined by *E/H* phase difference at individual frequency points for the same returns stroke in Fig. 6.15

The *E/H* phase difference at an individual frequency can also be used to derive the source distance. For example, the 3000 Hz in Fig. 6.15 is corresponding to a phase difference of -12.78 degree. Phase difference between *E* and *H* in theory depends on both range *r* and frequency *f*, as shown by Eq. (6.7). The source distance can then be found by searching from 100 m to 100 km with a 100 m step at 3000 Hz in Eq. (6.7) until it gives a phase difference of -12.78 degree. The searching result at 3000 Hz for the present stroke is 26.80 km. The E/H phase differences for other frequencies can be processed in a similar way and their results have been found and shown in Fig. 6.16. The average value of the results in Fig. 6.16 is 24.1 km, similar to that in Fig. 6.15.

6.4 Configuration of a single-station lightning locating system based on our proposed technique

Based on the technique stated in Section 6.3, a prototype single-station lightning locating system (S-LLS) has been developed and setup in field for experiment. At present, only the algorithm based on Eqs. (6.5) and (6.6) was employed.

The system is composed of three modules: Lightning Signal Sensing (LSS), Lightning Data Acquisition (LDA) and Lightning Data Display (LDD) modules (Fig. 6.17).

The LSS module is responsible for electromagnetic signals capture. It includes 1

flat-plate electrical antenna, 2 crossed-loop magnetic antennas, a CG/CC logic circuit and a lightning simulator for testing. As shown in Fig. 6.18, CG/CC logic circuit judges lighting signal waveform by a series of criteria including threshold voltage value, rise-time, decay time, extra pulse, pinnacle pulse, and reverse pulse. Threshold value is related to installation environment, a typical value is 100 mV. For a return stroke, the rise time of electric field waveform should be shorter than 18 μs and fall time should be longer than 10 μs. All those interference pulses except main peak should stay within an empirical limit when compare to main peak. Only signal meets the criteria above will be classified as Cloud-to-Ground discharge. CG/CC logic results also contain the judgment to the lightning signals' polarity. Lightning flash can be divided into four major categories, i) positive cloud to ground flash, ii) positive cloud to cloud flash, iii) negative cloud to ground flash, iv) negative cloud to cloud flash. The 3 analog signals (*E*-field and two *H*-field) and the CG/CC logic result are then transmitted to the LDA module for processing. The bandwidth for both the electric and magnetic antennas is much wider than 100 Hz – 200 kHz. The LSS module is enclosed in a glass-fiber dome, which is transparent to electromagnetic field in frequencies 5 Hz above.

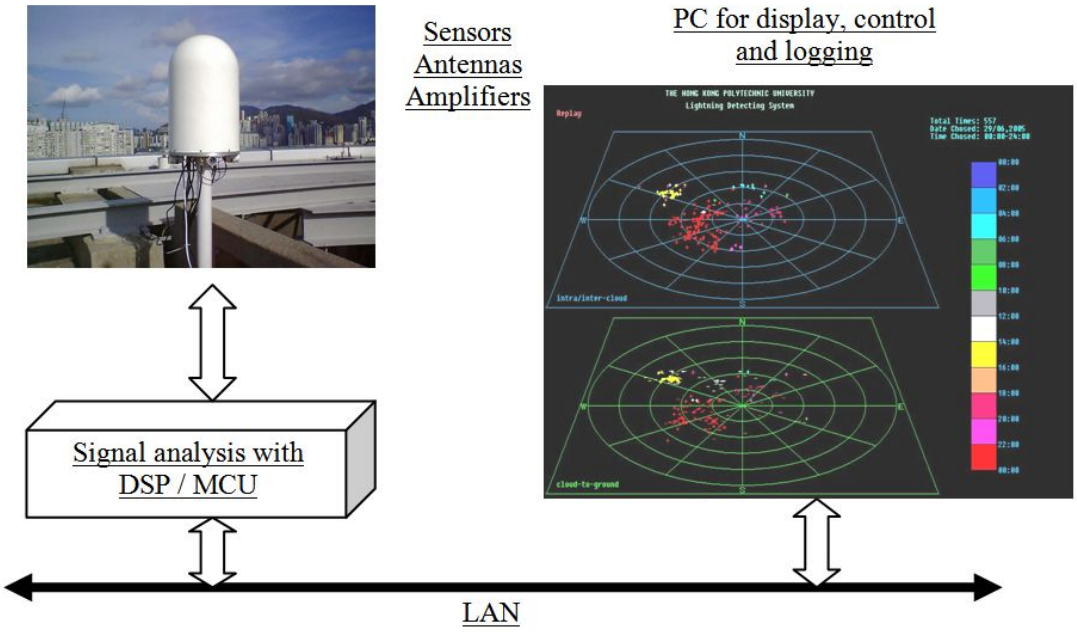

Fig. 6.17 Block diagram of the single station lightning locating system (S-LLS)

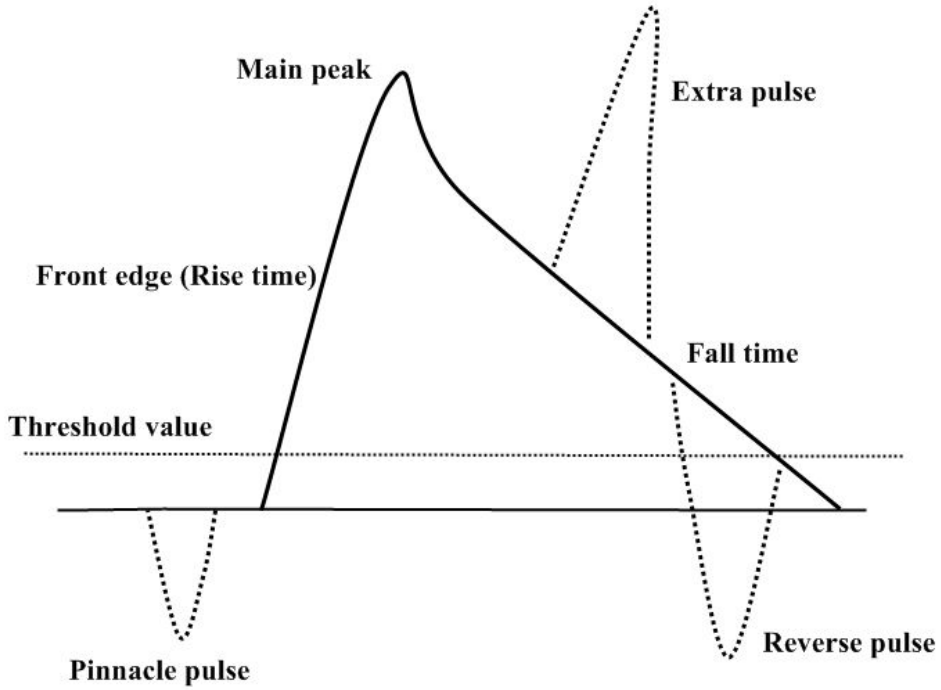

Fig. 6.18 Illustration of the criteria for CG lightning stroke waveform in the S-LLS

The LDA module is a micro-computer based data processor with imbedded A/D converters, which is programmed to process the signals from the LSS based on our proposed lightning locating theory. The three analog signals are time-stamped and sampled at a rate of 512 kHz, with a recording time of 16 ms for each impulsive event, triggered by the electric signal. Those digital data are then processed to determine the location of the impulse source. The CG/CC logic circuit on the LSS module provides information of type of the lightning impulse. For each lightning event, the LDA outputs the event occurring time, location, strength and flash type to an on-board memory and meanwhile transmits these data to LDD module.

The LDD module is a software pack installed on a common PC that is connected to the LDA module via internet. It offers real-time lightning monitoring and off-line data playback functions. Tasks of LDD include visualization, statistical analysis and permanent storage of lightning events. Up to 3 LDDs/users can be connected to the LDA simultaneously.

6.5 Experimental results with the S-LLS

For field experiment, the S-LLS developed has been setup at the Hong Kong Sea School (site location: latitude 22.217°N, longitude 114.214°E) since the summer of 2010. Lightning location data obtained by the S-LLS was compared with those by a 6-station LLN of Hong Kong Observatory (HKO).

The HKO website [Website_2 2013] provides location information of cloud-to-ground (CG) and cloud-to-cloud (CC) flashes detected by the network. Lightning records are updated every five minutes. It is claimed that for -CG flashes the HK-LLN has a spatial accuracy of 500 m and a detection efficiency of 90% up.

The HKO operates a network time server to enable synchronization of computers with the Hong Kong Observatory standard time. During the experiment, we used this HKO's network time server to synchronize our S-LLS by simply installing software recommended by the HKO. The time error, as tested by us, is less than ±0.01 second, which is enough for matching lightning events between the HK-LLN and S-LLS.

Fig. 6.19 is a lightning map captured from HKO website on 19 May of 2010, showing the -CG positions for a half-hour period from 16h30m to 16h59m. There are three major clusters of lightning flash. The biggest one is at the southwestern direction of the map. Other two are at eastern and northeastern directions of the map. Fig. 6.20 is a lightning map showing locations for all negative lightning impulses/strokes observed by the S-LLS during the same time period as Fig. 6.19. Distance interval between circles is 30 km. The cluster of flash in the southwest of Fig. 6.20 is well consistent with that of Fig. 6.19, indicating that the S-LLS is effective and sensitive to flashes at least in this region. There are many strokes nearby the S-LLS at azimuth of about 225 degree. This is because that the magnetic fields produced by these close and strong

lightning strokes make the outputs of the two magnetic loops of the S-LLS saturated, resulting in an estimation of source azimuth at about 225 degree. From this point, the gains of magnetic loop circuits of the S-LLS should be improved for locating very close lightning strokes. Fig. 6.20 also shows some flashes in the eastern and northeastern directions of the map. To get quantitative information on the locating accuracy, comparisons of individual strokes between S-LLS and HK-LLN were done. Table 6.4 is the comparison result for 8 time-synchronized negative strokes occurring in the range of 30 to 60 km to the S-LLS, as shown by the black boxes in Figs.6.19 & 6.20. The location accuracy for these strokes is in the range of 0.1 to 3.7 km (or 0.1% to 9%).

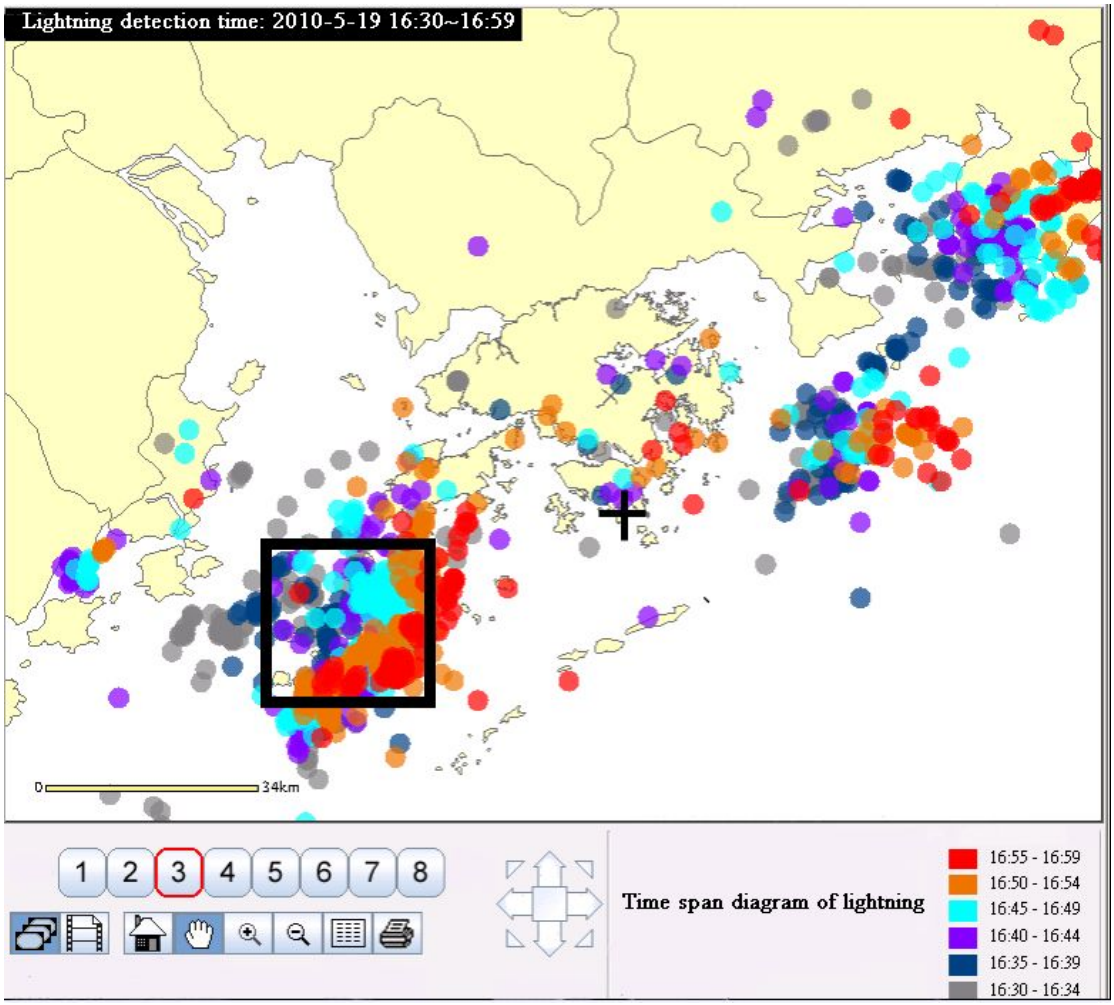

Fig. 6.19 Lightning map for negative CG for time period of 16h30m-16h59m on 19 May of 2010 from HK-LLN. Black cross "+" indicates S-LLS site

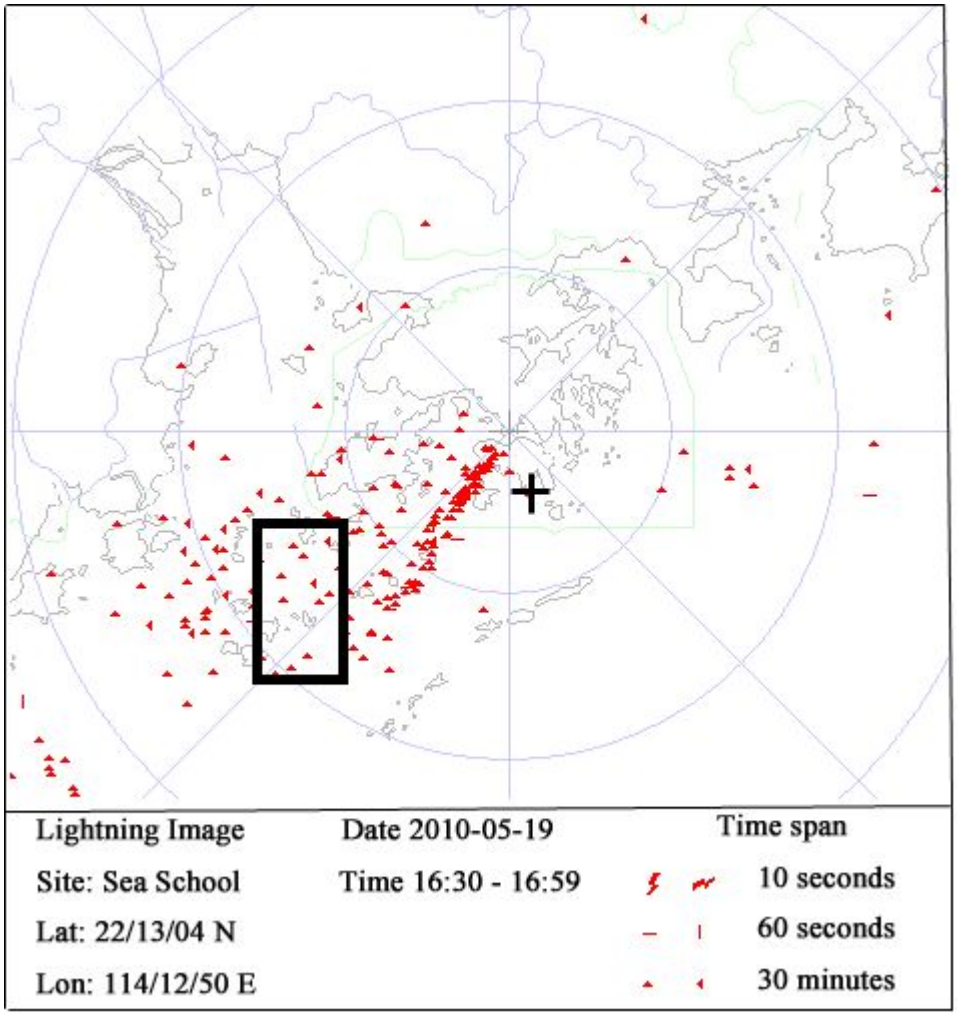

Fig. 6.20 Lightning map for negative impulses/strokes for the same time period as in Fig. 6.19 but from S-LLS. Black cross "+" indicates S-LLS site

Table 6.4 Comparisons of 8 negative strokes between S-LLS and HK-LLN for time period of 16h30m-16h59m on 19 May of 2010, shown by black boxes in Figs.6.19 & 6.20

Lightning strokes time (hh:mm:ss)	**Locating system**	**Longitude (Deg.)**	**Latitude (Deg.)**	***r* (km) Distance**	***θ* (Deg.) Azimuth**	***Δr***	***Δθ***
16:33:35.554	S-LLS	113.7760	22.0180	50.2	243.8	-1.4	1.3
	HK-LLN	113.7688	22.0028	51.6	242.5		
16:39:35.620	S-LLS	113.8140	21.9800	48.9	237.3	-1.5	2.1
	HK-LLN	113.8114	21.9585	50.4	235.2		
16:43:32.777	S-LLS	113.8640	22.1450	36.9	257.3	-0.4	-2.4
	HK-LLN	113.8569	22.1579	37.3	259.7		
16:46:19.685	S-LLS	113.8500	22.0970	39.8	250.3	-3.7	-5.3
	HK-LLN	113.8037	22.1206	43.5	255.6		
16:48:24.268	S-LLS	113.8760	22.0840	37.8	246.8	-2.4	-5.1
	HK-LLN	113.8423	22.1052	40.2	251.9		
16:52:06.668	S-LLS	113.7450	21.8840	60.8	232.5	-0.1	-3.7
	HK-LLN	113.7220	21.9126	60.9	236.2		
16:57:29.101	S-LLS	113.8600	21.9670	45.8	232.6	1.7	0.7
	HK-LLN	113.8764	21.9724	44.1	231.9		
16:59:00.599	S-LLS	113.9030	22.0780	35.6	244.1	2.2	-3.7
	HK-LLN	113.9131	22.1043	33.4	247.8		

*r and θ are the distance and azimuth of a stroke referred to the S-LLS, respectively.

*Δr andd $\Delta\theta$ are the difference in distance and azimuth between the S-LLS and HK-LLN, respectively.

Figs.6.21 & 6.22 are similar to Figs.6.19 & 6.20 but for the time period of 18h05m to 18h34m on 19 May of 2010 in the same storm. Both the HKO-LLN and S-LLS show that the lightning flashes were mainly occurred in the southeast area in the map. In combination with Figs.6.19 & 6.20, it shows that the storm was moving from southwest to southeast. The strokes nearby the S-LLS at azimuths of about 225 degree are the result of signal saturations on the magnetic loops of the S-LLS. Table 6.5 is the comparison result of 8 negative strokes occurring in the range of 15 to 30 km to the S-LLS, as shown by the black boxes in Figs.6.21 & 6.22. The location accuracy for these strokes is in the range of 0.3 to 4 km (or 0.15% to 22%), but there is a large systematic azimuthal error with a range of 8 to 22 degree. The large azimuthal error is probably due to that these strokes are too close to the S-LLS at the southern direction, so that the north-south magnetic loop of the S-LLS are partially saturated, resulting in a large error in direction finding.

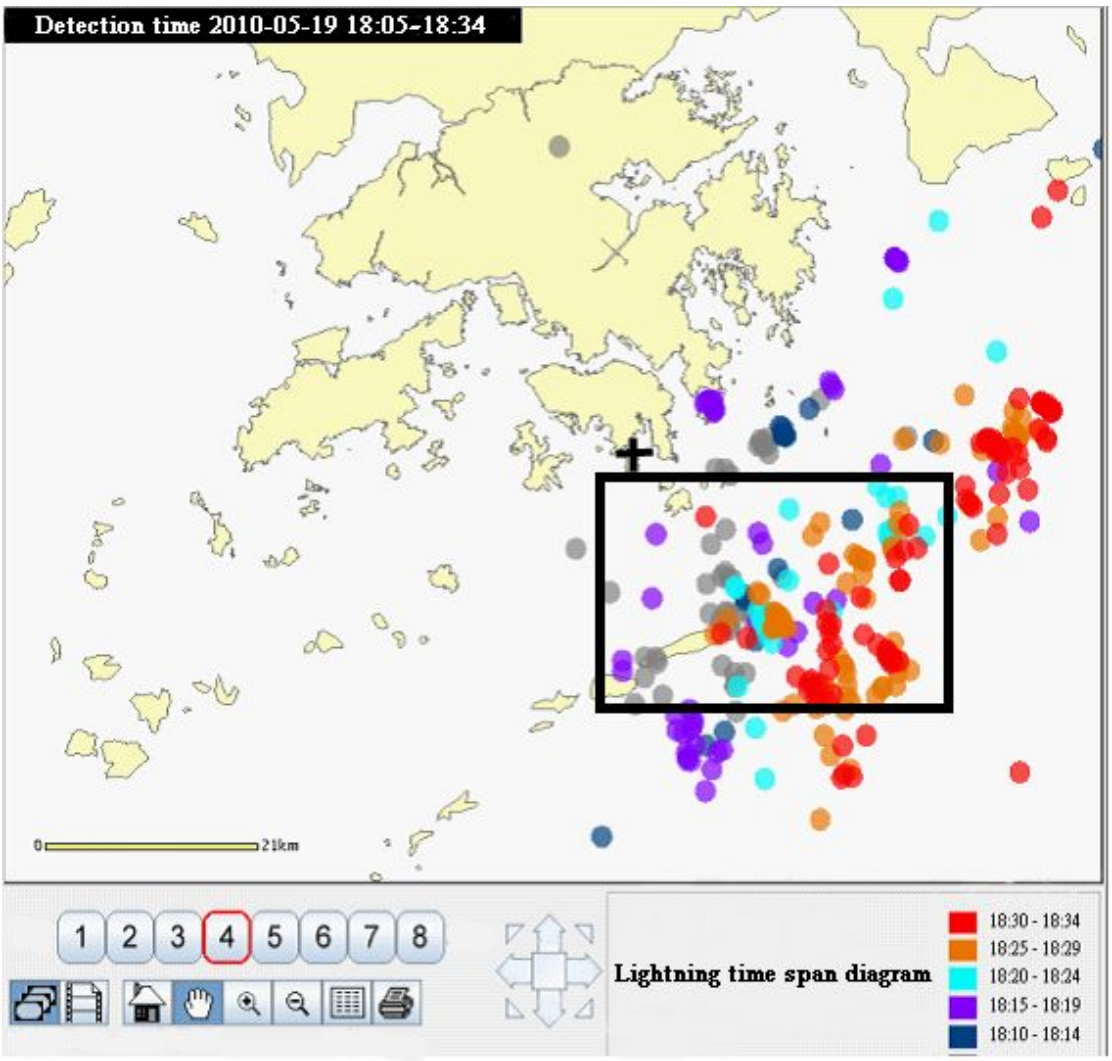

Fig. 6.21 Similar to Fig. 6.19 but for time 18h05m - 18h34m on 19 May of 2010

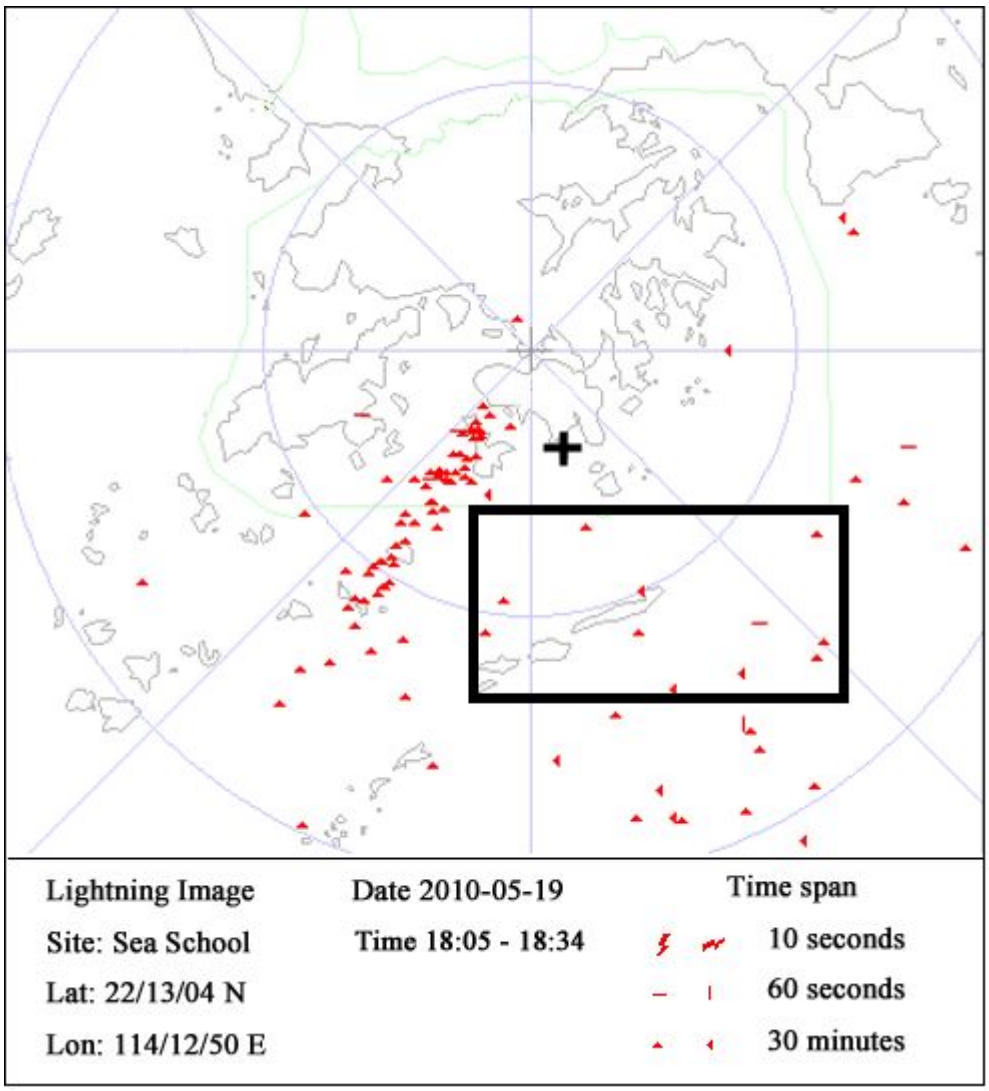

Fig. 6.22 Similar to Fig. 6.20 but for the same time as in Fig. 6.21

Table 6.5 Comparisons of 8 negative strokes between S-LLS and HK-LLN for time period of 18h05m-18h34m on 19 May of 2010, as shown by black boxes in Figs.6.21 & 6.22

Lightning Strokes time (hh:mm:ss)	**Locating system**	**Longitude (Deg.)**	**Latitude (Deg.)**	***r* (km) Distance**	***θ* (Deg.) Azimuth**	***Δr***	***Δθ***
18:05:18.117	S-LLS	114.2870	21.9370	32.1	166.5	3.9	8.4
	HK-LLN	114.3161	21.9825	28.2	158.1		
18:07:23.859	S-LLS	114.2660	22.0280	21.8	165.8	2.5	13.5
	HK-LLN	114.3013	22.0637	19.3	152.3		
18:07:24.974	S-LLS	114.1260	22.0730	18.5	209.3	4.0	21.8
	HK-LLN	114.1955	22.0886	14.5	187.5		
18:08:35.684	S-LLS	114.2580	22.0440	19.8	166.8	-1.2	22.3
	HK-LLN	114.3325	22.0639	21.0	144.5		
18:14:21.877	S-LLS	114.2760	22.0380	21.0	162.3	-1.8	15.2
	HK-LLN	114.3344	22.046	22.8	147.1		
18:25:35.241	S-LLS	114.2930	22.0340	22.0	158.3	-0.3	19.4
	HK-LLN	114.3526	22.0709	21.7	138.9		
18:30:16.730	S-LLS	114.4040	21.9640	34.3	145.3	1.5	16.2
	HK-LLN	114.4614	22.0316	32.8	129.1		
18:31:02.797	S-LLS	114.2980	22.0070	25.0	159.8	-3.0	15.7
	HK-LLN	114.3739	22.0137	28.0	144.1		

*r and θ are the distance and azimuth of a stroke referred to the S-LLS, respectively.

*Δr and $\Delta\theta$ are the difference in distance and azimuth between the S-LLS and HK-LLN, respectively.

Figs.6.23 & 6.24 are similar to Figs.6.19 &6.20 but for the time period of 18h05m to 18h34m on 24 June of 2010. Both show that the storm was in vicinity of Dong Guan City of Guangdong Province. However, the S-LLS gave a larger value of distance when compared with that of the HKO-LLN, indicating the performance of S-LLS to distant flashes is not as good as to close flashes. Similarly, comparisons for 8 negative strokes occurring in the range of 80 to 130 km to the S-LLS (shown by the black boxes in Figs.6.23 & 6.24) were made, and the results are summarized in Table 6.6. The location accuracy for these strokes is in the range of 12.4 to 26 km (or 13% to 24%), much larger than that in Tables 6.4 & 6.5.

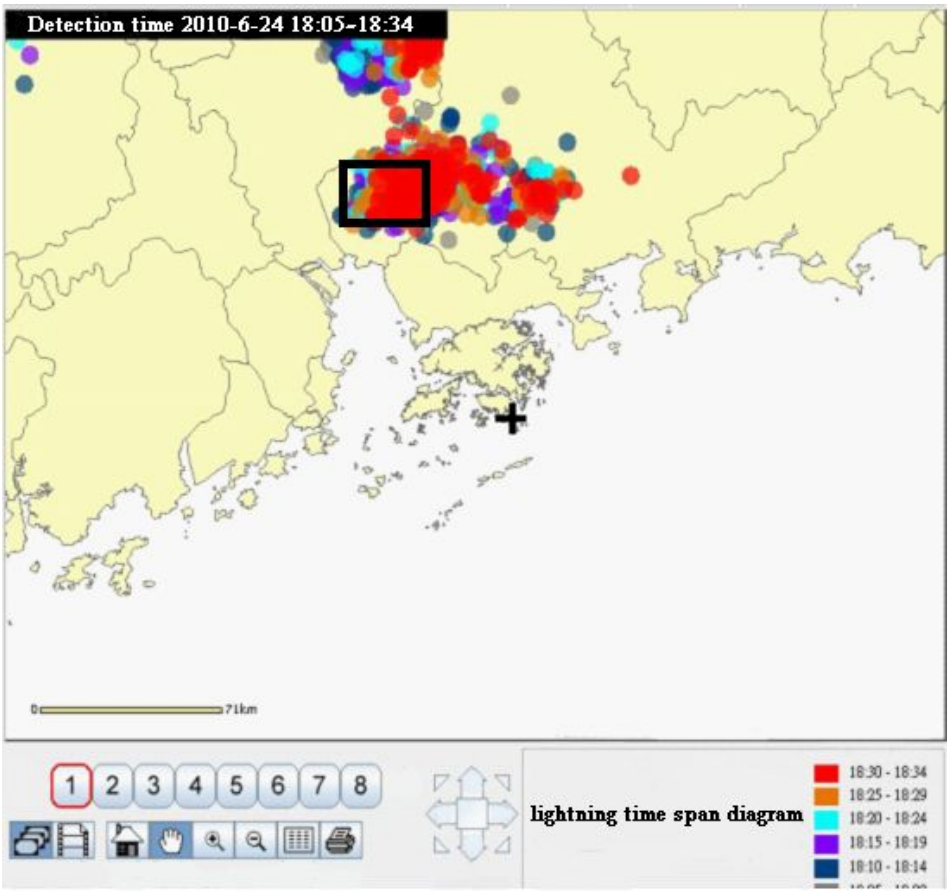

Fig. 6.23 Similar to Fig. 6.19 but for time 18h05m - 18h34m on 24 June of 2010

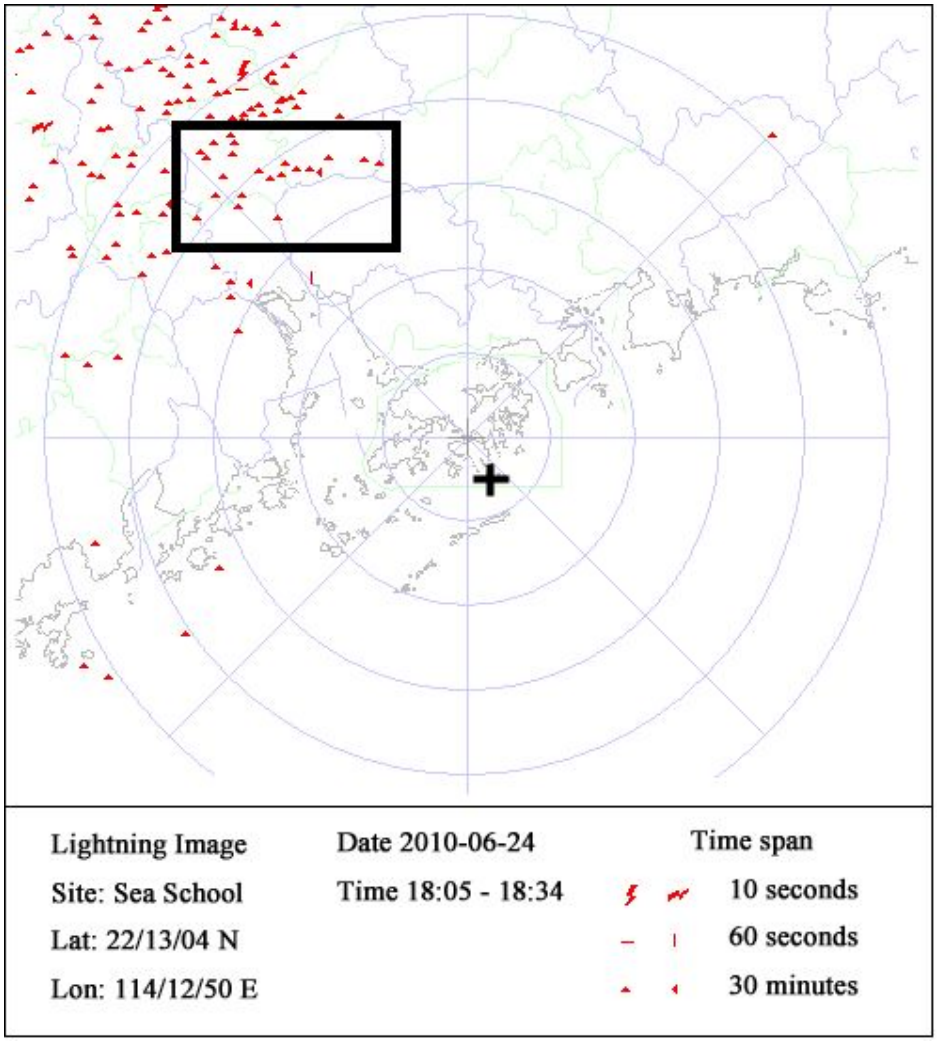

Fig. 6.24 Similar to Fig. 6.20 but for the same time as in Fig. 6.23

Table 6.6 Comparisons of 8 negative strokes between S-LLS and HK-LLN for time period of 18h05m-18h34m on 24 June of 2010, as shown by black boxes in Figs.6.23 & 6.24

Lightning strokes time (hh:mm:ss)	**Locating system**	**Longitude (Deg.)**	**Latitude (Deg.)**	***r* (km) Distance**	***θ* (Deg.) Azimuth**	***Δr***	***Δθ***
18:09:48.357	S-LLS	113.7460	22.8230	82.5	324.5	-15.4	-5.6
	HK-LLN	113.7386	22.9826	97.9	330.1		
18:11:56.420	S-LLS	113.4280	22.9830	117.0	316.5	15.7	-5.5
	HK-LLN	113.6052	22.9365	101.3	322.0		
18:25:37.552	S-LLS	113.6190	23.0720	112.7	327.3	21.8	-5.4
	HK-LLN	113.8068	22.9450	90.9	332.7		
18:26:41.637	S-LLS	113.7710	23.2400	122.2	338.2	22.6	-2.6
	HK-LLN	113.8954	23.0651	99.6	340.8		
18:26:57.414	S-LLS	113.5950	23.2980	135.6	332.1	19.6	-0.3
	HK-LLN	113.6891	23.1444	116.0	332.4		
18:28:08.980	S-LLS	113.6360	23.3130	135.2	334.1	26	-2.2
	HK-LLN	113.7863	23.1189	109.2	336.3		
18:29:02.619	S-LLS	113.8500	23.1030	105.1	339.2	12.4	-0.4
	HK-LLN	113.8992	23.0011	92.7	339.6		
18:32:28.434	S-LLS	113.6170	23.2690	131.7	332.4	25.2	-3.6
	HK-LLN	113.7907	23.0939	106.5	336.0		

*r and θ are the distance and azimuth of a stroke referred to the S-LLS, respectively.

*Δr and $\Delta\theta$ are the difference in distance and azimuth between the S-LLS and HK-LLN, respectively.

In summary, the S-LLS can give accurate distance information with an error less than 4 km for close lightning strokes in ranges of 15 to 60 km. However, for distant lightning strokes in ranges of 80 to 130 km, the error in distance can be as large as 26 km. The S-LLS did not performed well for very close lightning strokes mainly due to the signal saturations on magnetic loop circuits of the S-LLS. In addition, due to shielding by a mountain in the northeast of the site, the S-LLS has poor sensitivity to flashes occurred in that direction.

6.6 Conclusion

An improved approach for locating close lightning return stroke was proposed and practiced. The approach was examined by applying it to broadband electric and magnetic field waveforms observed simultaneously at one station for several strokes in a distance range of about 10 to 50 km. The results show that the proposed approach did well to those observed electric and magnetic waveforms.

Based on the proposed approach, a prototypal single-station lightning location system (S-LLS), which can be seen as a modified VLF/LF broadband magnetic DF added with a lightning distance finding function, was built up and tested in field. Comparisons of individual lightning stroke locations between the S-LLS and the Hong Kong local lightning location network (HK-LLN) were made. The results show

that the S-LLS has a good location accuracy of 0.1 - 4 km for close lightning strokes in ranges of 15 to 60 km, but has a poor location accuracy of 12.4 - 26 km for distant lightning strokes in ranges of 80 to 130 km. For very close and strong lightning strokes (say less than 15 km), due to signal saturations on the magnetic loops the S-LLS did not provide accurate stroke locations. This defect may be overcome by improving the gains of magnetic loops of the S-LLS.

The S-LLS is capable to provide early warning of lighting event for some critical places such as playground, sports venues, and power plant and those regions that haven't been covered by a LLN. .

Chapter 7

Discussion and Summary

This thesis focused mainly on lightning direction finder (DF) technique and its "site error".

First, a thorough review and a detailed investigation of the properties of "site error' have been done. The "site error" of a DF is found to be a function of both the source azimuth and signal frequency. In azimuth domain, the "site error" usually shows either a two-cycle variation or an odd-cycle variation or a combination of the both. In frequency domain, the "site error" usually shows a fluctuation with some mono-polar or bi-polar impulsive variations superposed on a relative flat variation curve.

Second, modeling and interpretation of the "site error" have been done. Based on the model established, it is found that the odd-cycle variations in azimuthal domain and the mono-polar impulsive fluctuations in frequency domain are due to the reflection of lightning incident signals by "electric-dipole-wise" structures nearby a DF, while the two-cycle ones in azimuthal domain and the bi-polar ones in frequency domain are due to that by the "magnetic-dipole-wise" structures. Using of broadband magnetic loop antenna or averaging process of the azimuths in frequency domain for a DF may give the source azimuth with high accuracy.

Third, a practical method for “site error” estimations and corrections for DF/TOA type LLN, which are currently used in world-wide, has been proposed. Although TOA locating technique can achieve a location accuracy of 500 m, it needs at least 4 sensors to detect a stroke. However, a large proportion of lightning strokes are usually detected by only 2 sensors, leading a DF locating technique with “site error” involved. Therefore, “site error” corrections are still necessary to a DF/TOA network. The “site error” for an individual DF can be obtained by comparison the DF detected azimuth with the TOA resultant azimuth for the same lightning strokes. Once the “site error” for a DF is obtained, it can be used to correct the DF detected azimuth especially for those strokes detected by only 2 sensors in the LLN. The method has been examined with the data from a 25-station DF/TOA LLN in China. The results show that this “site error” correction method could indeed upgrade the whole LLN performance because 2-sensor located strokes account for a large proportion of the LLN data.

In last, a single-station lightning location system (S-LLS) based on a broadband magnetic DF plus an improved lightning distance derivation method has been built and put in field experiments. Experimental results show that the S-LLS has a good location accuracy of 0.1 - 4 km for close lightning strokes in ranges of 15 to 60 km. It is capable to locate distant lightning strokes as far as 130 km but with lower location accuracy.

In future work, based on an appropriate lightning return stroke model and a more accurate distance finding technique, the S-LLS may be also used to obtain the magnitude and waveform of a return stroke current. In addition, the effect of earth path on lightning-produced electromagnetic pulse amplitude has been identified by Ding [Ding et al., 2012], which is helpful to the precise peak current derivation.

References

1. Biagi et al., 2007

Biagi, C. J., K. L. Cummins, K. E. Kehoe, and E. P. Krider: NLDN performance in Southern Arizona, Texas and Oklahoma in 2003-2004, *J. Geophys. Res*., Vol. 112, D05208, 2007.

2. Boccippio et al., 1998

Boccippio, D. J.,Wong, C.,Williams, E. R., Boldi, R., Christian, H. J., and Goodman, S. J: Global validation of single-station Schumann resonance lightning location, *J. Atmos. Sol.-Terr. Phys*., Vol. 60, pp. 701–712, 1998.

3. Brundell et al., 2002

Brundell, J. B., Rodger, C. J., and Dowden, R. L: Validation of single station lightning location technique, *Radio Sci*., Vol. 37, 2002.

4. Casper and Bent, 1992

P. W. Casper and R. B. Bent: Results from the LPATS USA National Lightning Detection and Tracking System for the 1991 Lightning Season, *The 21st International Conference on Lightning Protection*, Berlin, Germany, 1992.

5. Chen and Liu, 1990

Chen, M., and Liu Xinsheng: The transmission line model and current velocity of lightning return strokes. *Plateau Meteorology*, Vol. 9, pp. 54-63, 1990.

6. Chen, 2008

Chen Huaichen: Tutorial of digital signal processing, *Publishing House of Electronics Industry*, 2008.

7. Chen, 2009

Chen, M: Review of new progresses in the area of lightning detection and protection technique, *HKIE Transaction*, Vol.16, No.1, pp. 1-6, 2009.

8. Chen et al., 2011

Chen, M., Z. Dong, Y. Du, and Y. Zhang: Detection efficiency of a Regional Lightning Location Network in China, 2011 *Asia-Pacific EMC Symposium*, Jeju Island, Korea, May 16~19, 2011.

9. Chen et al., 1991

Chen, M.,X. Liu, C. Guo, Z. Ge: A parametric method of site error estimation for a lightning location system, *Acta Meteor. Sinica*, Vol. 5, pp. 370-380, 1991.

10. Chen et al., 1993

Chen, M., X. Liu and C. Guo: Site errors and its structure of a lightning location

system in Beijing region, *Acta Meteor. Sinica*, Vol. 51, No.1, pp. 66-74, 1993.

11. Chen et al., 2007

Chen, M., H. Wang, and Y. Du: A compact, Integrated lightning detector for making optical and electromagnetic measurements of lightning, *Proceeding of 13th International Conference on Atmospheric Electricity*, August 13-18, 2007, Beijing, China, pp. 835-837, 2007.

12. Chen et al., 2010

Chen, M., Zheng, D., Du, Y., Zhang, Y: Temporal and spatial characteristics of lightning activity versus terrain in Hong Kong. *Asia-Pacific Symposium on Electromagnetic Compatibility, APEMC*, pp. 1146-1149, 2010.

13. Christina et al., 2009

Stall, Christina A., Kenneth L. Cummins, E. Philip Krider, John A. Cramer: Detecting Multiple Ground Contacts in Cloud-to-Ground Lightning Flashes, *J. Atmos. Oceanic Technology*., Vol. 26, pp. 2392–2402, 2009.

14. Cooray and Perez, 1994

Vernon Cooray and Hugo Perez: Some features of lightning observed in Sweden, *J. Geophys. Res*., Vol. 99, pp. 10683-10688, 1994.

15. Cummins and Murphy, 2009

Cummins, K. L., M. J. Murphy: An overview of lightning locating systems: History, techniques, and data uses, with an in depth look at the U.S. NLDN. *IEEE Trans. Electromag. Compat*., Vol. 51, pp. 499–518, 2009.

16. Cummins et al., 1998

Cummins, K. L., M. J. Murphy, E. A. Bardo, W. L. Hiscox, R. B. Pyle, and A. E. Pifer: A combined TOA/MDF technology upgrade of the US national lightning detection network, *J. Geophys. Res*, Vol. 103, pp. 9035-9044, 1998.

17. Ding et al., 2012

Xueyun DING, Mingli CHEN and Yaping DU: Study of the effect of propagation path on lightning-produced electromagnetic pulses based on LLN data, *International Conferenc on Lightning Protection*, 2012.

18. Guo, 1997

Guo Shuohong: Electrodynamics, *High Education Press*, 1997.

19 Guo and Krider, 1983

Guo, C., and E. P. Krider: The optical power radiated by lightning return strokes, *J. Geophys. Res*., Vol.88, pp. 8621-8632, 1983.

20. Hiscox et al., 1984

Hiscox. W. L., E. P. Krider, A. E. Pifer and M. A. Uman: A systematic method for identifying and correcting “site errors” in a network of magnetic direction finders, *International Aerospace and Ground Conference on Lightning and Static Electricity*. Orlando, Florida, June 1984.

21. Honma et al., 2011

Honma, N., K. L. Cummins, M. J. Murphy, A. E. Pifer, and T. Rogers: Improved Lightning Locations in the Tohoku Region of Japan using Propagation and Onset corrections, *XIV International Conference on Atmospheric Electricity*, Rio de Janeiro, Brazil, 2011.

22. Horner, 1954

Horner, F: The accuracy of the location sources of atmospherics by radio direction finding, *Proc. IEEE* Vol. 101, pp. 383-390, 1954.

23. Horner, 1957

Horner, F: Very-low frequency propagation and direction finding, *Proc. IEEE* Vol. 101b, pp. 73–80, 1957.

24. Horner, 1960

Horner, F: The design and use of instruments for counting local lightning flashes,

Proc. Inst. Electr. Eng, pp. 321-330, 1960.

25. Jerauld et al., 2005

J. Jerauld, V. A. Rakov, M. A. Uman, K. J. Rambo, D. M. Jordan, K. L. Cummins, and J. A. Cramer: An evaluation of the performance characteristics of the U.S. National Lightning Detection Network in Florida using rocket-triggered lightning, *J. Geophys. Res*., Vol. 110, No. D19, pp. 19106, 2005.

26. Jordan and Uman, 1983

Jordan, D.M. and Uman, M.A: Variation in Light Intensity With Height and Time From Subsequent Lightning Return Strokes. *J. Geophys. Res*., Vol. 88, 1983.

27. Kemp and Jone, 1971

Kemp, D.T. and D. L. Jones: A new technique for the analyses of transient ELF electromagnetic disturbances within the Earth-ionosphere cavity, *J. Atmos. Terr. Phys*, Vol. 33, pp. 567-572, 1971.

28. Korol and Nickolaenko, 1993

Korol, M. A. and Nickolaenko, A. P: A technique to derive the distance from near discharge. *J. Atmos. Electr*., Vol. 13, pp. 1-7, 1993.

29. Krider, 1973

Krider, R.E: The location of lightning flashes at ranges less than 100 km, *J. Atmos. Terr. Phys*., Vol. 35, pp. 283-90, 1973.

30. Krider et al., 1976

Krider, E.P., R. C. Noggle and M. A. Uman: A gated, wide-band, magnetic direction finder for lightning return strokes, *J. Appl. Meteor*., Vol. 15, pp. 301, 1976.

31. Krider and Noggle, 1975

Krider, E. P., and R. C. Noggle: Broadband Antenna Systems for Lightning Magnetic Fields, *Journal of Applied Meteorology*, pp. 252, 1975.

32. Krider et al., 1977

Krider, E. P., C. D. Weidman, and R. C. Noggle: The electric fields produced by lightning stepped leaders, *J. Geophys. Res*., Vol. 82, pp. 951-960, 1977.

33. Krider et al., 1980

Krider, E. P., R. C. Noggle, A. E. Pifer, and D.L. Vance: Lightning direction finding systems for forest fire detection, *Bull. Amer. Meteor. Soc*., Vol. 61, pp. 980-6, 1980.

34. Lin et al., 1980

Lin, Y.T., Uman, M.A., and Standler, R.B: Lighting return stroke model, *J. Geophys. Res*., Vol. 85, pp. 1571, 1980.

35. Lu et al., 2006

Lu Hongmin, Zhao Yongjiu, and Zhu Manzuo: The basis of electromagnetic field and wave, *Science Press*. 2006.

36. Lopez and Passi, 1991

Lopez R. E. and R. M. Passi: Simulation in site error estimation for direction finders, *J. Geophys. Res*., Vol. 96, pp. 15287-15296, 1991.

37. Mach et al., 1986

Mach, D. M., D. R. MacGorman, W. D. Rust and R. T. Arnold: Site errors and detection efficiency in a magnetic direction-finder network for locating lightning strikes to ground, *Journal of Atmospheric and Oceanic Technology*, Vol. 3, pp. 67-74, 1986.

38. Mardiana, 2007

Mardiana R: Development of Web-based Lightning Information from Single Station, *Proceedings of the International Conference on Electrical Engineering and Informatics*, Institut Teknologi Bandung, Indonesia June 17-19, 2007.

39. Mei et al., 2007

Mei Zen, Chen Shuiming, Gu Qinwei, Huang Xinzhang: Statistic of Lightning Accidents During 1998~2004 in China, *High Voltage Engineering*, Vol. 33 No. 12

December 2007.

40. Nagano et al., 2007

I. Nagano, S. Yagitani, M. Ozaki, Y. Nakamura and K. Miyamura: Estimation of lightning location from single station observations of sferics, *Electronics and Communications in Japan*, Part I, Vol. 90(1), pp. 25-34, 2007.

41. Nickolaenko and Hayakawa, 2002

Nickolaenko. A.P., Hayakawa, M: Resonances in the Earth-ionosphere Cavity. *Kluwer Academic Publishers*, Dordrecht, Boston, London, 380pp, 2002.

42. Nucci et al., 1988

Nucci, C.A., Mazzetti, C., Rachidi, F., Ianoz, M: On lightning return stroke models for LEMP calculations. *Proceedings of the international conference on Lightning protection*, Graz, 1988.

43. Orville, 1987

Orville, R.E., Jr: An analytical solution on obtain the optimum source location using multiple direction finder on a spherical surface, *J. Geophys. Res*., Vol. 92, No. D9, pp.l0877-10886, 1987.

44. Passi and Lopez, 1989

Passi, R. M., and R. E. Lopez: A Parametric Estimation of Systematic Errors in Networks of Magnetic Direction Finders, *J. Geophys. Res*., Vol. 94, pp. 13319-13328, 1989.

45. Qie et al., 2001

Xiushu Qie, Ye Yu, Huaibin Wang and Cuihua Zhang: Analysis on Some Features of Ground Flashes in Chinese Inland Plateau, *Plateau Meteorology*, Vol. 20, 2001.

46. Rakov and Uman, 2003

Rakov V, Uman M: Lightning: physics and effects, *Cambridge University Press*. 2003.

47. Rakov et al., 1994

Vladimir A. Rakov, Martin A. Uman, and Rajeev Thottappilli: Review of lightning properties from electric field and TV observations, *Journal of Geophysical Research*, Vol. 99, No. D5, pp. 10745-10750, 1994.

48. Ramachandran et al., 2007

V. Ramachandran, J. N. Prakash, A. Deo and S. Kumar: Lightning stroke distance estimation from single station observation and validation with WWLLN data, *Ann. Geophys*, Vol. 25, pp. 1509–1517, 2007.

49. Richard and Auffray, 1985

Richard P., Auffray G: VHF-UHF interferometric measurements, application to lightning discharge mapping. *Radio Science*, Vol. 20(2), pp. 171-192, 1985.

50. Rodger and Russell, 2002

Rodger, C.J., and N.A. Russell: Lightning multiplicity measurements by the U. S. National Lightning Detection Network, *Proceedings of the 27th General Assembly of the International Union of Radio Science*, Maastricht, Holland, 2002.

51. Shao et al., 1995

Shao, X. M., Krehbiel, P. R., Thomas, N. J., Rison, W: Radio interferometric observations of cloud-to-ground lightning phenomena in Florida, *J. Geophys.Res*., Vol. 100, pp. 2749-2783, 1995.

52. Shen et al., 2003

Shen Peixuan, Mao Jietai, Li Jianguo, Zhang Aichen, Sang Jianguo, Pan Naixian: Atmospheric Physics (in Chinese), *Peking University Press*, 2003.

53. Shvets et al., 1997

Shvets A. V., Nickolaenko A. P., and Hayakawa M: Characteristics of nearby lightning discharges observed at Singapore, *J. Atmos Solar-Terr Phys USA*, Vol. 59,

pp.1717-1726, 1997.

54. Sommerfeld, 1926

Sommerfeld: Propagation of waves in wireless telegraphy, *J. Ann Phys*, Vol. 81, pp.1135-1153, 1926.

55. Song et al., 2011

Song Xin, Wang Keqi and Li Difei: Research and Application of Field Mill Electric Field Meter in the Lightning Early Warning, *Automation and Instrumentation*, Vol. 26(2), 2011.

56. Stansfield, 1947

Stansfield, R. G.: Statistical theory of d.f. fixing, *Journal of the Institution of Electrical Engineers*, Vol. 94, pp. 762-770, 1947.

57. Thomas et al., 2004

Thomas, R. J., Krehbiel, P. R., Rison, W., Hunyady, S. J., Winn, W. P., Hamlin, T., Harlin, J: Accuracy of the lightning mapping array, *J. Geophys. Res*., Vol. 109, No. D14, pp. 1-34, 2004.

58. Tian et al., 2009

Tian Xiaorui, Shu Lifu, Wang Mingyu, Zhao Fengjun: Spatial and Temporal

Distribution of Lightning Fire and Forecasting Model for Daxing'anling, *Forest Research*, Vol. 1, 2009.

59. Uman, 1987

Martin A. Uman: The lightning discharge, *International Geophysics Series*, Vol. 39, pp. 356, 1987.

60. Volland, 1995

Volland H: Long wave sferics propagation within the atmospheric waveguide, *Handbook of Atmospheric Electrodynamics*, Volume II, pp. 65-93, *CRC Press*, Boca Raton, 1995.

61. Wait, 1962

Wait, J. R: Electromagnetic Waves in Stratified Media, *Macmillan*, New, York, 1962.

62. Wang et al., 2000

Wang Daohong, Xiushu Qie and Changming Guo: Thunder and Artificial Triggered Lightning, *Shanghai Jiaotong University Press*, 2000.

63. Website_1, 2013

http://webflash.ess.washington.edu/

64. Website_2, 2013

http://www.weather.gov.hk/wxinfo/llis/gm_index.htm